Electronic Supplementary Information (ESI)

Spin-Driven Multiferroic Properties of $PbMn_7O_{12}$ Perovskite

Alexei A. Belik,[*,†] Yana S. Glazkova,[†,‡] Noriki Terada,[§] Yoshitaka Matsushita,[§] Alexey V. Sobolev,[‡] Igor A. Presniakov,[‡] Naohito Tsujii,[§] Shigeki Nimori,[§§] Kanji Takehana,[§§] and Yasutaka Imanaka[§§]

[†] *International Center for Materials Nanoarchitectonics (WPI-MANA), National Institute for Materials Science (NIMS), Namiki 1-1, Tsukuba, Ibaraki 305-0044, Japan*

[‡] *Department of Chemistry, Lomonosov Moscow State University, Leninskie Gory, 119992 Moscow, Russia*

[§] *National Institute for Materials Science (NIMS), Sengen 1-2-1, Tsukuba, Ibaraki 305-0047, Japan*

[§§] *Tsukuba Magnet Laboratory, NIMS, 3-13 Sakura, Tsukuba, Ibaraki 305-0003, Japan*

* To whom all correspondence should be addressed. E-mail: Alexei.Belik@nims.go.jp

A construction of our high-pressure cell allows us to treat two samples (two Au/Pt capsules) at the same time (see Figure below and for example, Yamaura, K. *J. Solid State Chem.* **2016**, *236*, 45-54).

$PbMn_7O_{12}$-3-1 and $PbMn_7O_{12}$-3-2 samples were prepared from the same starting mixture and in one high-pressure cell. Small difference in their properties (Figure 4 in the main text) again confirms that variations in real synthesis conditions (for example, some temperature gradients along a high-pressure cell) have some effects.

$PbMn_7O_{12}$-N sample was prepared/used for Neutron diffraction.

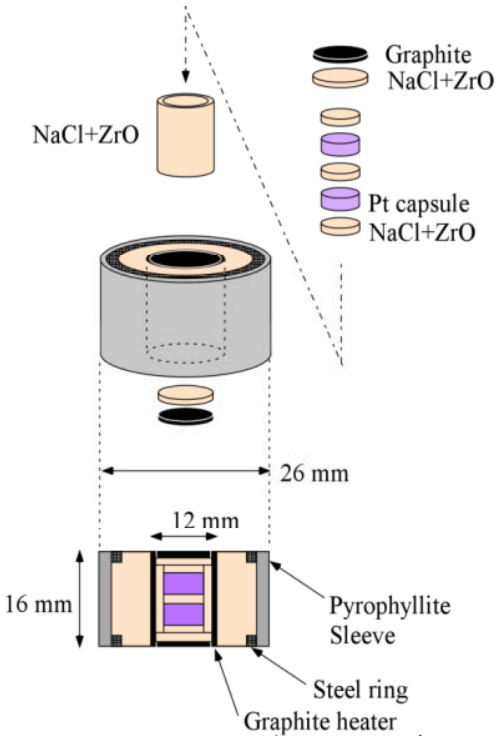

T_{N3} = 43 K for $PbMn_7O_{12}$ coincides with T_C = 43 K of Mn_3O_4. Mn_3O_4 is a very common impurity in systems containing Mn and O. However, we can exclude the presence of Mn_3O_4 in our samples. No signs of Mn_3O_4 were detected on high-resolution synchrotron X-ray powder diffraction patterns of sample 2 (Figure S1b: a 85 % peak of Mn_3O_4 should have been detected at $2\theta \approx 14.531$ deg). If the amount of Mn_3O_4 is below a detection limit, no specific heat anomaly is expected because specific heat probes bulk properties. Detection of the specific heat anomaly at T_{N3} = 43 K for $PbMn_7O_{12}$ (sample 2: Figures S11 and S12; and sample 3-1: Figure 3 in the main text) confirms that this anomaly is intrinsic for $PbMn_7O_{12}$. [Note that magnetic measurements may show the presence of Mn_3O_4 below a detection limit of laboratory or synchrotron XRPD (Belik, A. A. *J. Phys. Soc. Jpn*. **2014**, *83*, 074703).]

Table S1. Lattice parameters of $PbMn_7O_{12}$ (sample 3-2) from low-temperature and high-temperature laboratory X-ray powder diffraction data. An error of the *a* lattice parameter is about 0.0003, and the *c* lattice parameter – 0.0002.

T (K)	*a* (Å)	*c* (Å)
5	10.5073	6.4116
10	10.5075	6.4118
20	10.5075	6.4117
30	10.5077	6.4117
40	10.5082	6.4121
50	10.5072	6.4113
60	10.5092	6.4123
70	10.5078	6.4111
80	10.5088	6.4116
90	10.5091	6.4115
100	10.5095	6.4114
110	10.5093	6.4108
120	10.5109	6.4112
130	10.5110	6.4108
140	10.5119	6.4110
150	10.5122	6.4107
160	10.5132	6.4109
170	10.5136	6.4107
180	10.5142	6.4109
190	10.5144	6.4106
200	10.5149	6.4106
210	10.5158	6.4108
220	10.5166	6.4109
230	10.5174	6.4112
240	10.5182	6.4112
250	10.5185	6.4111
260	10.5187	6.4110
270	10.5201	6.4112
280	10.5214	6.4114
290	10.5211	6.4111
300	10.5220	6.4109

T (°C)	*a* (Å)	*c* (Å)
25	10.5218	6.4102
57	10.5240	6.4116
88	10.5262	6.4133
117	10.5285	6.4152
127	two-phased	
127	two-phased	
137	7.4343	
167	7.4360	
197	7.4377	
227	7.4394	
257	7.4413	
287	7.4432	
317	7.4450	

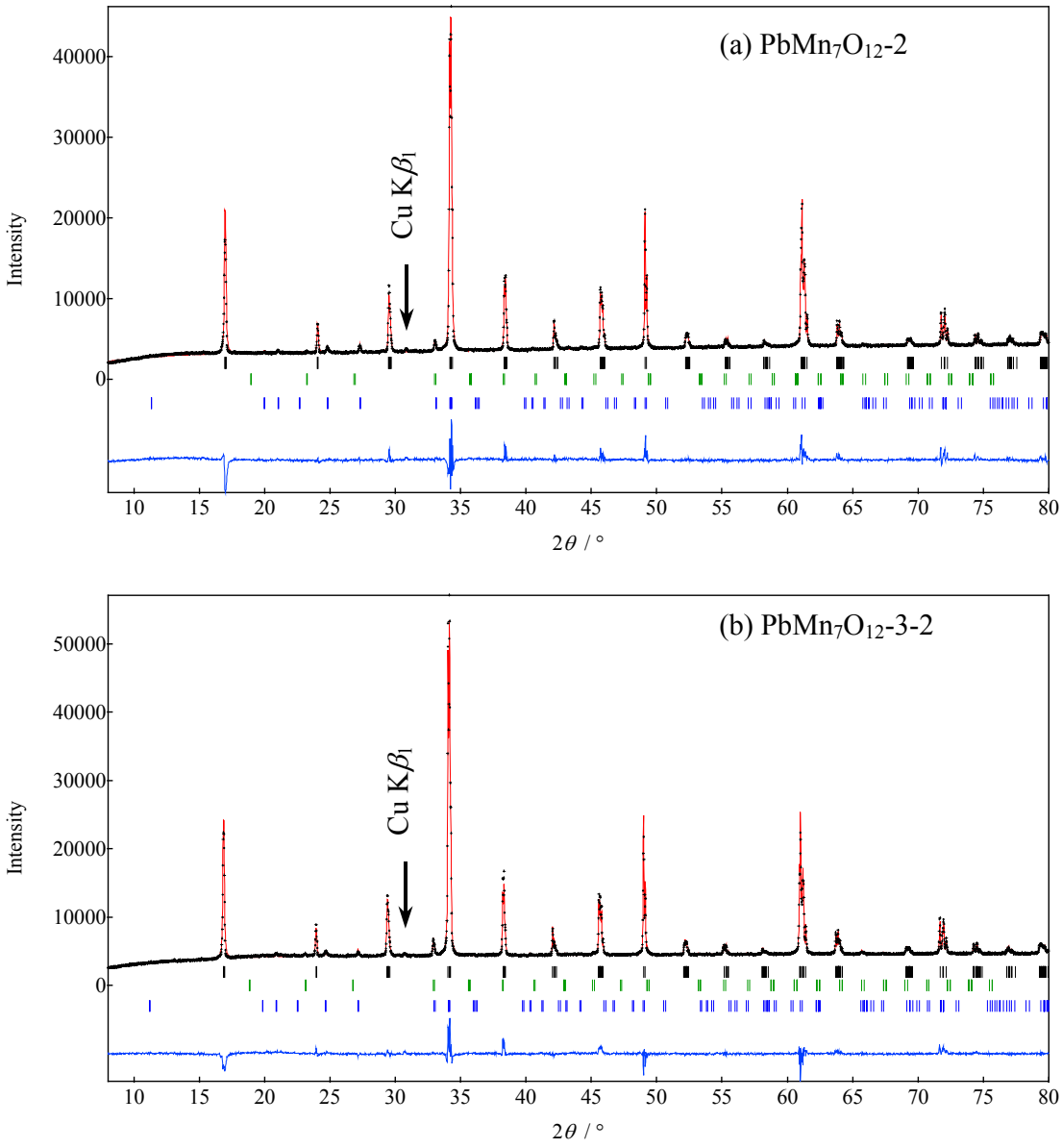

Figure S1a. X-ray powder diffraction data of $PbMn_7O_{12}$. Experimental (black crosses), calculated (red line), and difference (blue line) laboratory XRPD patterns of $PbMn_7O_{12}$ (a: sample 2; b: sample 3-2) at 295 K (measured with CuKα radiation) on a RIGAKU MiniFlex600 diffractometer. The bars show possible Bragg reflection positions for $PbMn_7O_{12}$ (black), Mn_2O_3 impurity (green), and $Pb_3(CO_3)_2(OH)_2$ impurity (blue) (from top to bottom). Arrows show a very small contribution from the strongest sample reflections originating from the Cu Kβ_1 radiation.

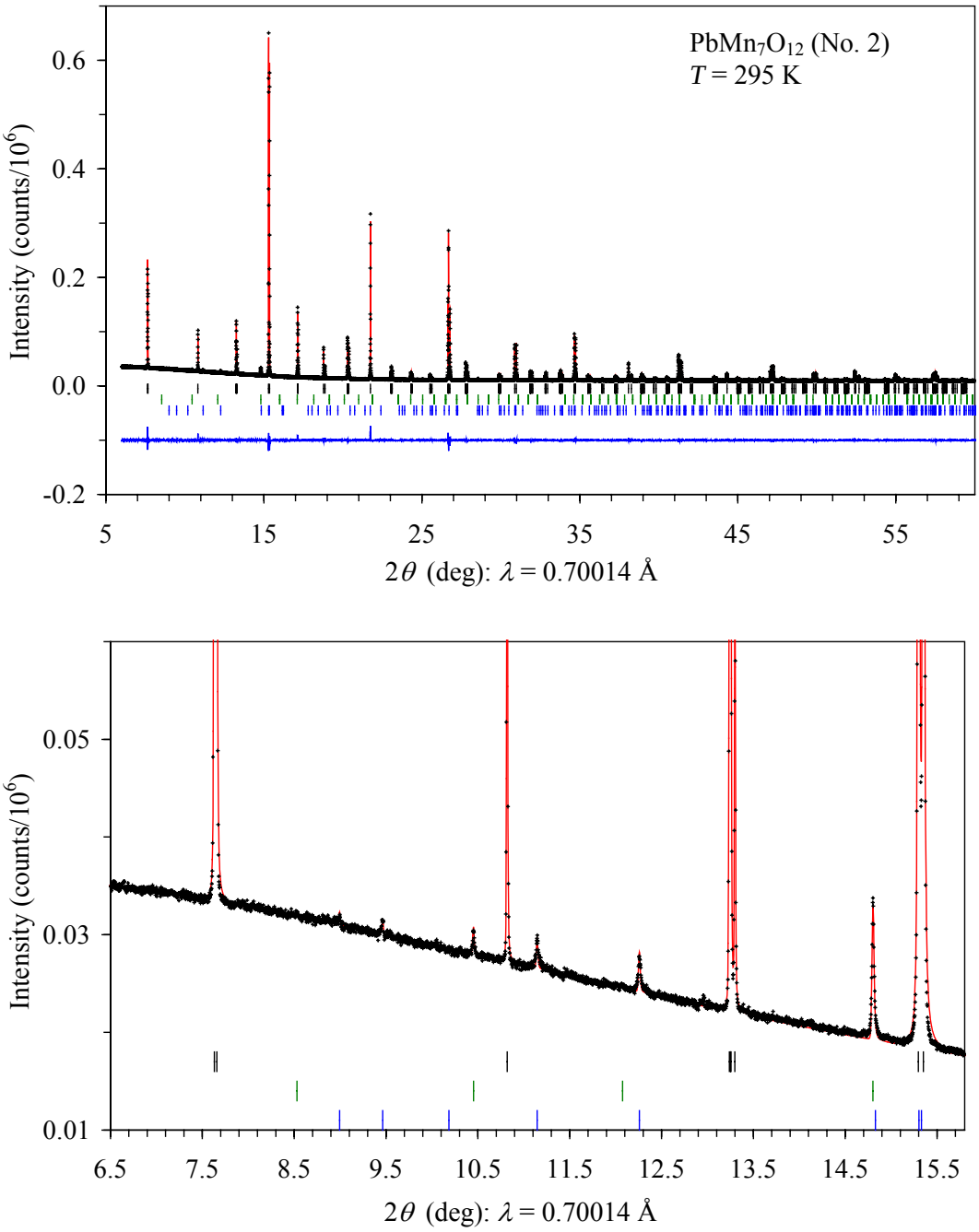

Figure S1b. (Up) Experimental (black crosses), calculated (red line), and difference (blue line) synchrotron XRPD patterns of $PbMn_7O_{12}$ (sample 2) at 295 K (λ = 0.70014 Å). The bars show possible Bragg reflection positions of $PbMn_7O_{12}$ (black) and Mn_2O_3 (green) and $Pb_3(CO_3)_2(OH)_2$ (blue) impurities. (Down) The lower panel emphasizes impurity reflections. The weight fractions of impurities were estimated to be 3.8 % (Mn_2O_3) and 0.7 % ($Pb_3(CO_3)_2(OH)_2$) from the refined scale factors during the Rietveld refinements [Belik, A. A.; Glazkova, Y. S.; Katsuya, Y.; Tanaka, M.; Sobolev, A. V.; Presniakov, I. A. *J. Phys. Chem. C* **2016**, *120*, 8278-8288.]

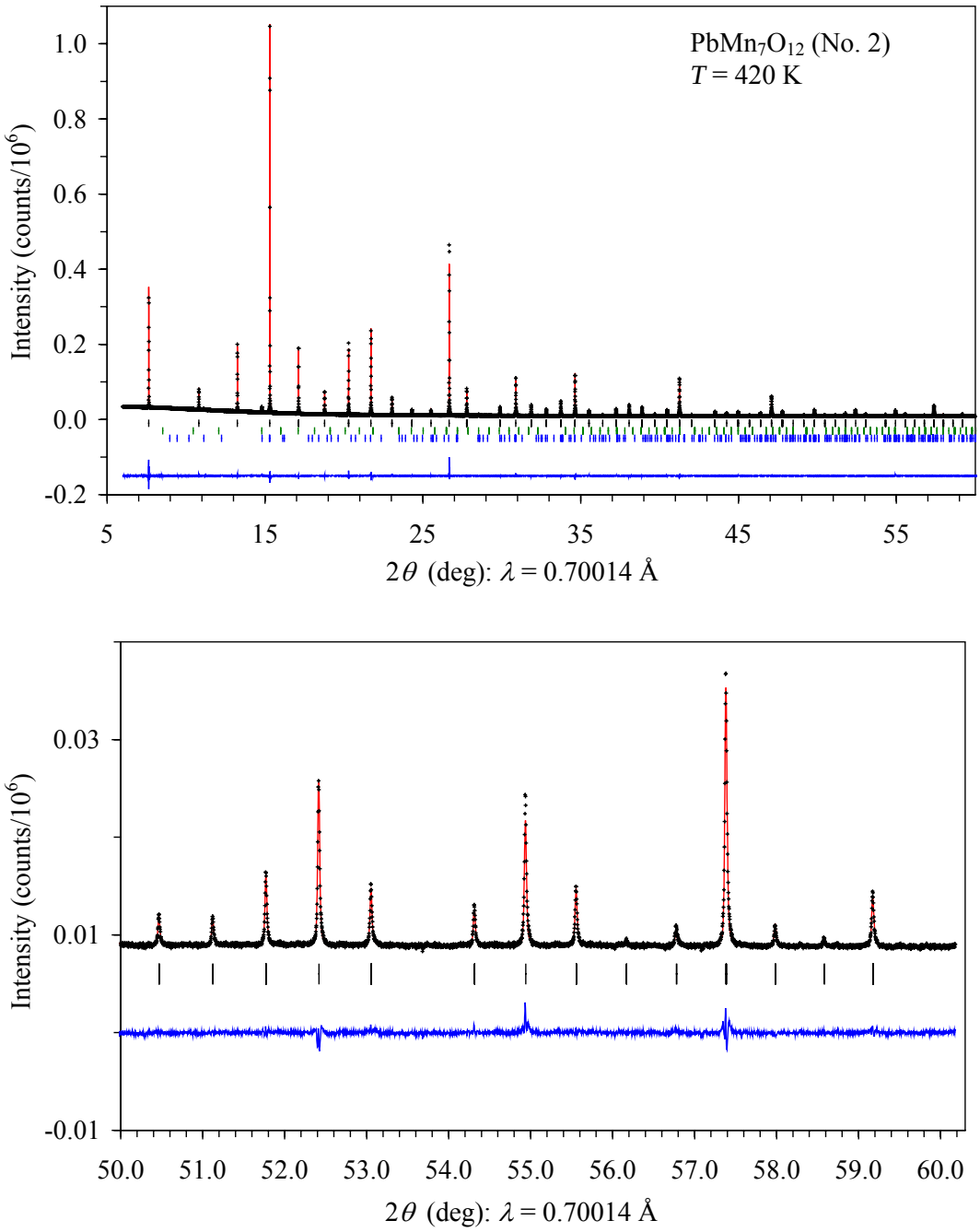

Figure S1c. (Up) Experimental (black crosses), calculated (red line), and difference (blue line) synchrotron XRPD patterns of $PbMn_7O_{12}$ (sample 2) at 420 K (λ = 0.70014 Å). The bars show possible Bragg reflection positions of $PbMn_7O_{12}$ (black) and Mn_2O_3 (green) and $Pb_3(CO_3)_2(OH)_2$ (blue) impurities. [Belik, A. A.; Glazkova, Y. S.; Katsuya, Y.; Tanaka, M.; Sobolev, A. V.; Presniakov, I. A. *J. Phys. Chem. C* **2016**, *120*, 8278-8288.]
(Down) The lower panel emphasizes the high 2θ region to illustrate that there is only one perovskite phase in $PbMn_7O_{12}$ (sample 2) (*cf.*, the appearance of two close perovskite phases was observed in Sánchez-Benítez, J.; Kayser, P.; Morales-García, A.; Martínez-Lope, M. J.; Mompeán, F. J.; Xu, J. M.; Jin, Z. M.; Alonso, J. A. Preparation, Crystal Structure, and Magnetotransport Properties of the New $CdCu_3Mn_4O_{12}$ Perovskite: A Comparison with Density Functional Theory Calculations. *J. Phys. Chem. C* **2014**, *118*, 9652−9658). Bragg reflections of impurities were omitted because impurities are not visible in this 2θ region.

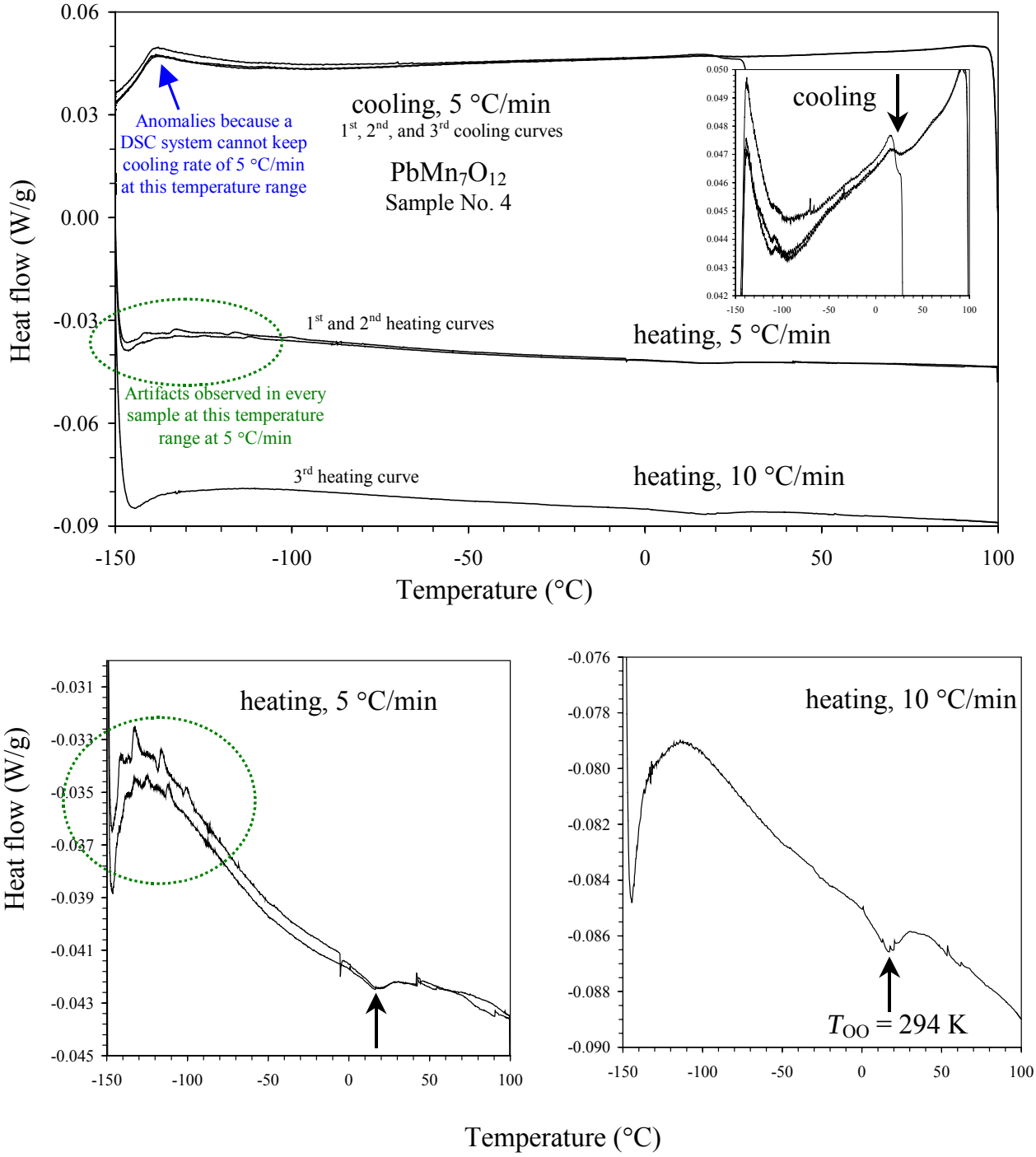

Figure S2. DSC data of $PbMn_7O_{12}$ (Sample 4). Differential scanning calorimetry (DSC) curves of $PbMn_7O_{12}$ at heating-cooling rate of 5-10 K/min. Measurements were performed between 123 and 373 K. Insets show details.

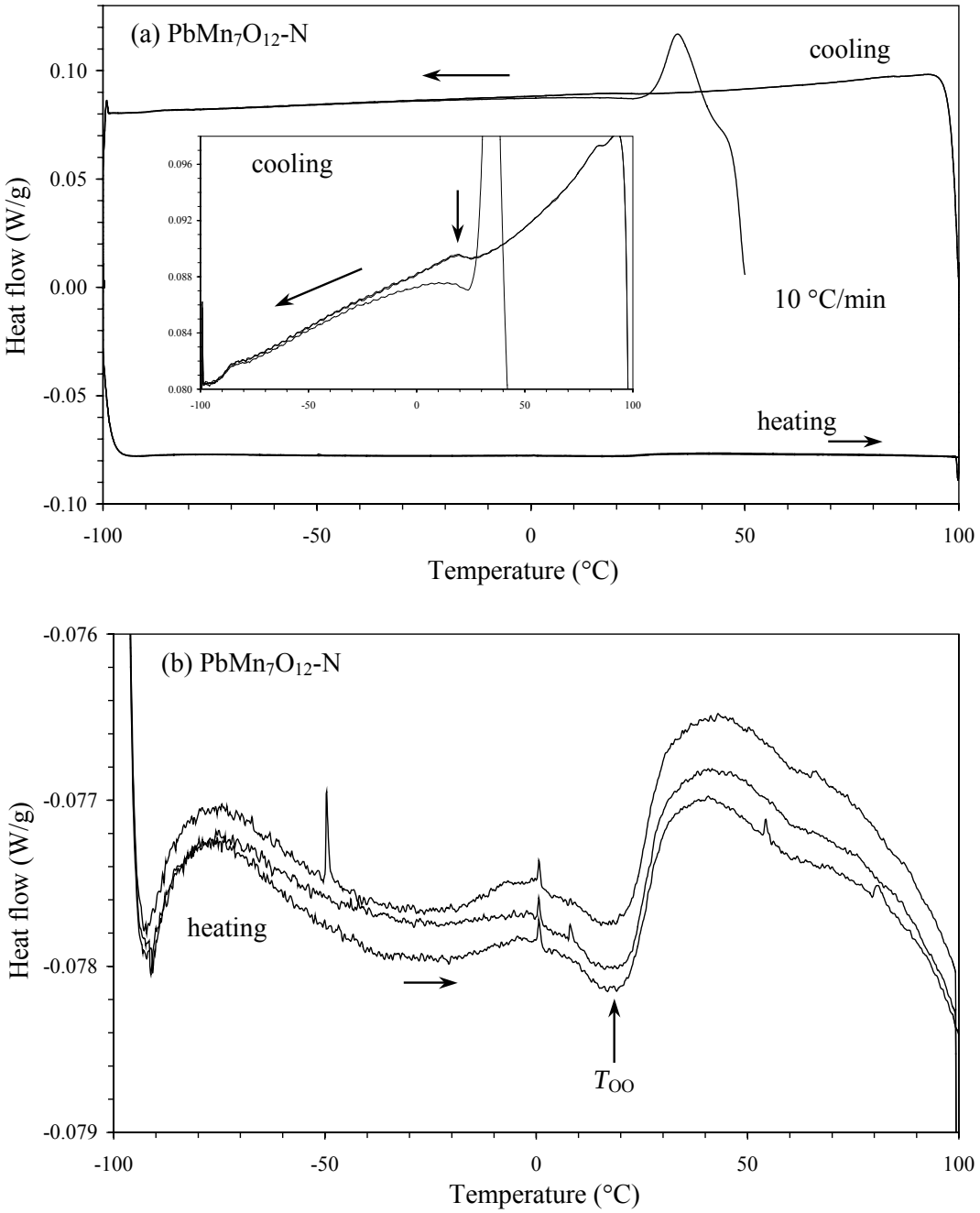

Figure S3. DSC data of $PbMn_7O_{12}$ (Sample N). Differential scanning calorimetry (DSC) curves of $PbMn_7O_{12}$ at heating-cooling rate of 10 K/min. Measurements were performed between 173 and 373 K. Insets show details.

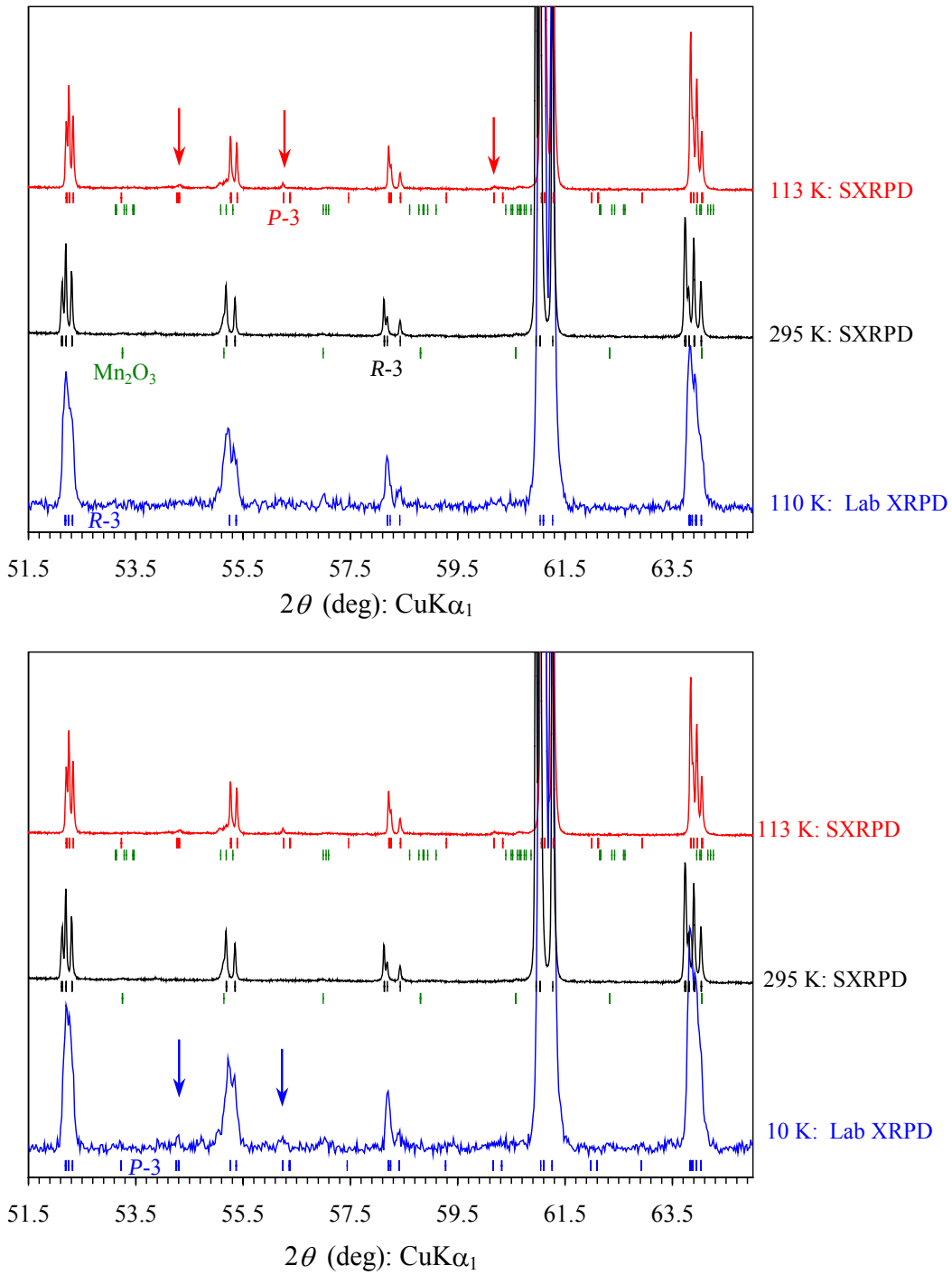

Figure S4a. X-ray powder diffraction (XRPD) data of $PbMn_7O_{12}$.
Synchrotron XRPD (SXRPD) patterns of $PbMn_7O_{12}$ at 113 K (red) and 295 K (black) [the 2θ data were recalculated to match the CuKα$_1$ radiation] [from Belik, A. A.; Glazkova, Y. S.; Katsuya, Y.; Tanaka, M.; Sobolev, A. V.; Presniakov, I. A. *J. Phys. Chem. C* **2016**, *120*, 8278-8288]. Laboratory XRPD patterns of $PbMn_7O_{12}$ at 110 K and 10 K (blue) measured with CuKα$_1$ radiation. The bars show possible Bragg reflection positions for $PbMn_7O_{12}$ and Mn_2O_3 impurity (green) [note that cubic Mn_2O_3 becomes orthorhombic at low temperatures: *Phys. Rev. B* **2013**, *87*, 184413]. Weak superstructure reflections observed on synchrotron XRPD patterns are marked by red arrows - they were clearly observed at 113 K; on the other hand, they cannot be detected on laboratory XRPD at 100 K. On laboratory XRPD patterns, those reflections can be probably seen at 10 K (blue arrows); see Figure S4b.

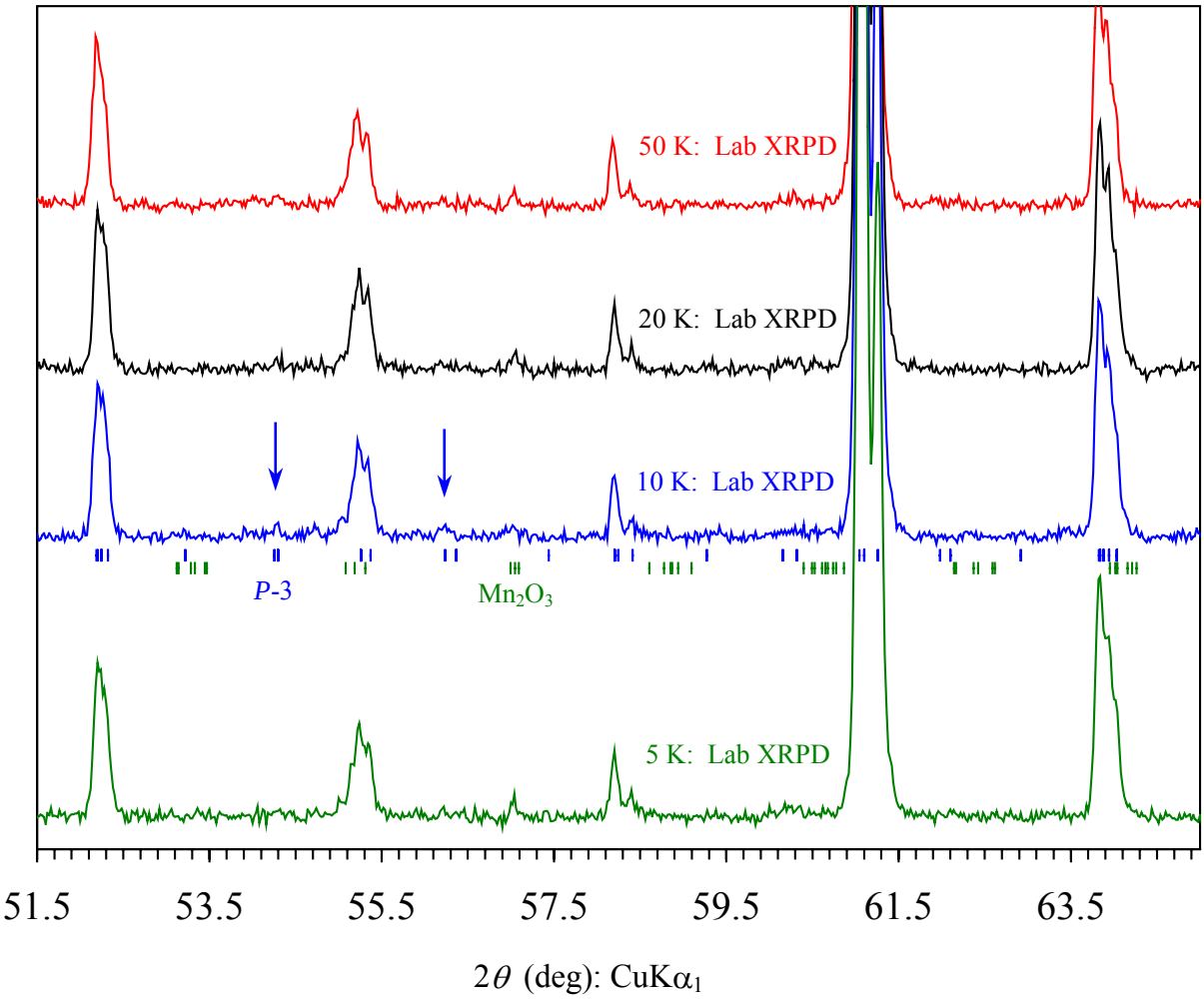

Figure S4b. X-ray powder diffraction (XRPD) data of $PbMn_7O_{12}$.
Laboratory XRPD patterns of $PbMn_7O_{12}$ (sample 3-2) at 50 K (red), 20 K (black), 10 K (blue), and 5 K (green) measured with $CuK\alpha_1$ radiation. The bars show possible Bragg reflection positions for $PbMn_7O_{12}$ (space group *P*-3) and Mn_2O_3 impurity (green) [note that cubic Mn_2O_3 becomes orthorhombic at low temperatures: *Phys. Rev. B* **2013**, *87*, 184413]. Superstructure reflections observed at 10 K (blue arrows) can hardly be visible at other temperatures. Therefore, their unambiguous assignment is impossible without results of synchrotron XRPD.

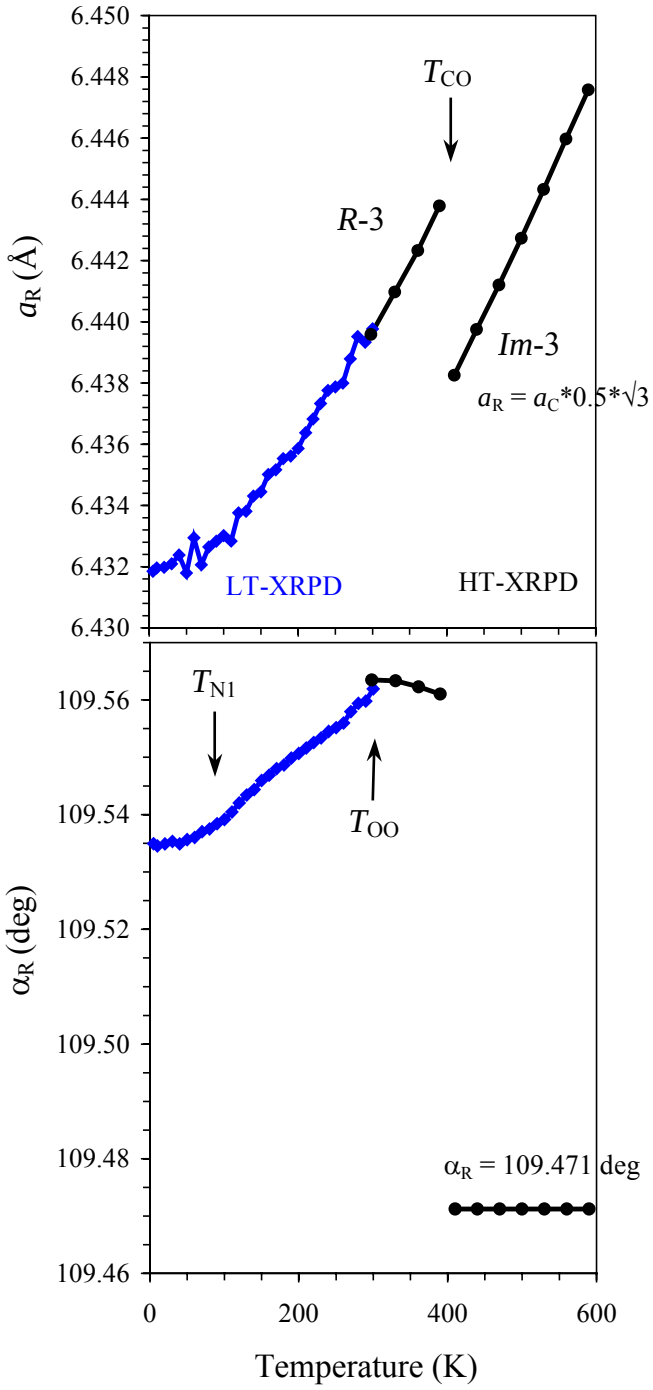

Figure S4c. Temperature dependence of the lattice parameters in $PbMn_7O_{12}$.
Temperature dependence of the lattice parameters (in rhombohedral axes) in $PbMn_7O_{12}$ (sample 3-2). For the cubic phase, $a_R = a_C*0.5*\sqrt{3}$ and α_R = 109.471 deg, where a_C is the lattice parameter of the *Im*-3 phase.

The lattice parameters in the rhombohedral axes are calculated as $a_R = a_H*\beta/3$ and $\alpha_R = 2\arcsin(3/(2\beta))$ with $\beta = (3+[c_H/a_H]^2)^{1/2}$, where a_H and c_H are the lattice parameters in the hexagonal axes of *R*-3 space group.

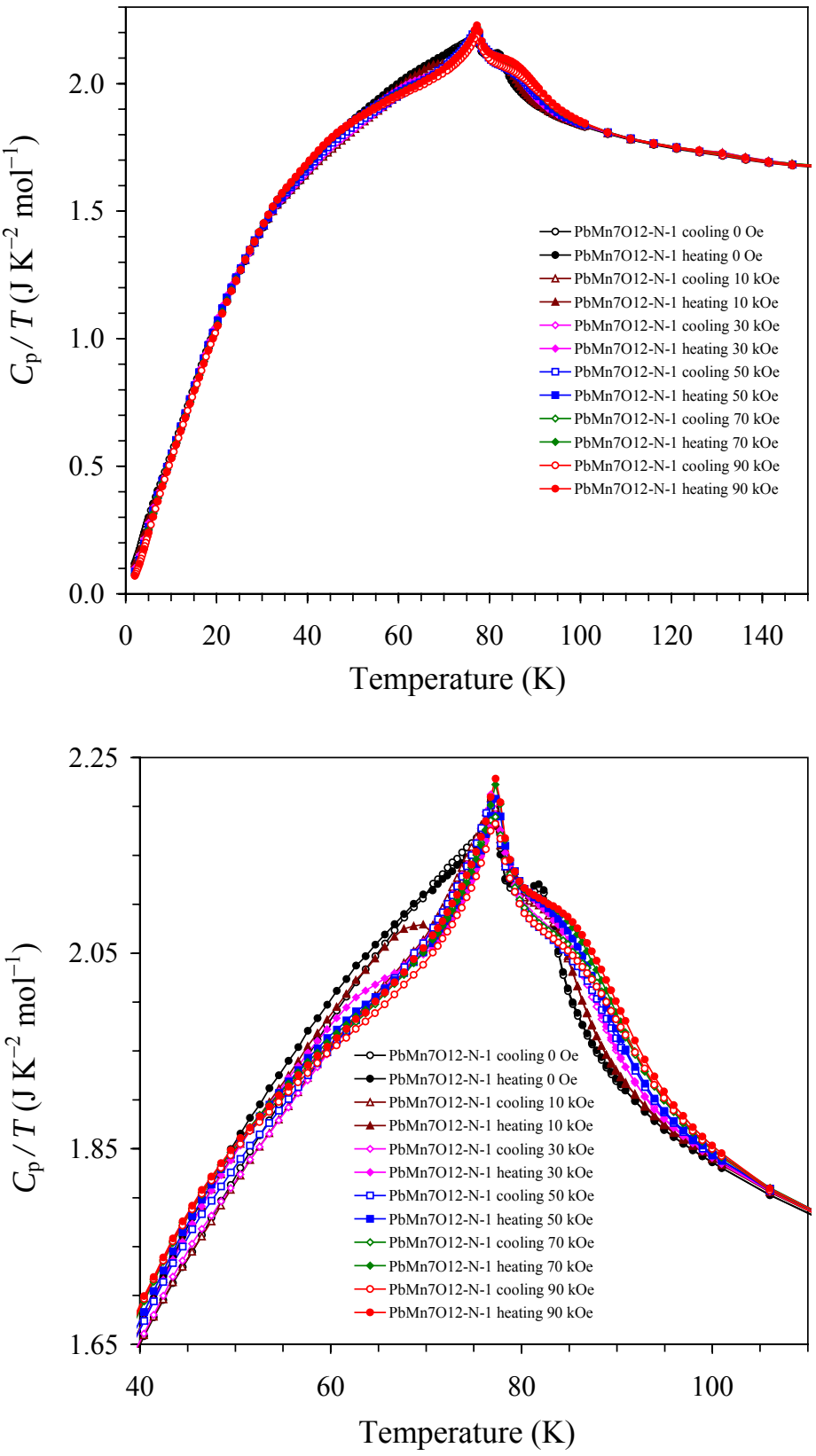

Figure S5. Specific heat of $PbMn_7O_{12}$ (Sample N). Specific heat data of $PbMn_7O_{12}$ (sample N) at different magnetic fields on cooling and heating (the measurements steps were changed during measurements).

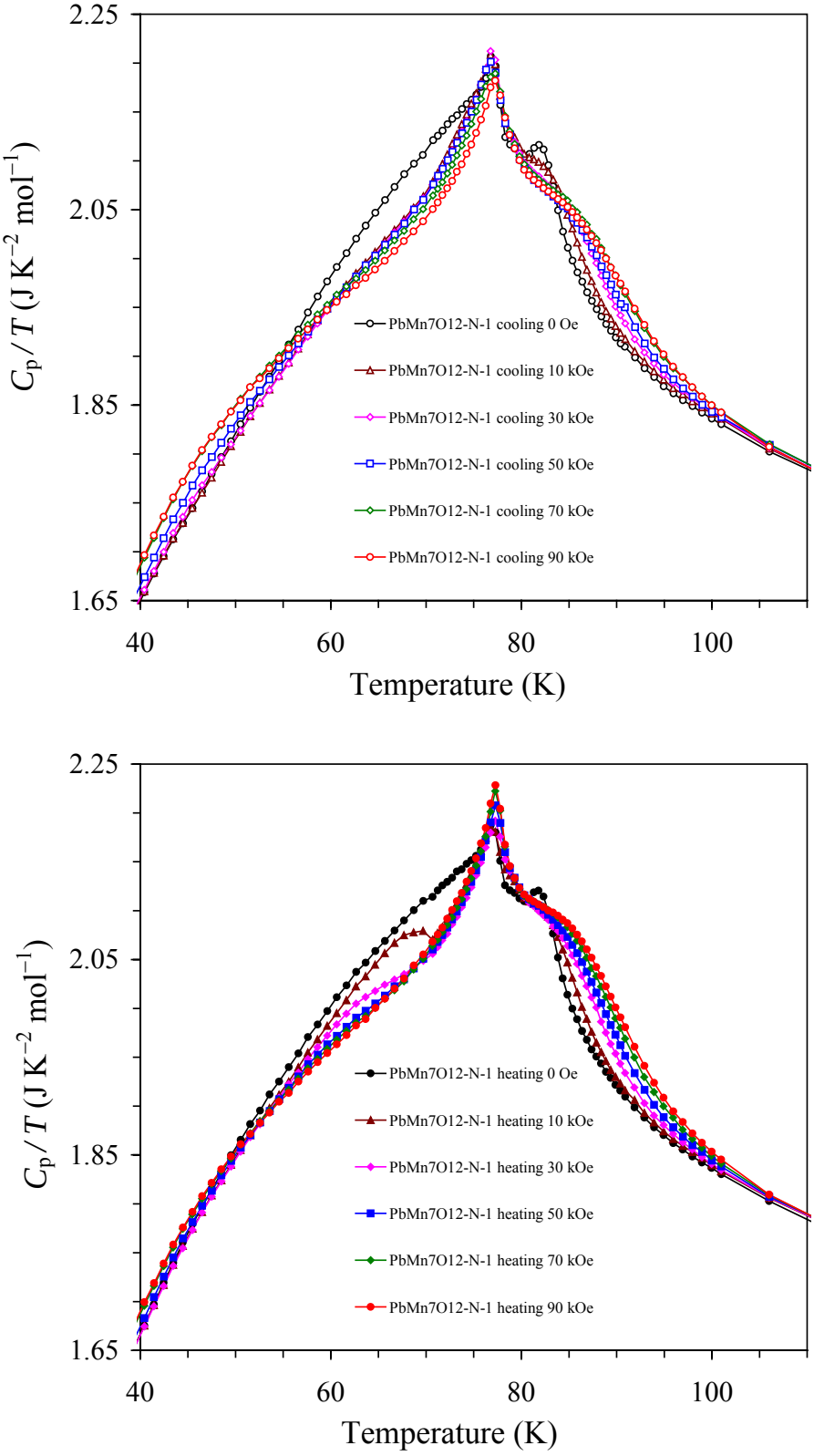

Figure S6. Specific heat of $PbMn_7O_{12}$ (Sample N). Specific heat data of $PbMn_7O_{12}$ (sample N) at different magnetic fields on cooling and heating (details).

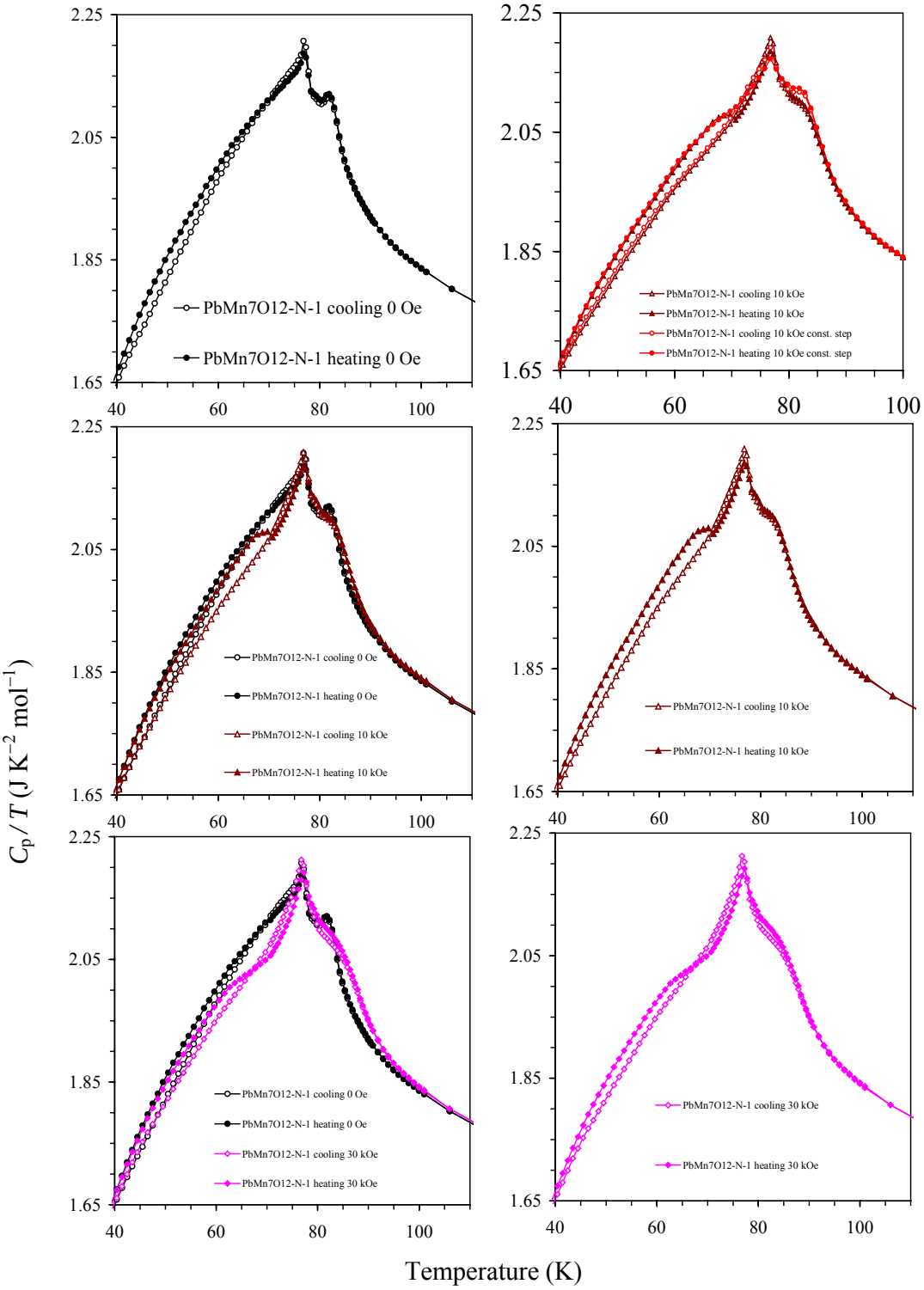

Figure S7. Specific heat of $PbMn_7O_{12}$ (Sample N). Specific heat data of $PbMn_7O_{12}$ (sample N) at different magnetic fields on cooling and heating (details). The measurement step was changed at 70 K (and at 90 K). A Multiview software of PPMS determines a measurement heat pulse again when a measurement step is changed. During this process, a large heat pulse is applied to a sample, and a magnetic state could be destroyed. This fact could be a reason of a sharper artifact at 10 kOe on heating at 70 K; the anomaly was smooth when a constant measurement step was used (the upper right panel).

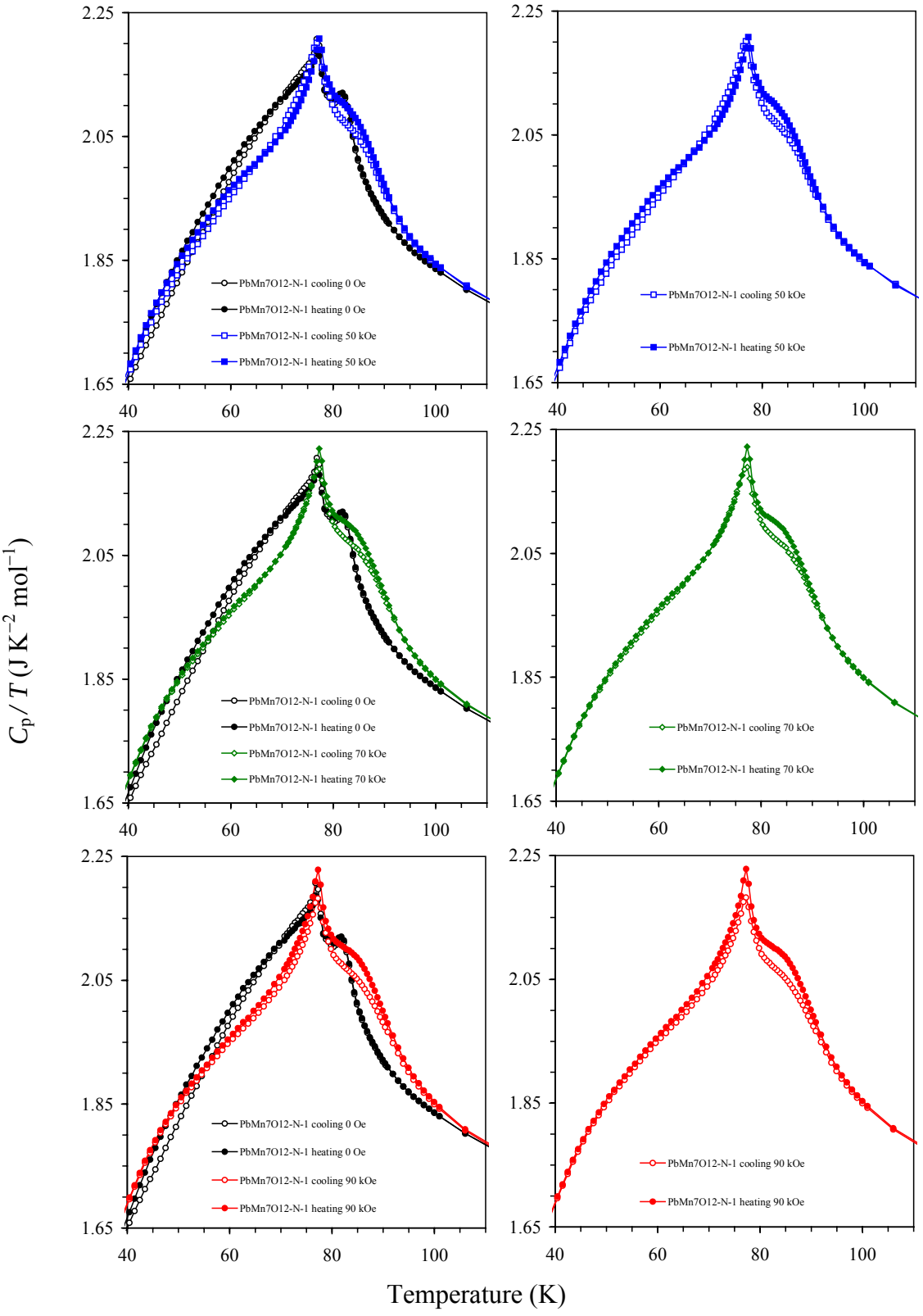

Figure S8. Specific heat of $PbMn_7O_{12}$ (Sample N). Specific heat data of $PbMn_7O_{12}$ (sample N) at different magnetic fields on cooling and heating (details).

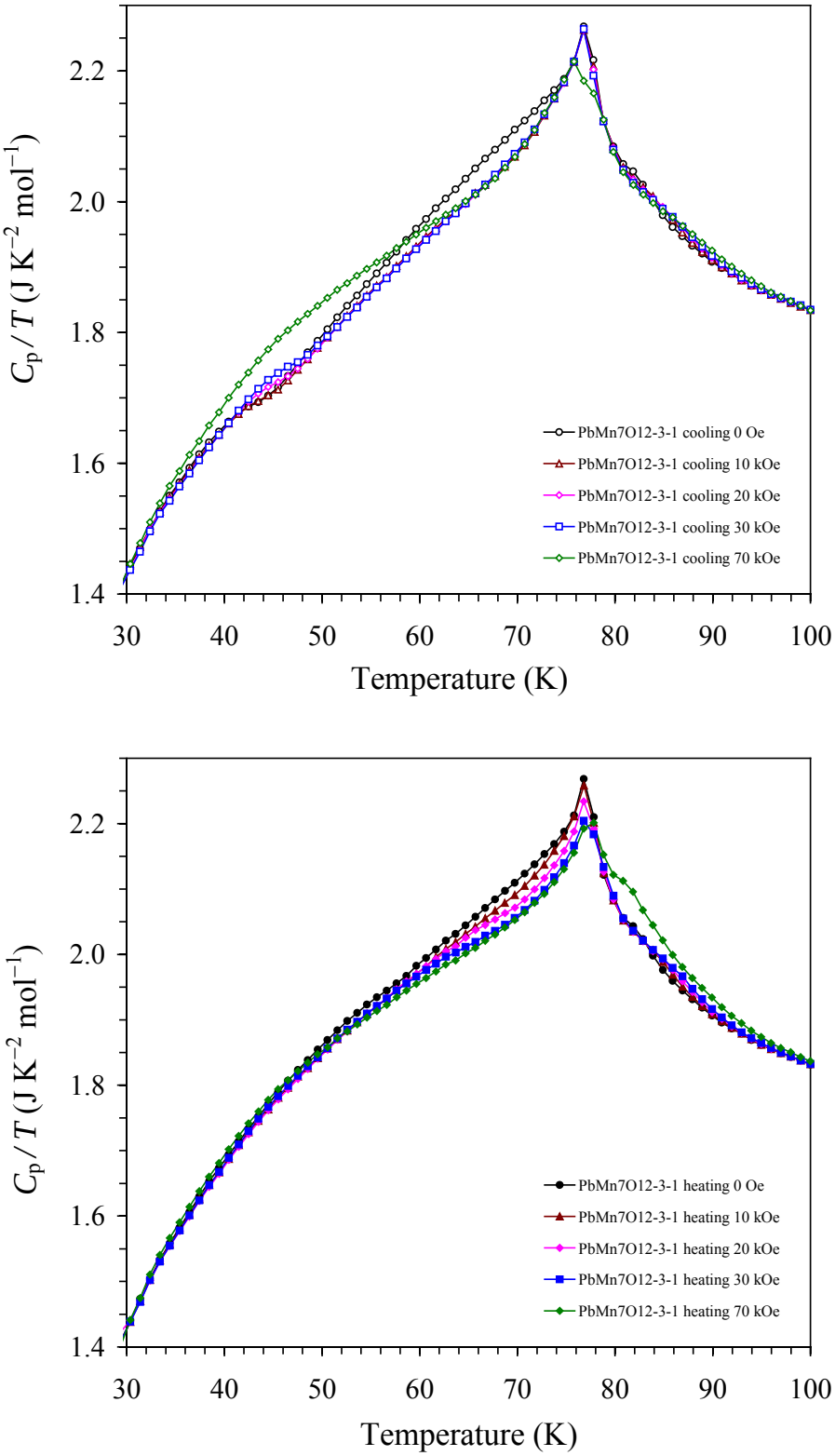

Figure S9a. Specific heat of $PbMn_7O_{12}$ (Sample 3-1). Specific heat data of $PbMn_7O_{12}$ (sample 3-1) at different magnetic fields on cooling and heating at a constant step of 1 K.

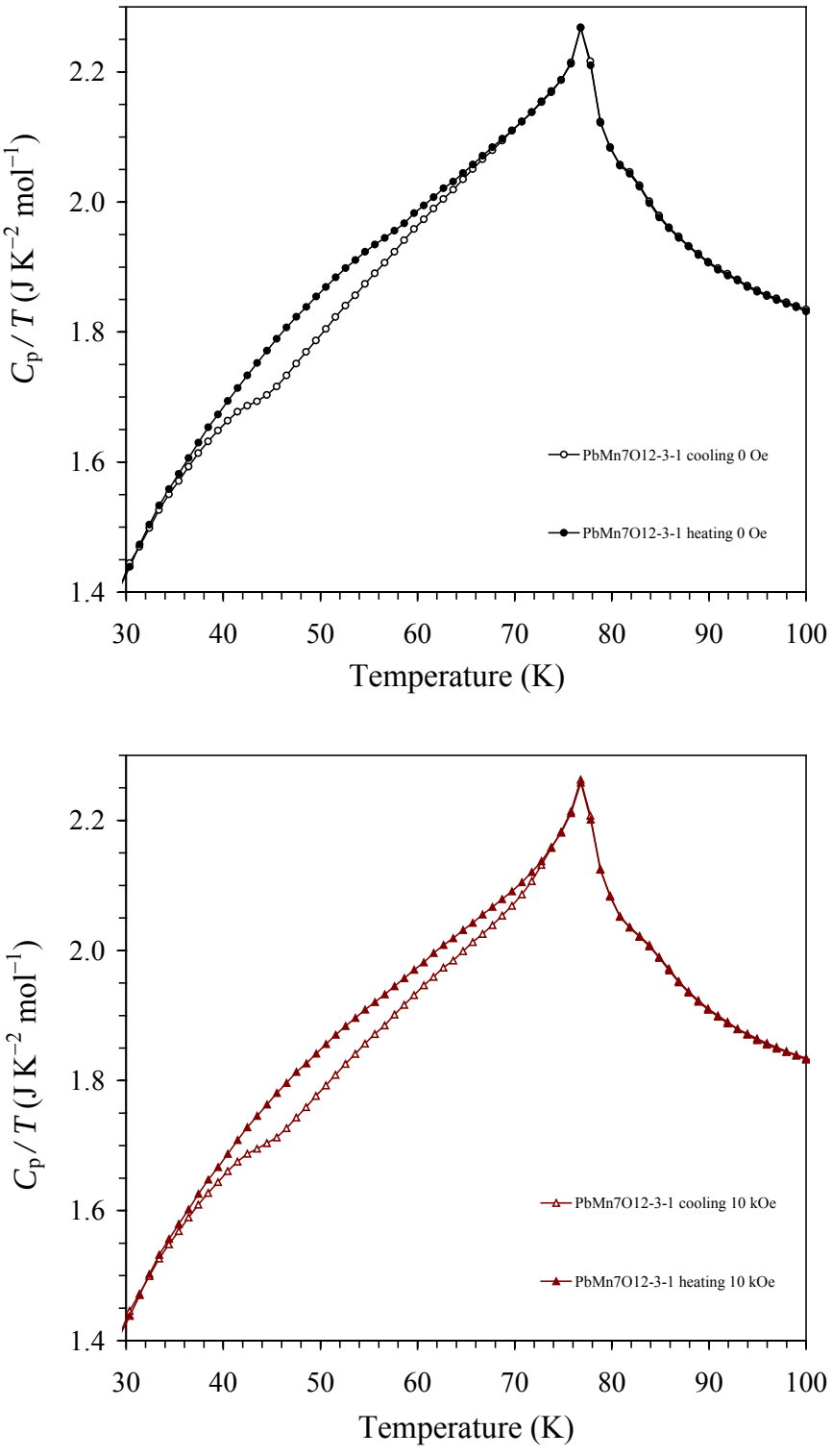

Figure S9b. Specific heat of $PbMn_7O_{12}$ (Sample 3-1). Specific heat data of $PbMn_7O_{12}$ (sample 3-1) at different magnetic fields on cooling and heating at a constant step of 1 K (details).

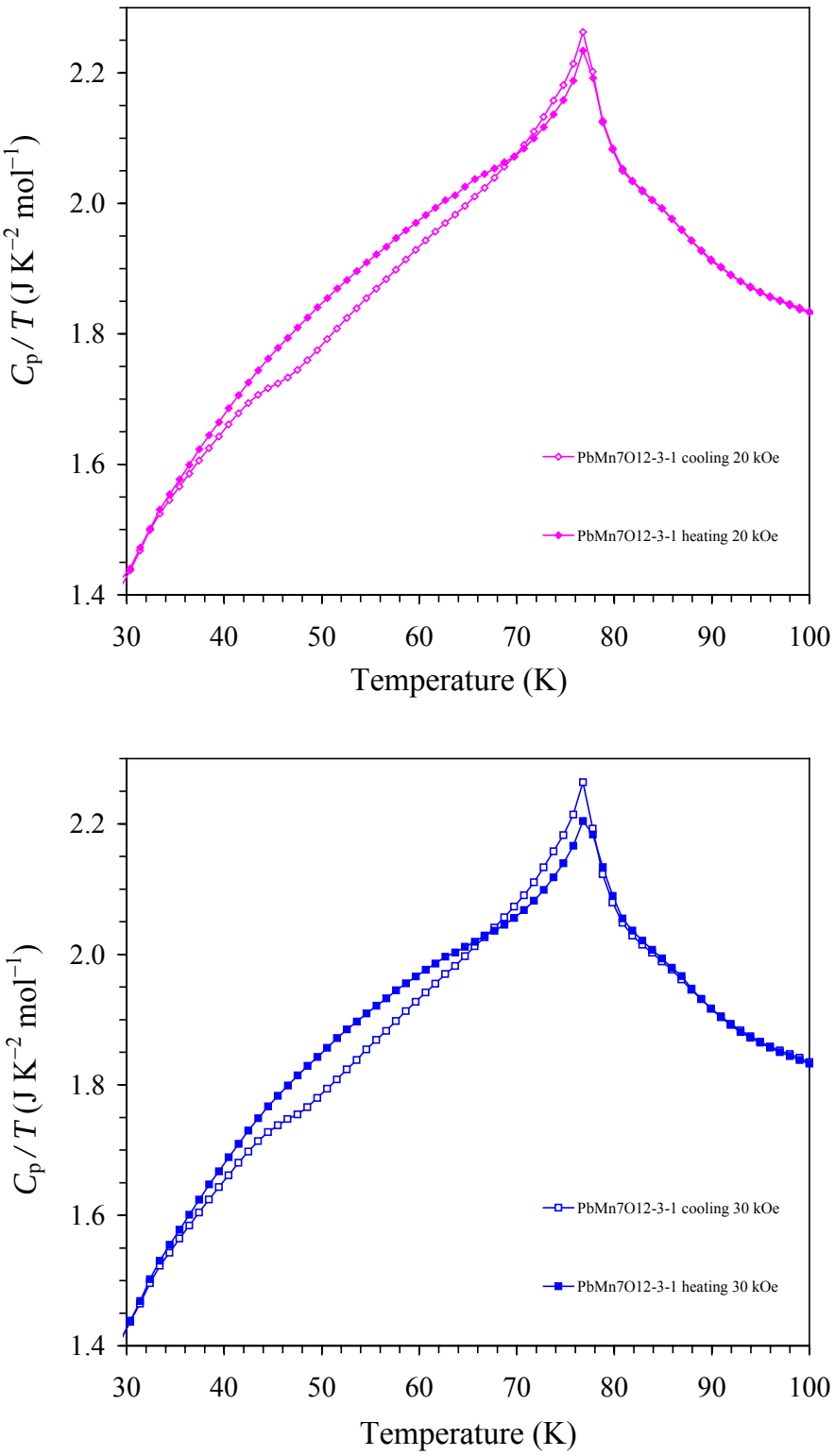

Figure S10a. Specific heat of $PbMn_7O_{12}$ (Sample 3-1). Specific heat data of $PbMn_7O_{12}$ (sample 3-1) at different magnetic fields on cooling and heating at a constant step of 1 K (details).

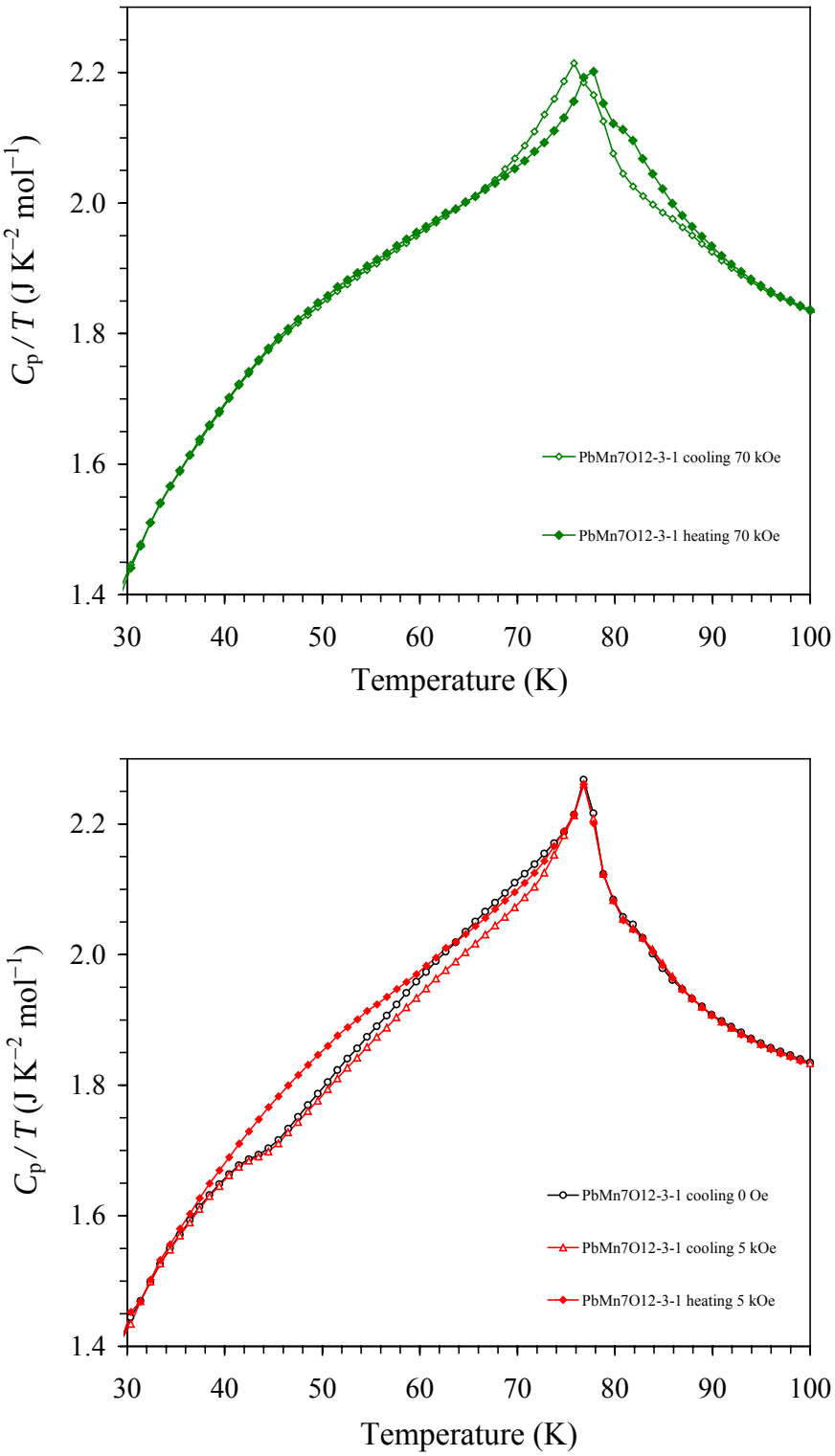

Figure S10b. Specific heat of $PbMn_7O_{12}$ (Sample 3-1). Specific heat data of $PbMn_7O_{12}$ (sample 3-1) at different magnetic fields on cooling and heating at a constant step of 1 K (details).

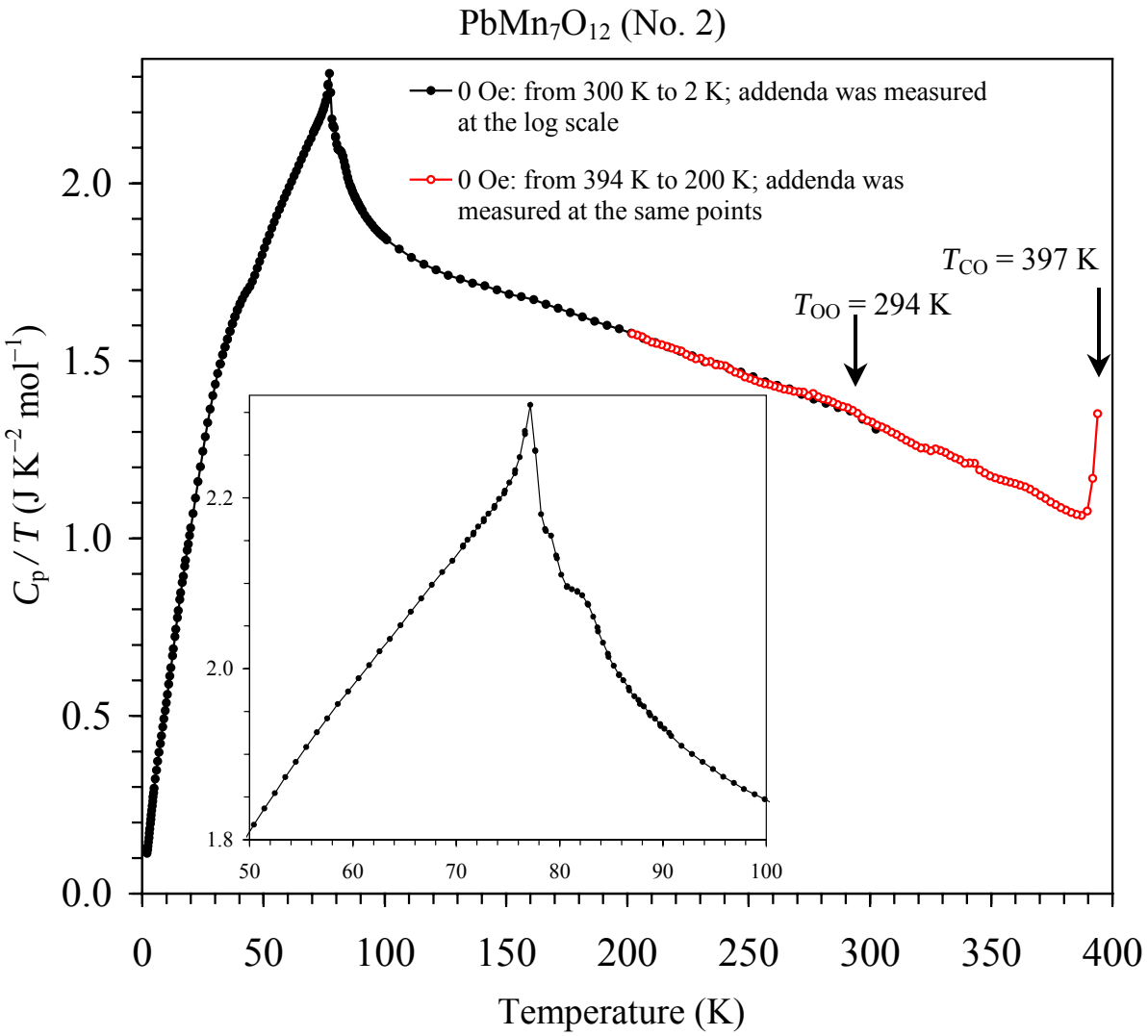

Figure S11. Specific heat of $PbMn_7O_{12}$ (Sample 2). Measurements were performed on cooling at 0 Oe. Specific heat could not detect anomalies near T_{OO} in agreement with a very small anomaly on the DSC curves. For measurements from 394 to 200 K, addenda was measured at the same temperature points as for the sample measurement (with a step of 2 K); Apiezon grease F was used to fix the sample.

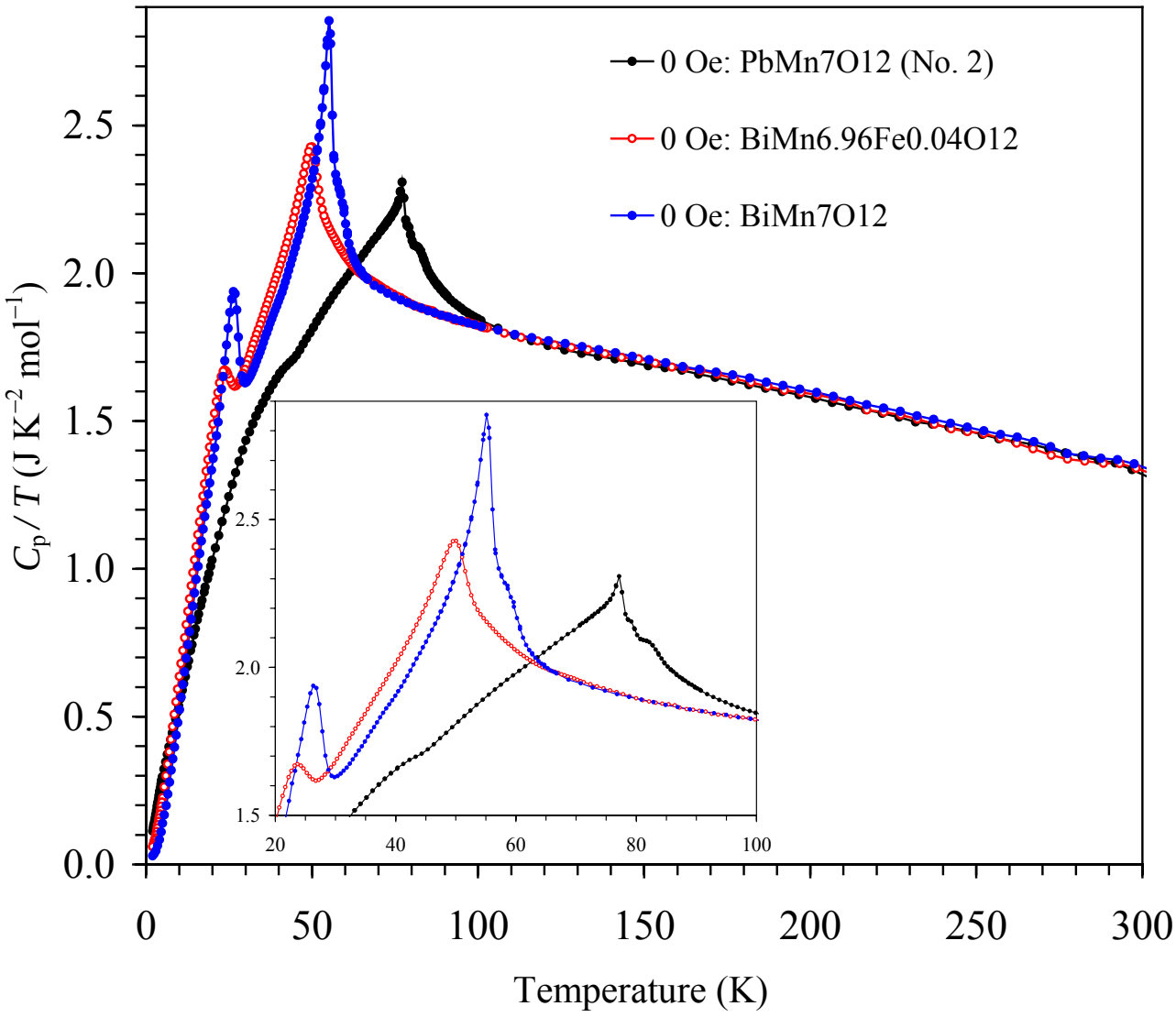

Figure S12a. Specific heat of $PbMn_7O_{12}$ (Sample 2). Specific heat of $PbMn_7O_{12}$ at 0 Oe in comparison with that of $BiMn_{6.96}{}^{57}Fe_{0.04}O_{12}$ (at 0 Oe) and $BiMn_7O_{12}$ (at 0 Oe) plotted as *C*p/*T* vs *T*. All measurements were performed on cooling. This figure illustrates that specific heat values are almost identical for these three compounds between about 100 K and 300 K in agreement with their close molecular weights.

Note that there is a clear shoulder at 59 K in single-phase $BiMn_7O_{12}$, slightly above T_{N1} = 55 K. This feature was also observed in [Imamura, N.; Karppinen, M.; Motohashi, T.; Fu, D.; Itoh, M.; Yamauchi, H. *J. Am. Chem. Soc.* **2008**, *130*, 14948-14949]. This fact suggests a more complex behavior of $BiMn_7O_{12}$.

A shoulder was also observed in $PbMn_7O_{12}$ (sample 2) at 79.3 K, slightly above T_{N2} = 77 K (see Figure S12b for details). It probably originates from Mn_2O_3 impurity.

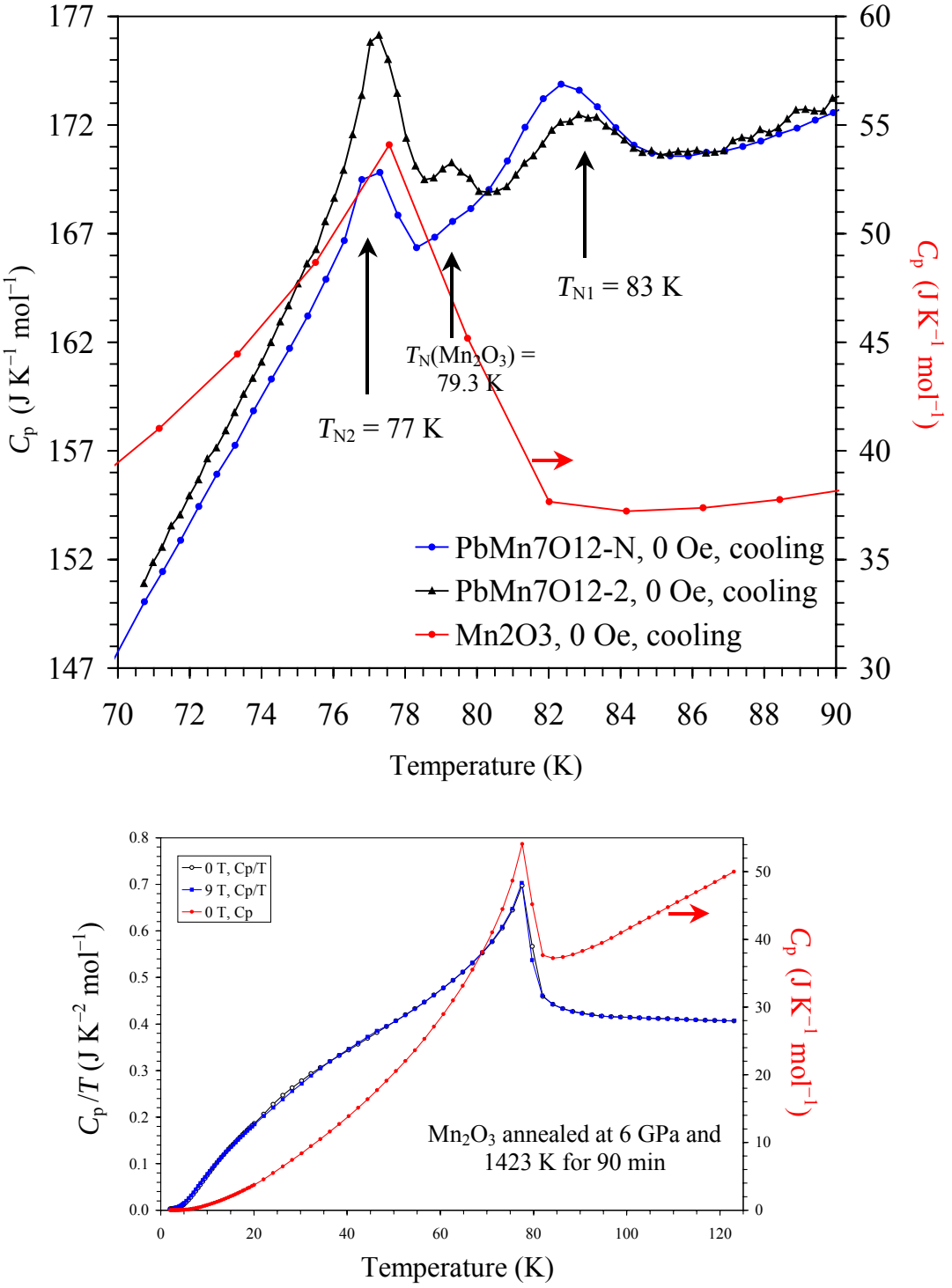

Figure S12b. Specific heat of $PbMn_7O_{12}$. (Up) Specific heat of two $PbMn_7O_{12}$ samples (2 and N) at 0 Oe plotted as *C*p vs *T*. All measurements were performed on cooling. A measurement step for sample 2 was 0.25 K to catch tiny details (addenda was measured with a step of 0.5 K between 70 and 90 K for this measurement; this measurement is different from the one on Figure S12a). An additional peak (in *C*p vs *T*) or a shoulder (in *C*p/*T* vs *T*) can be seen at 79.3 K in sample 2.

(Down) Specific heat of Mn_2O_3 annealed at 6 GPa and 1423 K for 90 min. The data are plotted as *C*p/*T* vs *T* (at 0 and 90 kOe) and *C*p vs *T* (at 0 Oe).

Note that synchrotron X-ray powder diffraction data were measured for sample 2 in [Belik, A. A.; Glazkova, Y. S.; Katsuya, Y.; Tanaka, M.; Sobolev, A. V.; Presniakov, I. A. *J. Phys. Chem. C* **2016**, *120*, 8278-8288] in a wide temperature range, and only one perovskite phase was detected. In other words, two close perovskite phases cannot explain the appearance of the additional peak.

On the other hand, Mn_2O_3 impurity has T_N of about 80 K. Therefore, the additional peak could originate from Mn_2O_3 impurity. $PbMn_7O_{12}$ (sample 2) has a larger amount of Mn_2O_3 impurity in comparison with $PbMn_7O_{12}$ (sample N); as a result, its specific heat anomaly could be seen. Very small difference in the peak position in pure Mn_2O_3 and Mn_2O_3 impurity in $PbMn_7O_{12}$ (sample 2) could be explain by the sample-dependent variation of T_N.

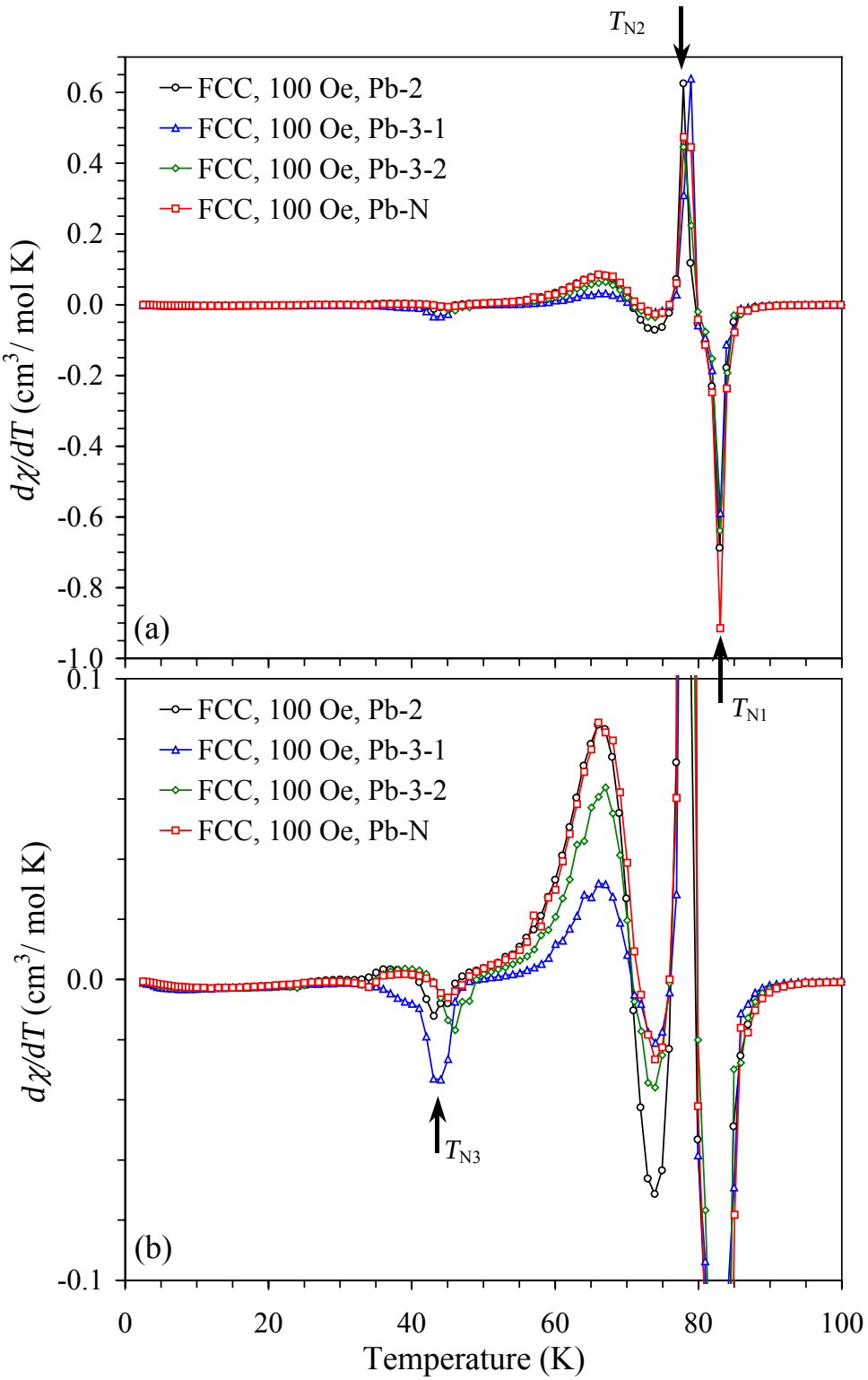

Figure S13. Magnetic Properties of $PbMn_7O_{12}$. FCC $d\chi/dT$ vs T curves at 100 Oe for different $PbMn_7O_{12}$ samples. Arrows show the Néel temperatures. (Up) full curves, (down) details.

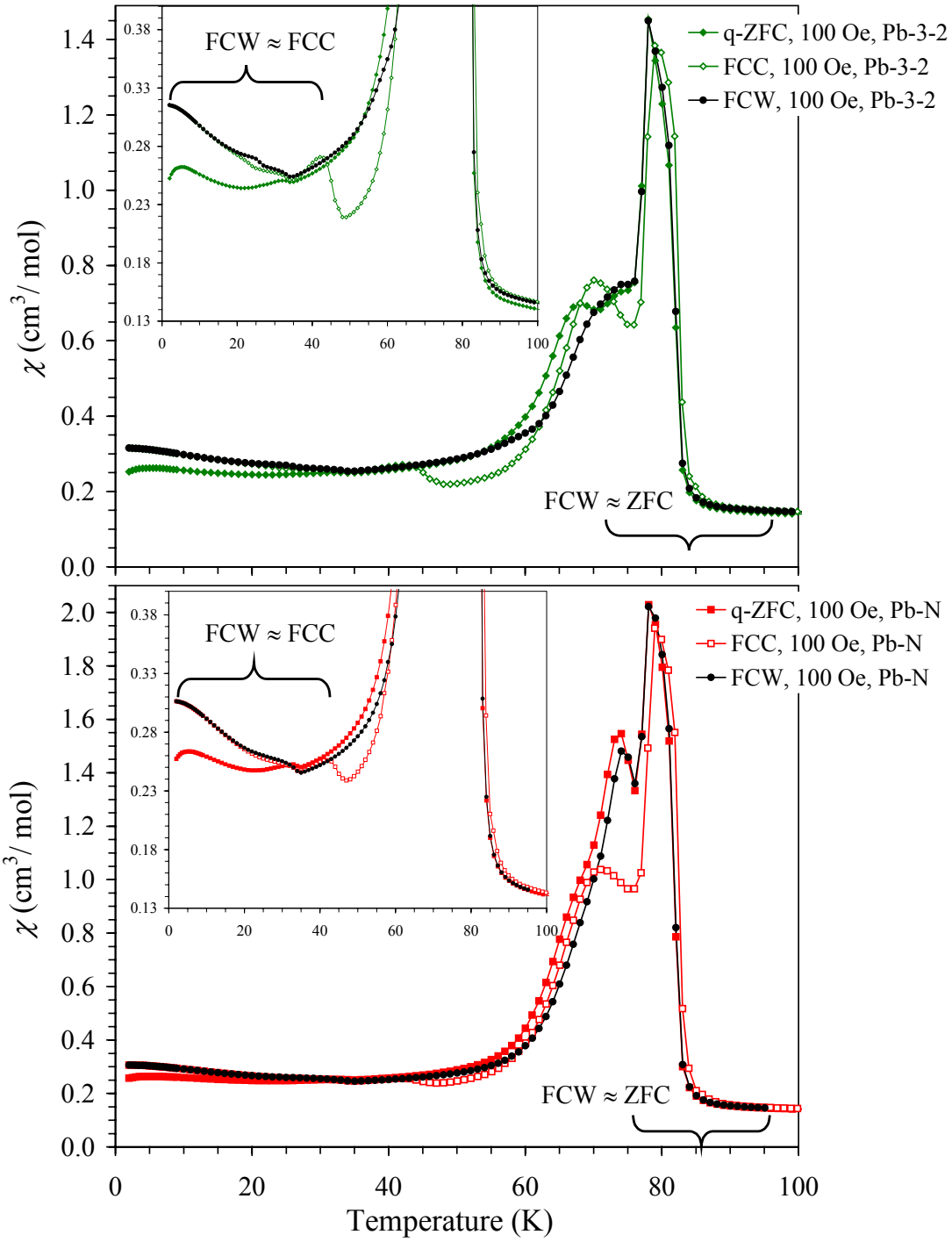

Figure S14. Magnetic Properties of $PbMn_7O_{12}$. ZFC, FCC, and FCW dc magnetic susceptibility curves of $PbMn_7O_{12}$ at 100 Oe. (Up) sample 3-2, (down) sample N. Temperature ranges where the FCC and FCW curves and the ZFC and FCW curves almost coincide with each other are marked.

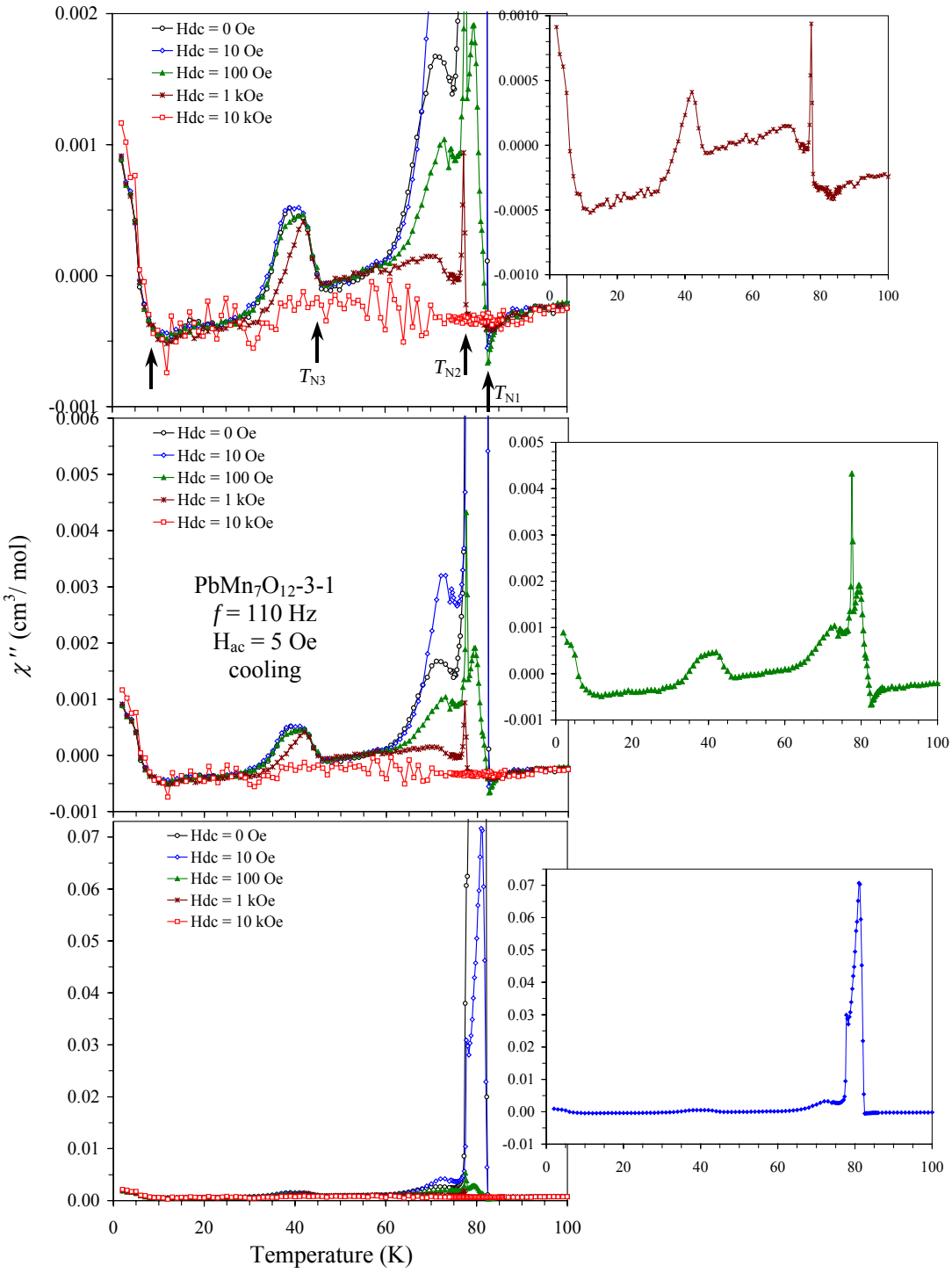

Figure S15. Magnetic Properties of $PbMn_7O_{12}$. Different details of imaginary parts of the ac susceptibility (χ'' vs T) for $PbMn_7O_{12}$ (sample 3-1) in different static magnetic fields (H_{dc}). Measurements were performed on cooling from 150 K to 2 K using an ac field with the amplitude H_{ac} = 5 Oe and frequency f = 110 Hz. Arrows show the Néel temperatures and additional anomalies below about 10 K, which match with frequency-dependent dielectric anomalies (Figures S23-S30); the additional anomalies are independent of H_{dc}.

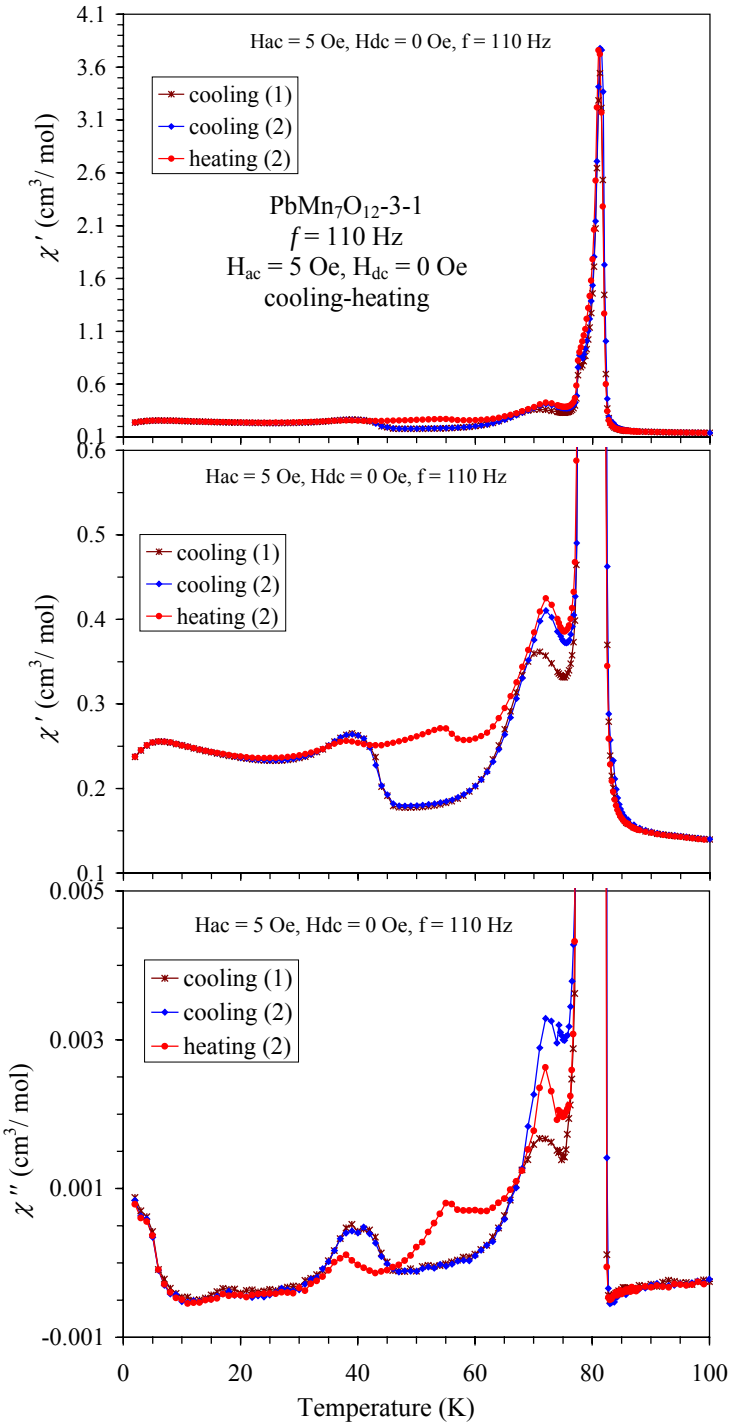

Figure S16. Magnetic Properties of $PbMn_7O_{12}$. Real parts (χ' vs T) and imaginary parts (χ'' vs T) of the ac susceptibility of $PbMn_7O_{12}$ (sample 3-1). Measurements were performed at a zero static magnetic field (H_{dc} = 0 Oe) on cooling (two times) and heating (one time) using an ac field with the amplitude H_{ac} = 5 Oe and frequency f = 110 Hz. [Cooling (2) and heating (2) were performed in the same run].

These data emphasize the hysteresis between cooling and heating curves. Please note that there is some difference near 70 K on two cooling curves (the same sample, sample holder, MPMS, and measurement protocol were used); this fact shows that the anomalies near 70 K are highly sensitive to the environment (for example, trapped fields inside a magnetometer).

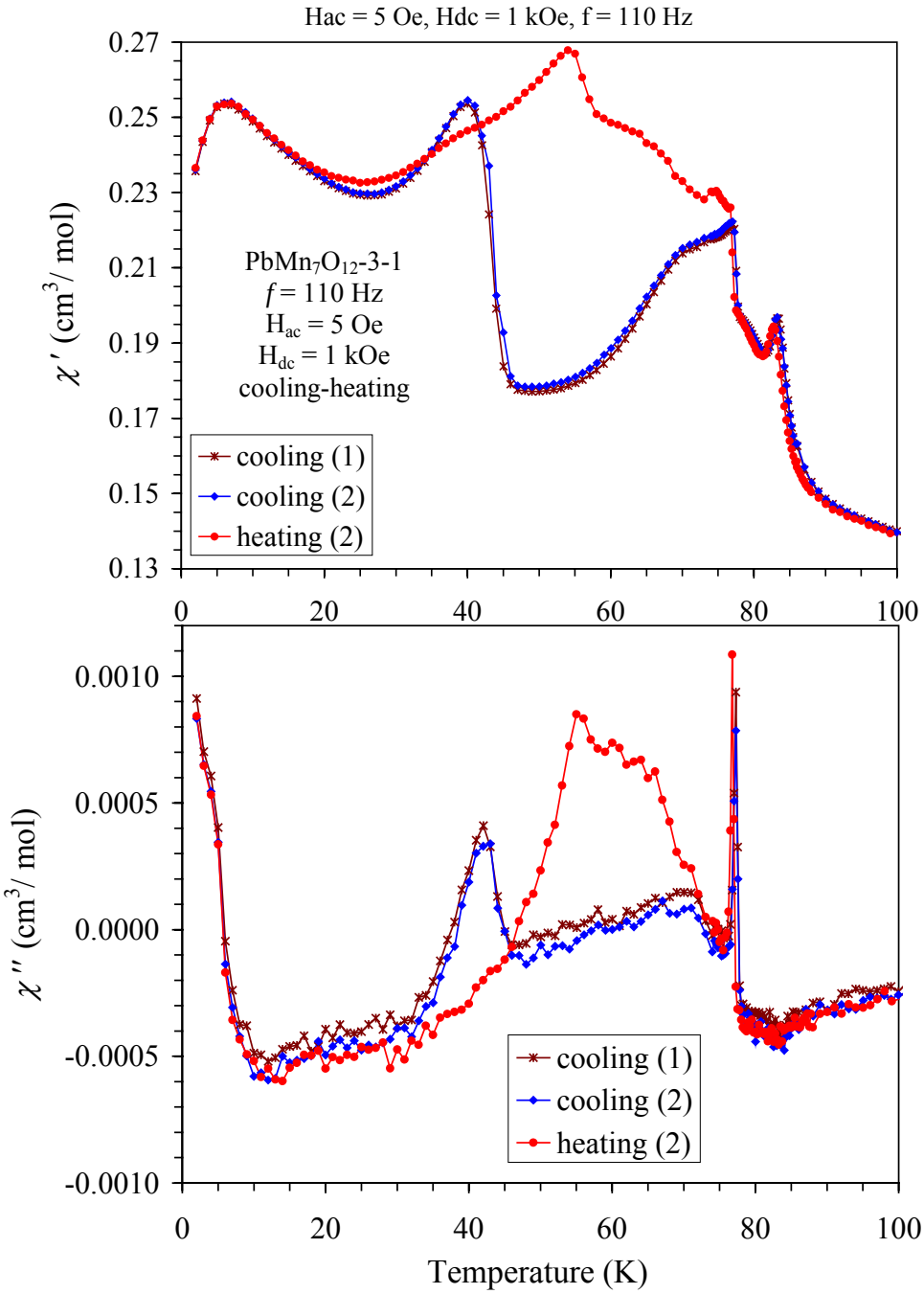

Figure S17. Magnetic Properties of $PbMn_7O_{12}$. Real parts (χ' vs T) and imaginary parts (χ'' vs T) of the ac susceptibility of $PbMn_7O_{12}$ (sample 3-1). Measurements were performed at H_{dc} = 1 kOe on cooling (two times) and heating (one time) using an ac field with the amplitude H_{ac} = 5 Oe and frequency f = 110 Hz. [Cooling (2) and heating (2) were performed in the same run]. In this case (H_{dc} = 1 kOe), two cooling curves coincide in the whole temperature range.

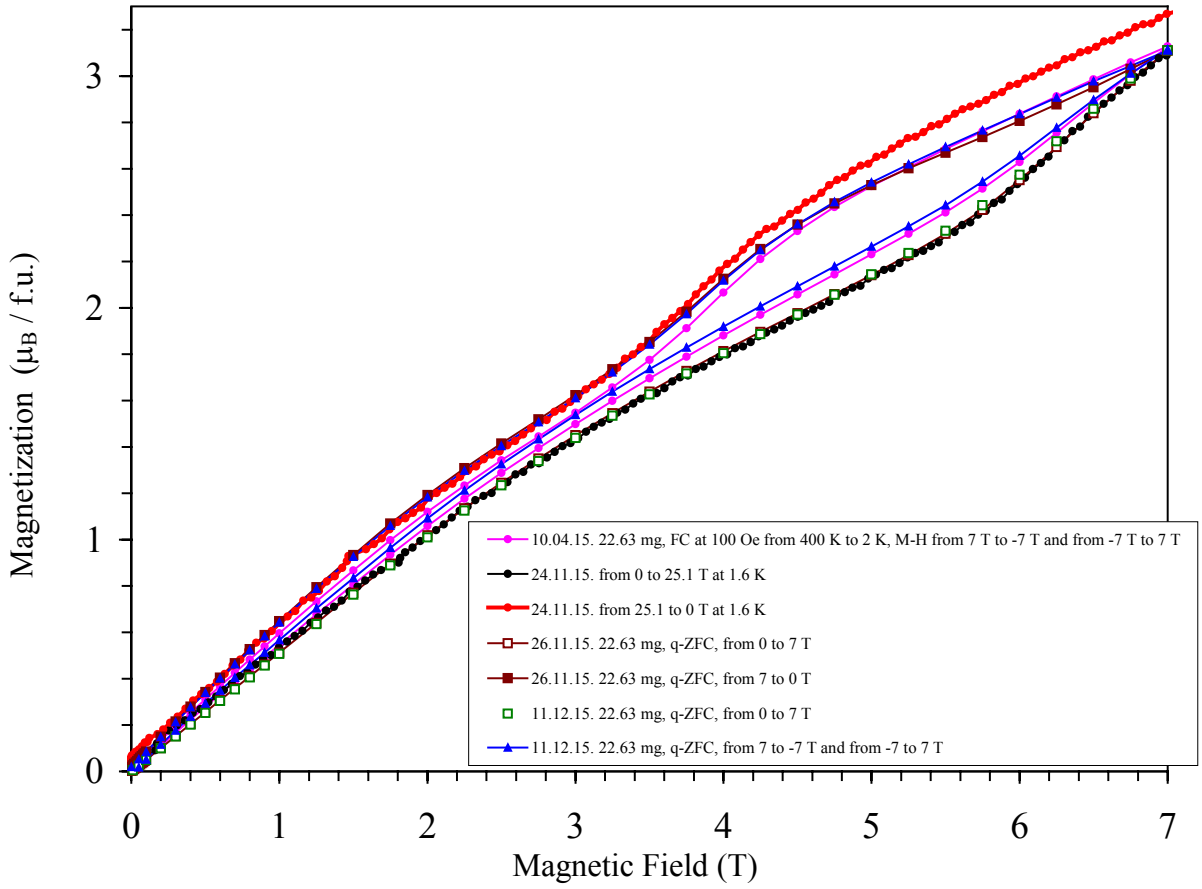

Figure S18a. Magnetic Properties of $PbMn_7O_{12}$.

M vs H curves of $PbMn_7O_{12}$ (sample 2; a pellet of 22.63 mg) measured with the NIMS hybrid magnet at 1.6 K (on 24.11.15. - dd.mm.yy.) and MPMS-7T at 2 K on different dates. The sample was arbitrary rotated for and after the measurement using the NIMS hybrid magnet. q-ZFC means that the sample was rapidly inserted (quenched) into a MPMS-7T kept at 10 K and having a nominal zero magnetic field. All three initial isothermal magnetization curves (two from 0 to 7 T and one from 0 to 25.1 T) are almost identical.

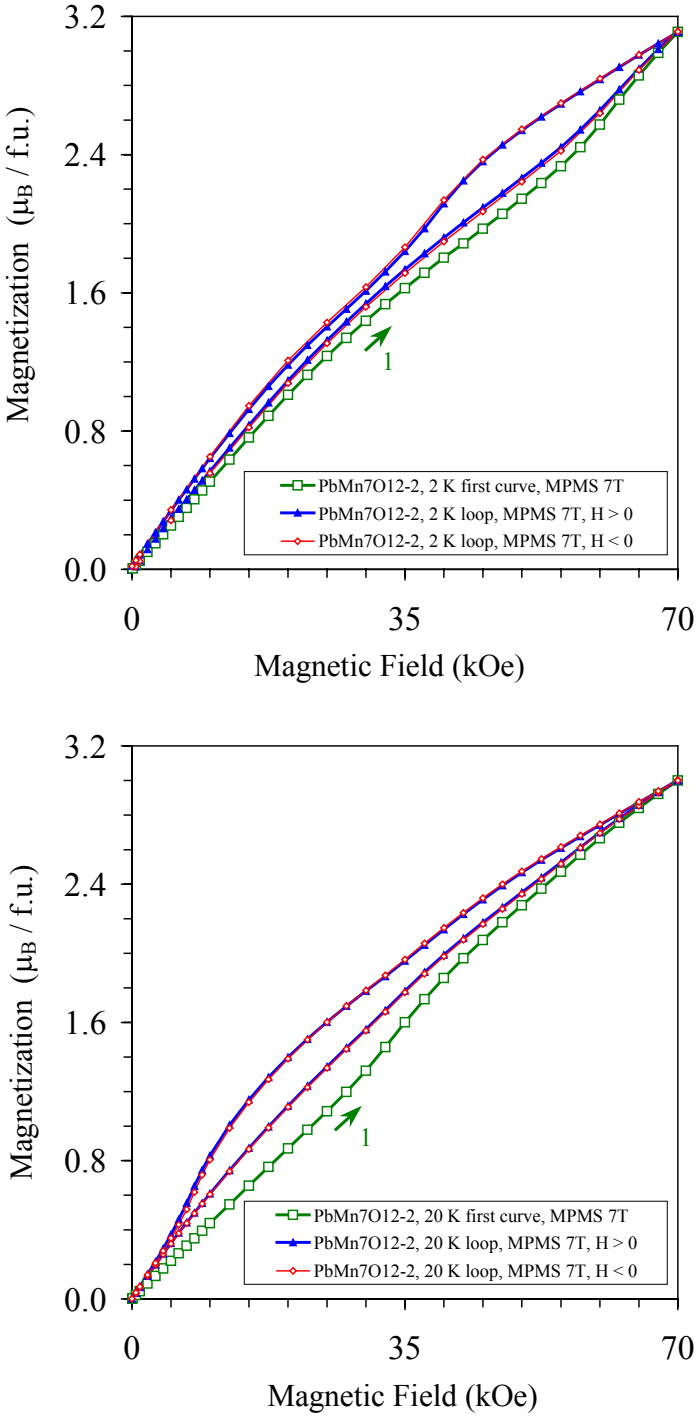

Figure S18b. Magnetic Properties of $PbMn_7O_{12}$.
M vs H curves of $PbMn_7O_{12}$ (sample 2; a pellet of 22.63 mg) measured with MPMS-7T at 2 K and 20 K plotted as M vs H for H ≥ 0 (blue triangles) and −M vs −H for H ≤ 0 (red diamonds); this plot is used to illustrate that the M vs H curves are symmetrical for H ≥ 0 and H ≤ 0. Three branches were measured: (1) from 0 to 70 kOe (green squares), from 70 kOe to −70 kOe, and from −70 kOe to 70 kOe.
[At 2 K: the sample was rapidly inserted into a magnetomer kept at 10 K and having an unspecified trapped field; then temperature was set to 2 K, and three branches were measured on an MPMS-7T: (1) from 0 to 70 kOe (green squares), (2) from 70 kOe to −70 kOe, and (3) from −70 kOe to 70 kOe (blue and red symbols).
At 20 K: the $PbMn_7O_{12}$ sample was inserted into a magnetometer kept at 110 K (above T_{N1}) and having a positive trapped field (confirmed by a superconducting Nb sample), cooled down from 110 K to 20 K, and three branches were measured on an MPMS-7T: (1) from 0 to 70 kOe (green squares), (2) from 70 kOe to −70 kOe, and (3) from −70 kOe to 70 kOe (blue and red symbols).]

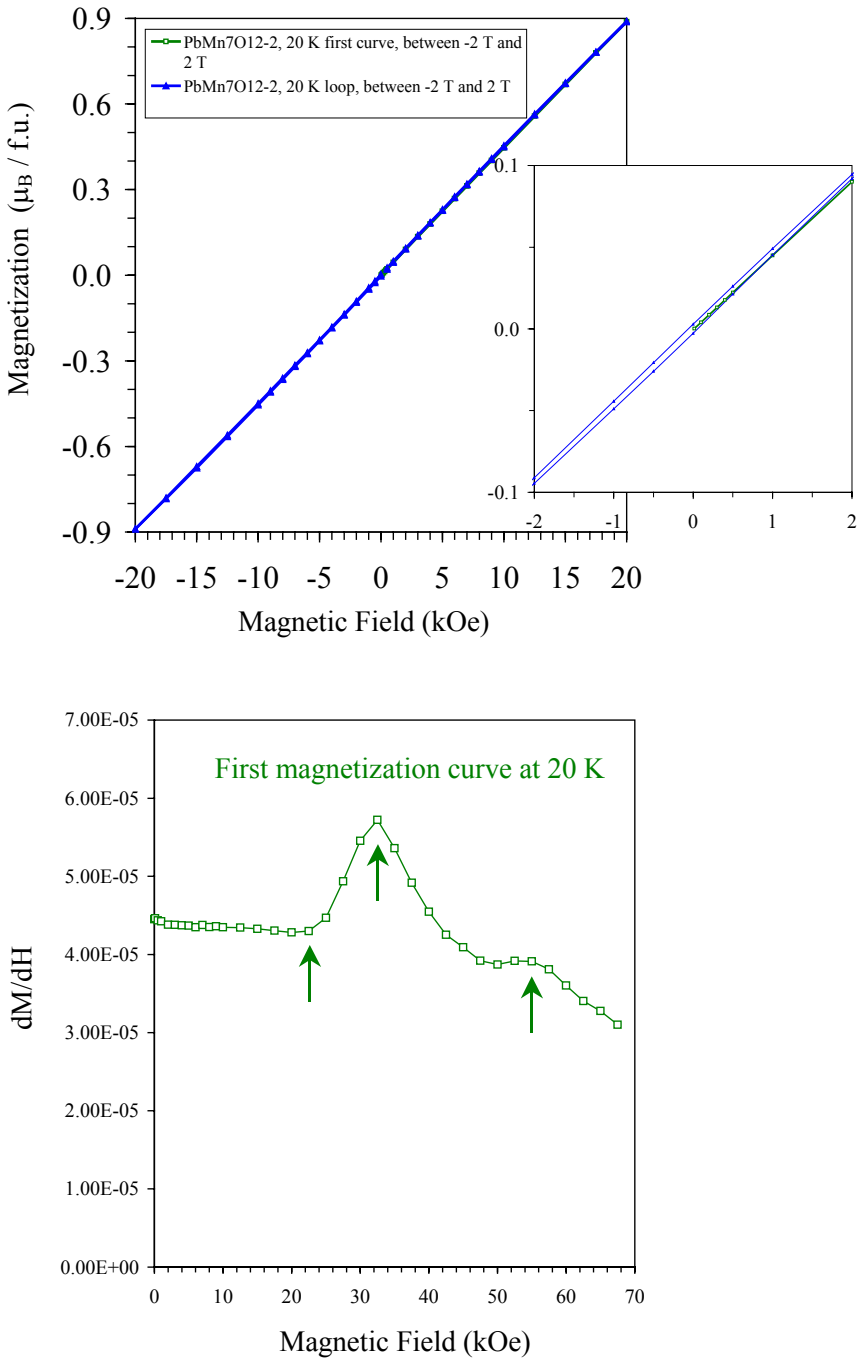

Figure S18c. Magnetic Properties of $PbMn_7O_{12}$.
M vs H curves of $PbMn_7O_{12}$ (sample 2; a pellet of 22.63 mg) measured with MPMS-7T. At 20 K, a field-induced transition is observed starting from 22.5 kOe with a maximum at about 32.5 kOe on the dM/dH vs H curve (down); and an additional kink is observed at 55.0 kOe.

Therefore, we checked an M vs H curve between –20 kOe and 20 kOe (up). [The $PbMn_7O_{12}$ sample was inserted into a magnetometer kept at 110 K (above T_{N1}) and having a positive trapped field (confirmed by a superconducting Nb sample), cooled down from 110 K to 20 K, and three branches were measured on an MPMS-7T: (1) from 0 to 20 kOe (green squares), (2) from 20 kOe to –20 kOe, and (3) from –20 kOe to 20 kOe (blue triangles).]
The M vs H curves were linear between –20 kOe to 20 kOe with a tiny hysteresis (the inset) confirming an antiferromagnetic ground state.

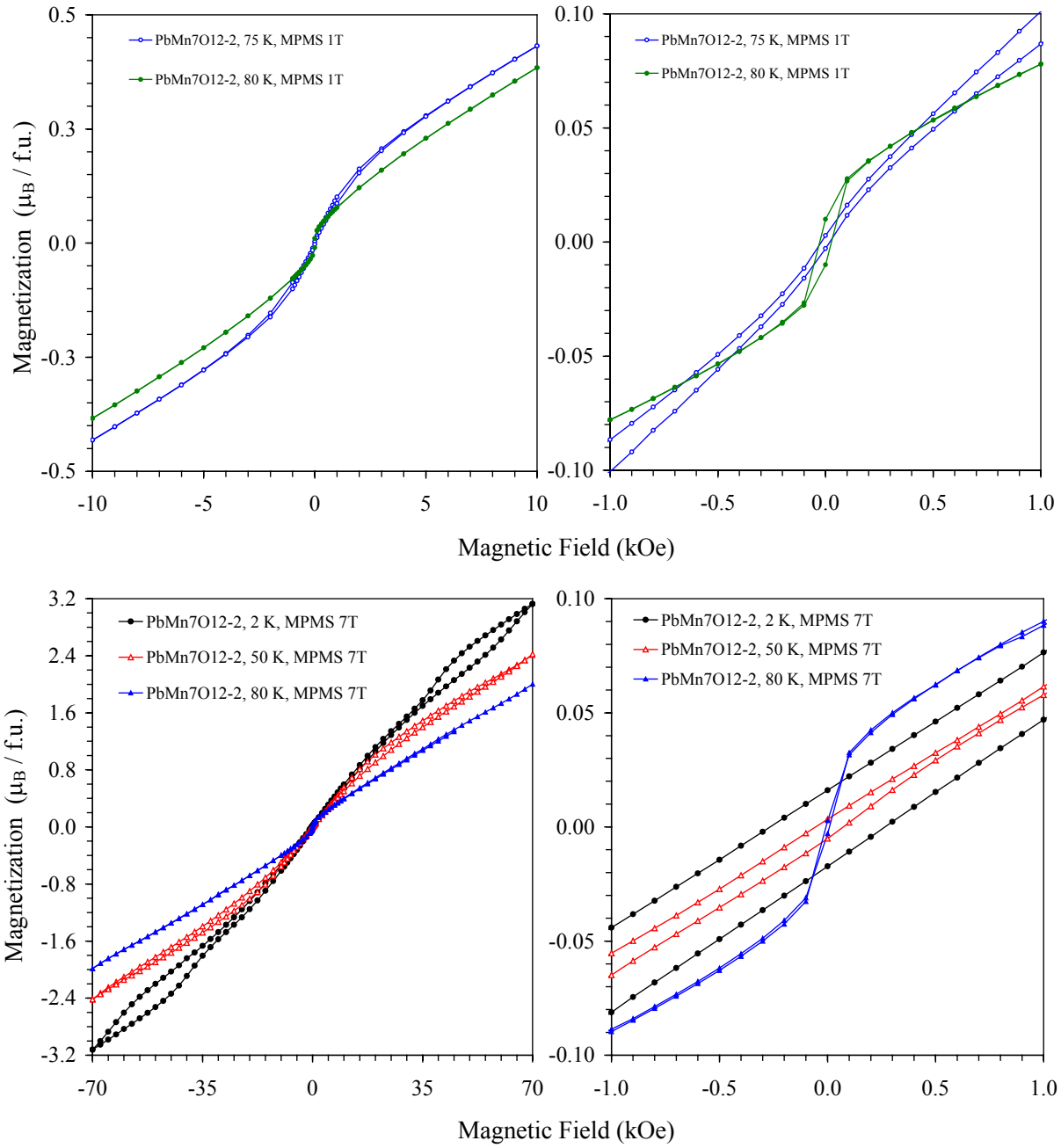

Figure S19. Magnetic Properties of $PbMn_7O_{12}$.

(Up) Full and detailed M vs H curves of $PbMn_7O_{12}$ (sample 2) at 75 and 80 K measured with an MPMS-1T.
(Down) Full and detailed M vs H curves of $PbMn_7O_{12}$ (sample 2) at 2, 50, and 80 K measured with an MPMS-XL(7T).

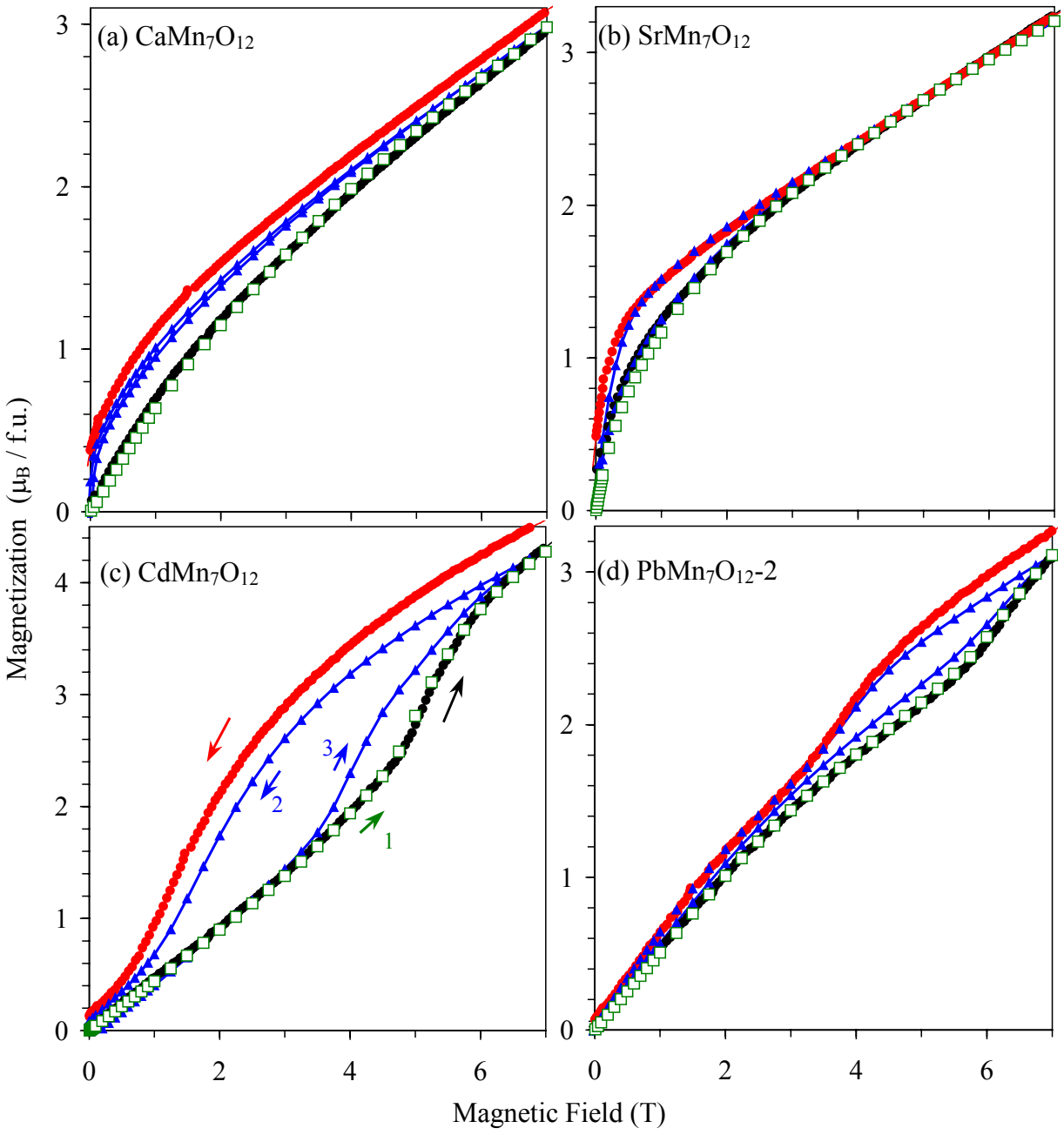

Figure S20a. Magnetic Properties of $PbMn_7O_{12}$.

High-field M vs H curves at 1.6 K together with M-H curves measured on an MPMS-7T at 2 K for (a) $CaMn_7O_{12}$ (sample 3-4 prepared at ambient pressure), (b) $SrMn_7O_{12}$ (sample 4-1), (c) $CdMn_7O_{12}$ (sample N), and (d) $PbMn_7O_{12}$ (sample 2). Three branches were measured on the MPMS-7T: (1) from 0 to 70 kOe (green squares), (2) from 70 kOe to −70 kOe, and (3) from −70 kOe to 70 kOe (blue triangles).

High-field M vs H measurements were performed at 1.6 K from 0 Oe to 251 kOe (black curves) and from 251 kOe to 0 Oe (red curves) on the NIMS hybrid magnet.

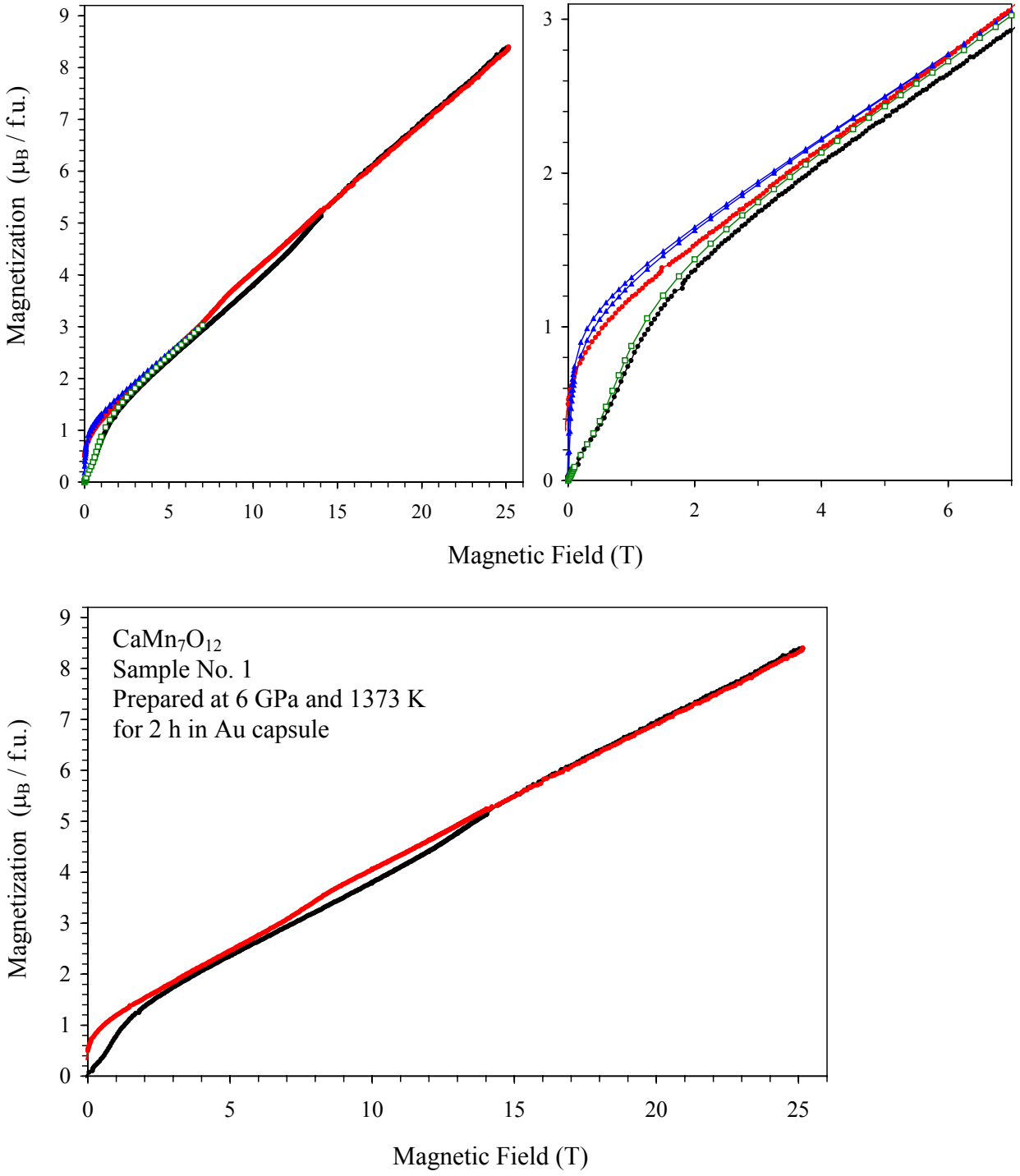

Figure S20b. Magnetic Properties of $CaMn_7O_{12}$.

High-field M vs H curves at 1.6 K together with M-H curves measured on an MPMS-7T at 2 K for $CaMn_7O_{12}$ (sample 1 prepared at high pressure).

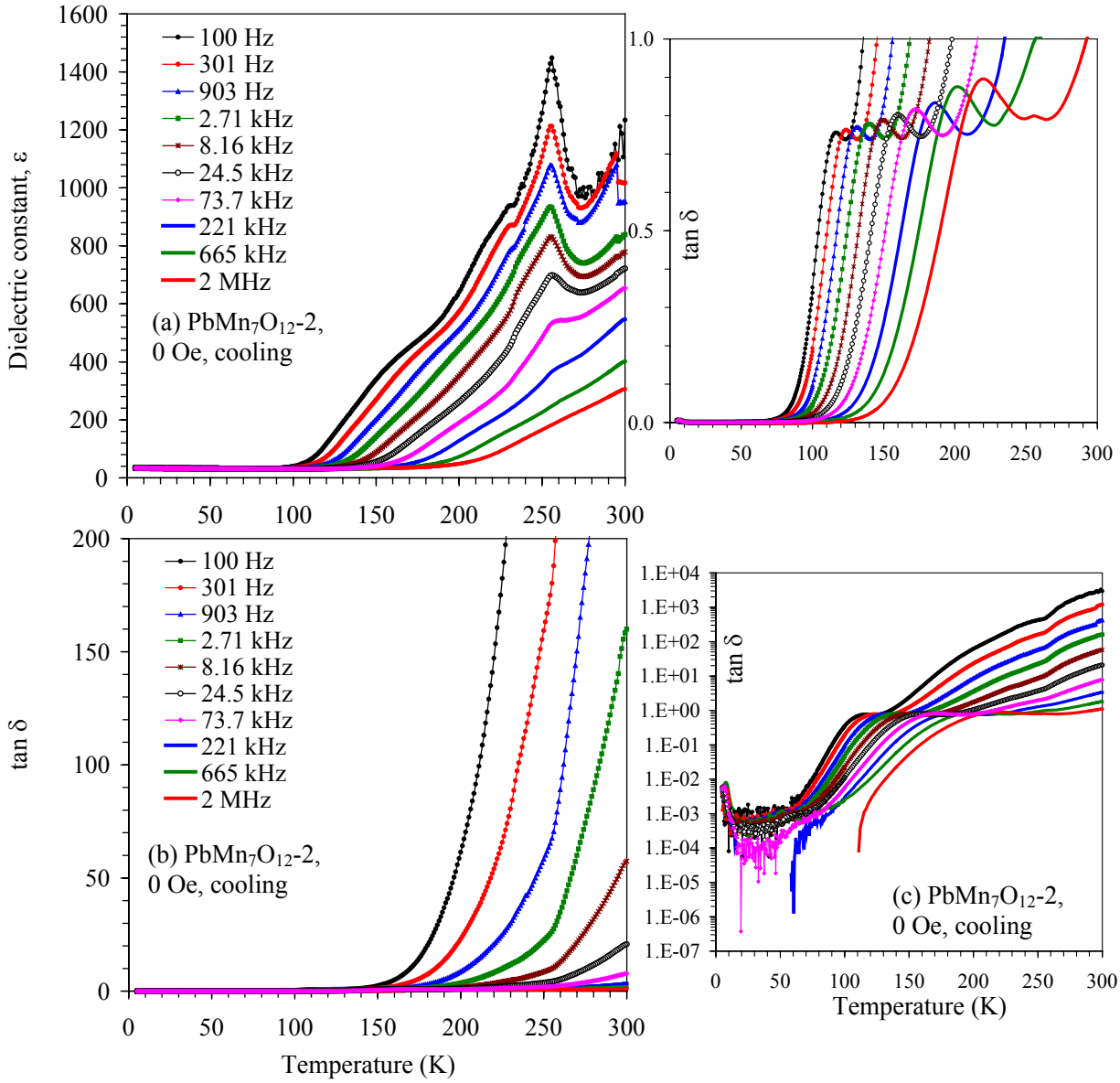

Figure S21a. Dielectric Properties of $PbMn_7O_{12}$.

(Up, left) Dielectric constant in the linear scale and (up, right and down) dielectric loss in the linear and logarithmic scales at different frequencies for $PbMn_7O_{12}$ (sample 2) on cooling at 0 Oe. Note that anomalies near 250 K on dielectric constant are (instrumental) artifacts (we observed such anomalies on many different samples).

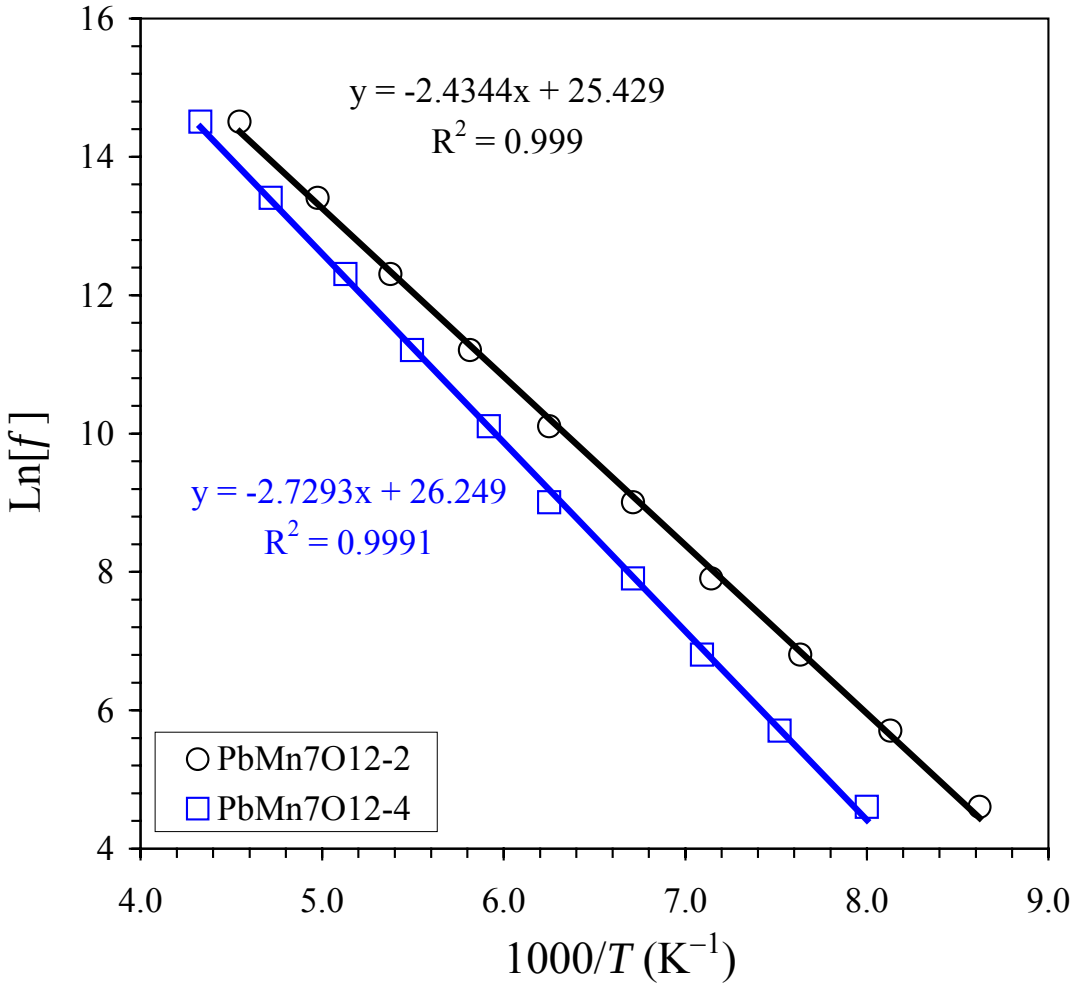

Figure S21b. Dielectric Properties of $PbMn_7O_{12}$ (samples 2 (black) and 4 (blue)).
The ln(f) vs 1000/T plot of the peak temperature of dielectric loss.

Dependence of the maximum of dielectric loss (tanδ), shown on the upper right part of Figures S21a and the down part of S30b, was analyzed using an Arrhenius law:

$f = f_0 * \exp(-E_a/(k_B T))$,

where f_0 is a pre-exponential constant, E_a is an activation energy, and k_B is the Boltzmann constant.

The obtained parameters are $\ln(f_0) = 25.4(2)$ and $E_a = 0.210(2)$ eV for sample 2 and $\ln(f_0) = 26.2(2)$ and $E_a = 0.235(2)$ eV for sample 4.

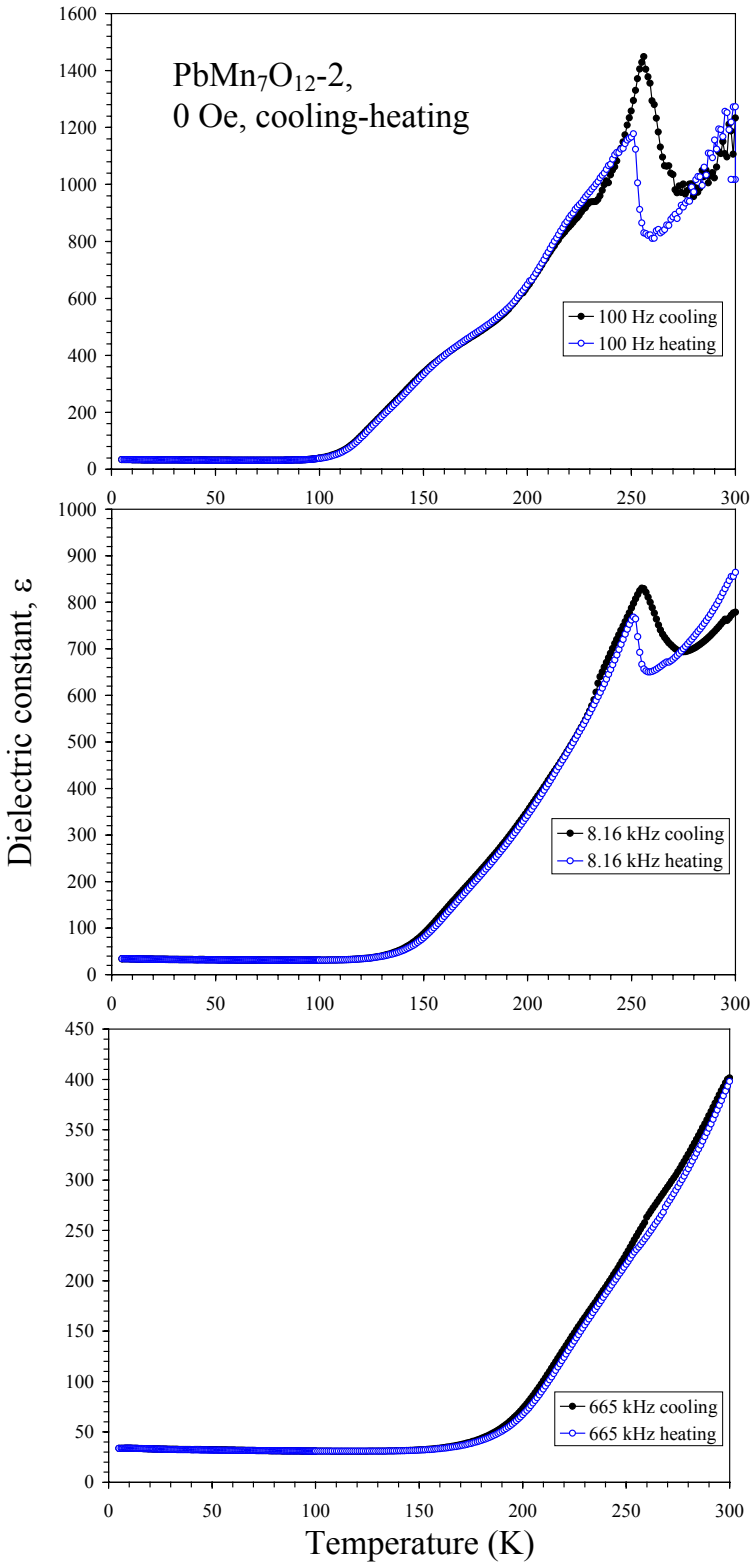

Figure S22. Dielectric Properties of $PbMn_7O_{12}$.
Dielectric constant in the linear scale for $PbMn_7O_{12}$ (sample 2) on cooling and heating at 0 Oe at different frequencies. These curves illustrate an extrinsic origin of anomalies near 250 K.

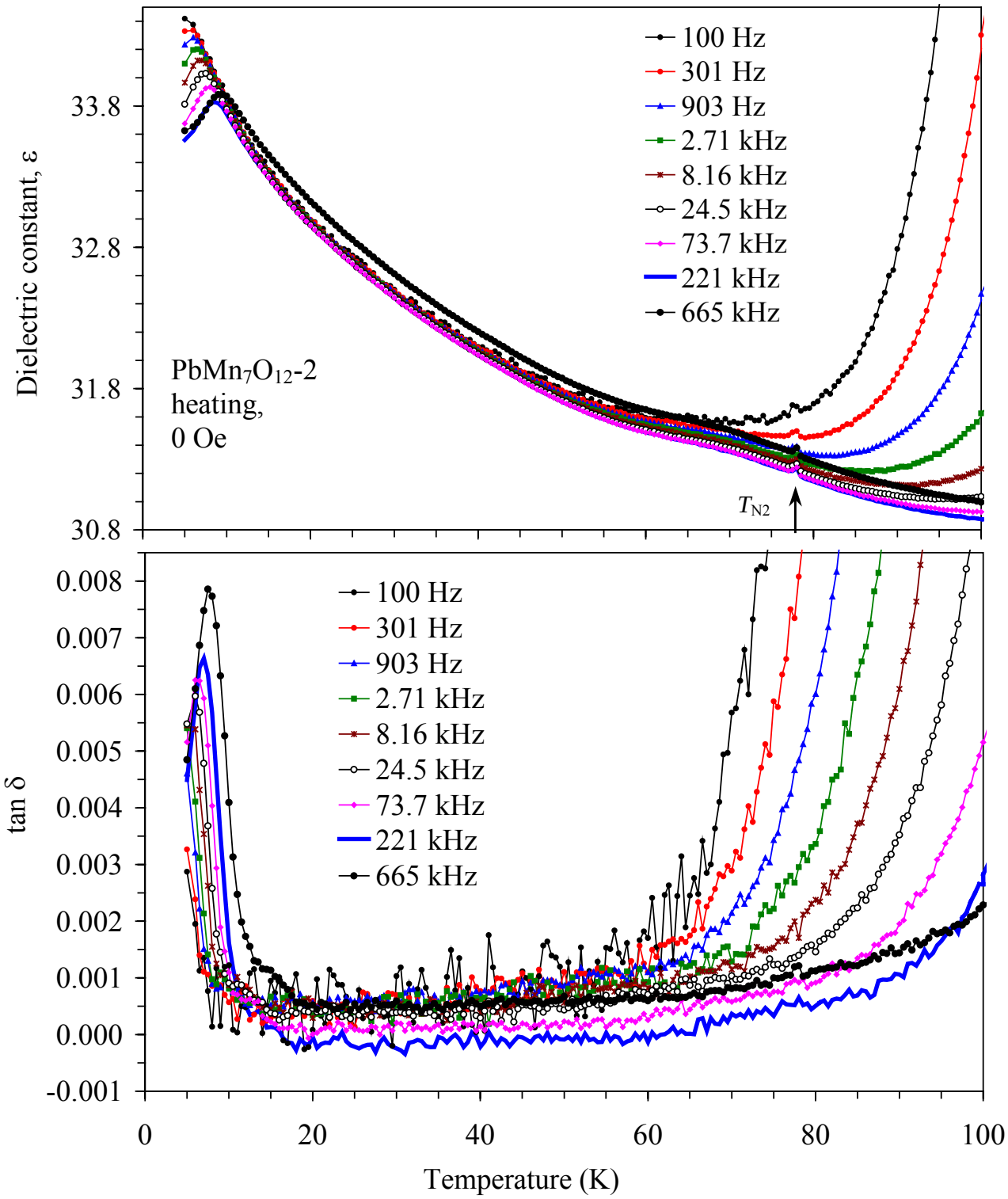

Figure S23. Dielectric Properties of $PbMn_7O_{12}$.
(Up) Dielectric constant and (down) dielectric loss at different frequencies for $PbMn_7O_{12}$ (sample 2) on heating at 0 Oe.

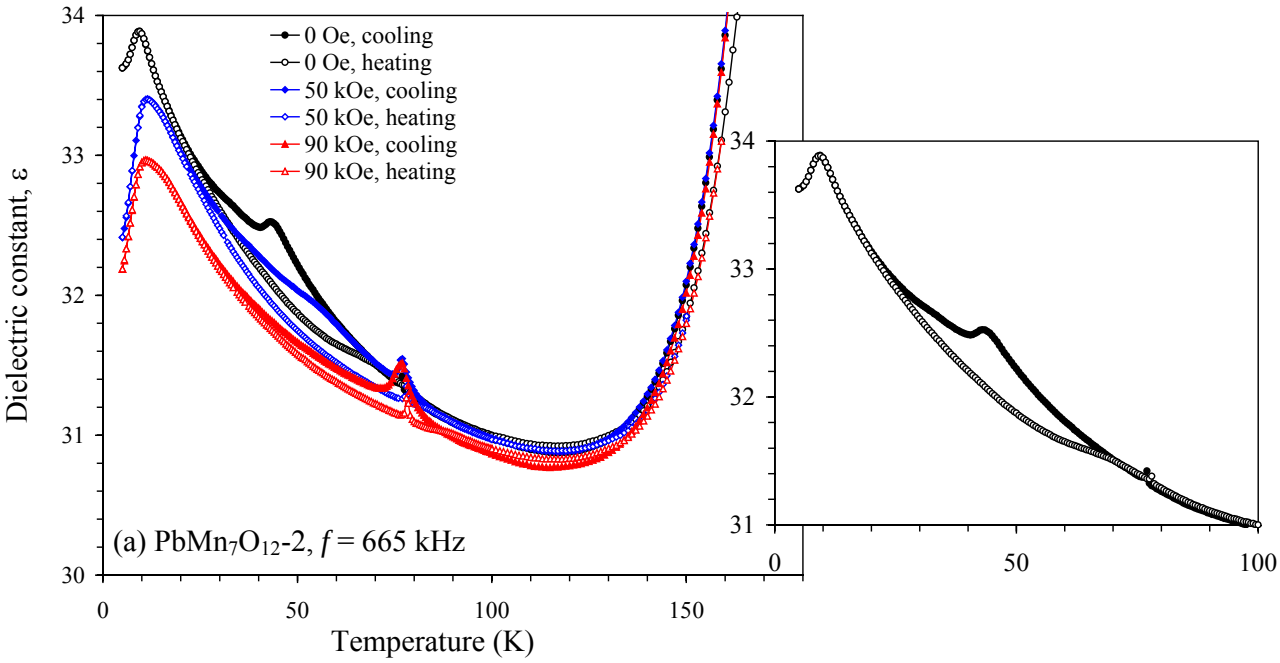

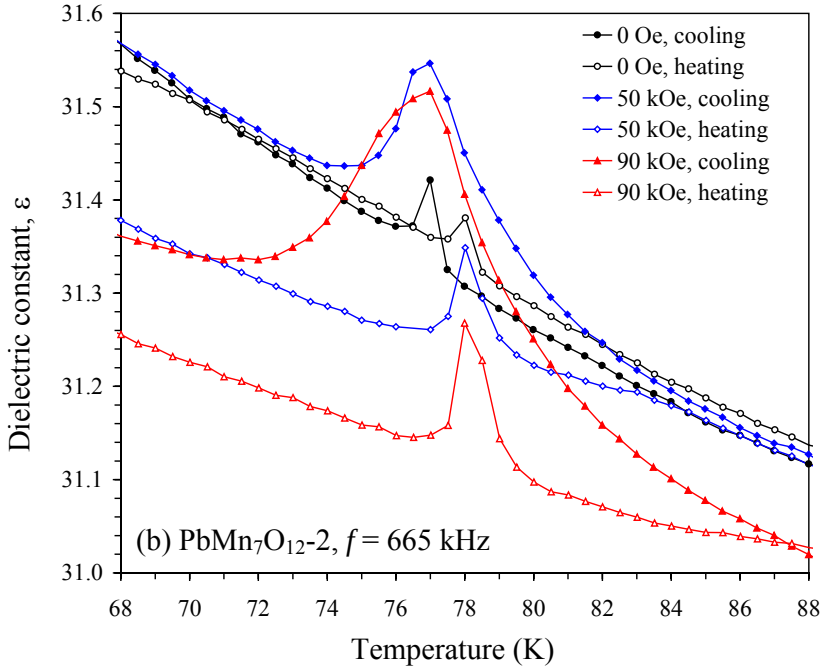

Figure S24. Dielectric Properties of $PbMn_7O_{12}$.
(Up) Dielectric constant at frequency of 665 kHz for $PbMn_7O_{12}$ (sample 2) on heating and cooling at 0, 50, and 90 kOe.
(Down) Details of the same curves between 68 and 88 K.

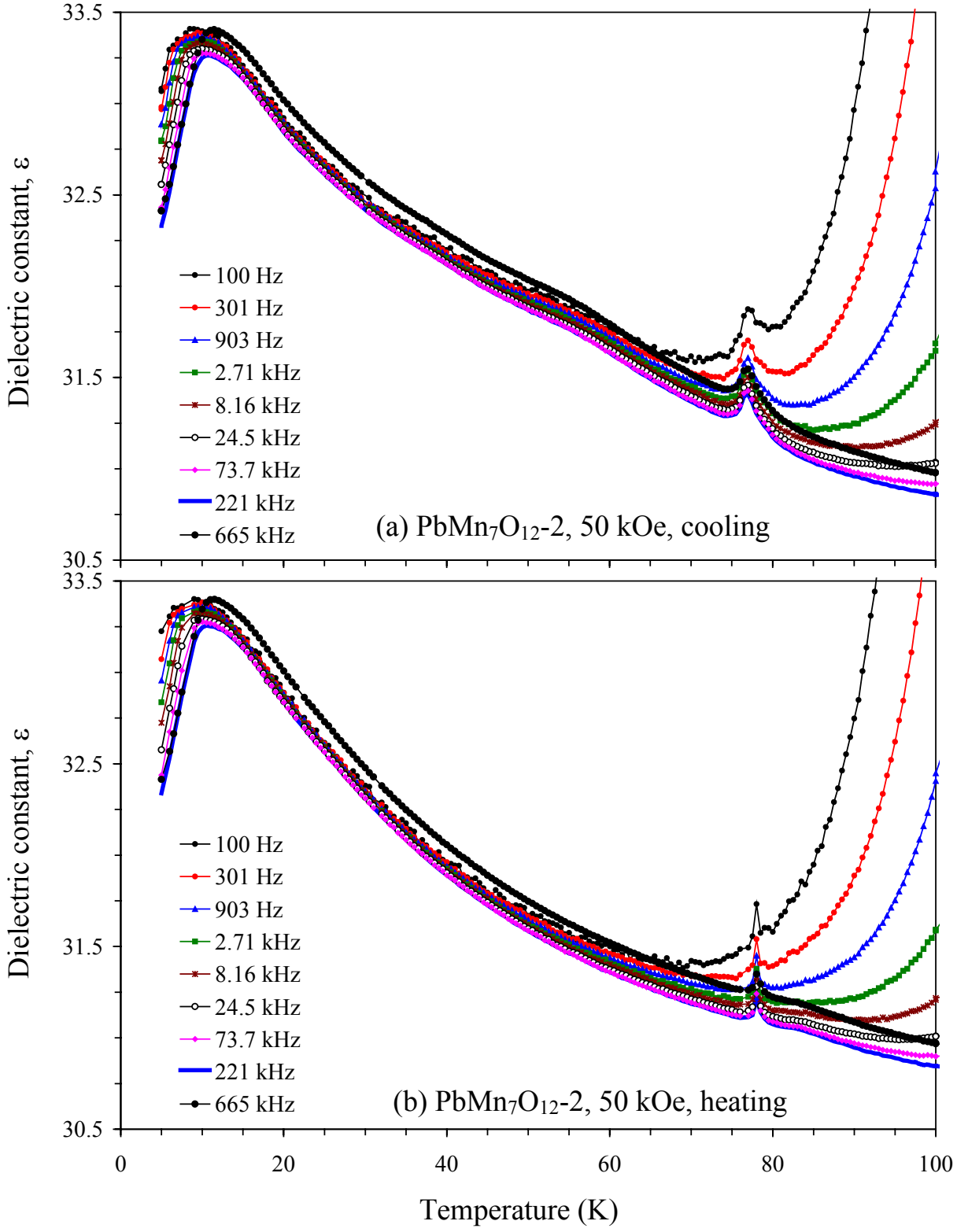

Figure S25. Dielectric Properties of $PbMn_7O_{12}$.
(Up) Dielectric constant at different frequencies for $PbMn_7O_{12}$ (sample 2) on cooling at 50 kOe.
(Down) Dielectric constant at different frequencies for $PbMn_7O_{12}$ (sample 2) on heating at 50 kOe.

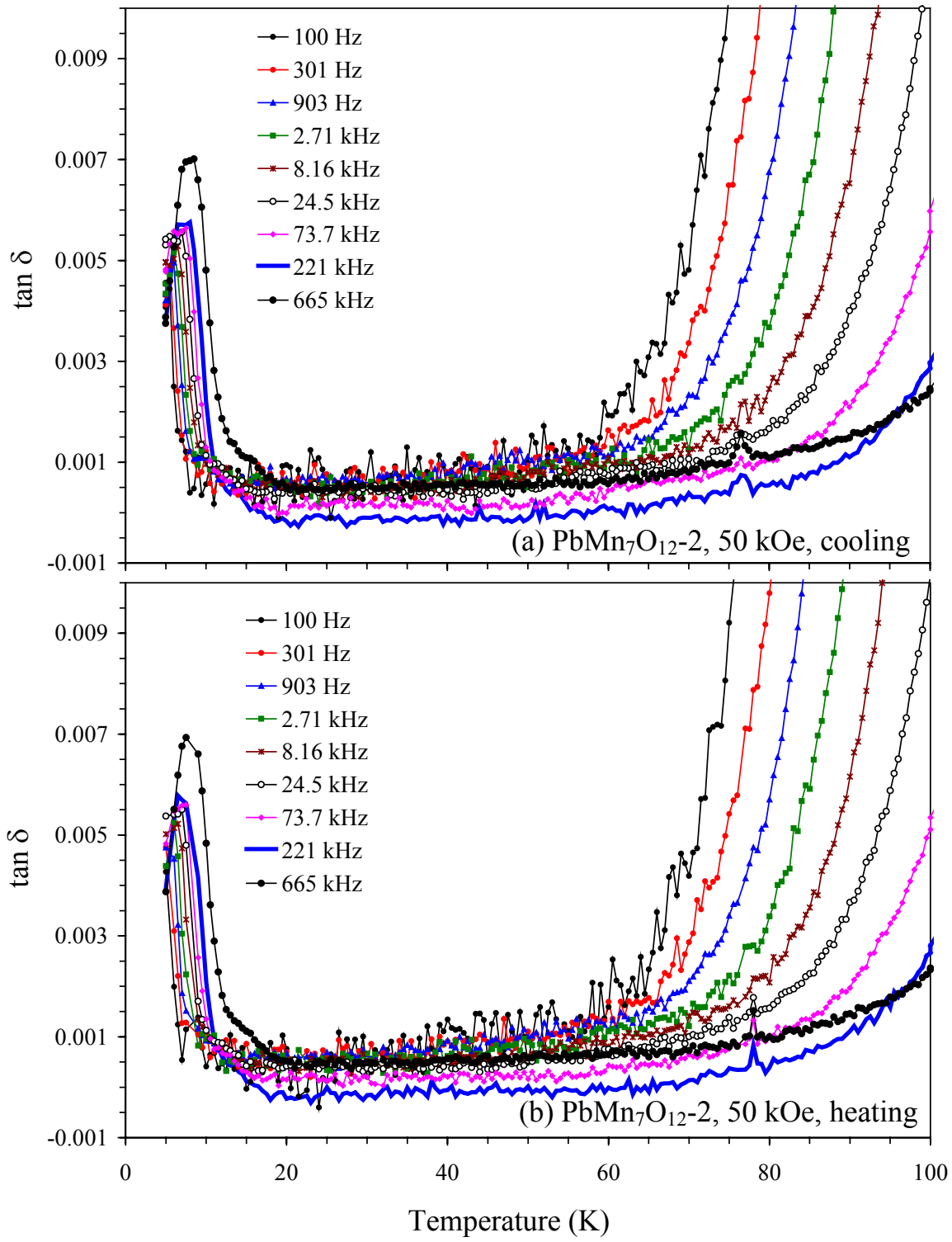

Figure S26. Dielectric Properties of $PbMn_7O_{12}$.
(Up) Dielectric loss at different frequencies for $PbMn_7O_{12}$ (sample 2) on cooling at 50 kOe. (Down) Dielectric loss at different frequencies for $PbMn_7O_{12}$ (sample 2) on heating at 50 kOe.

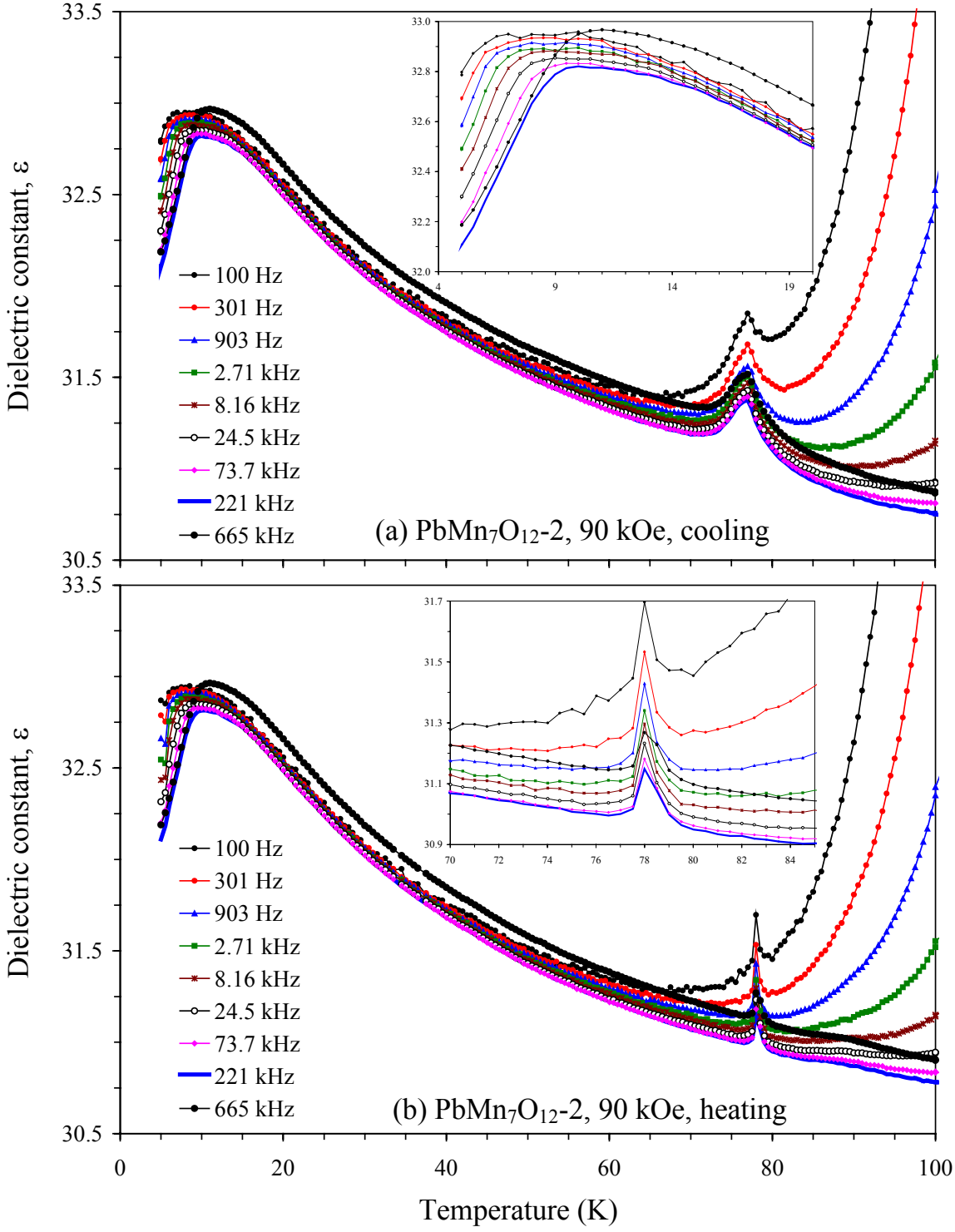

Figure S27. Dielectric Properties of $PbMn_7O_{12}$.
(Up) Dielectric constant at different frequencies for $PbMn_7O_{12}$ (sample 2) on cooling at 90 kOe.
(Down) Dielectric constant at different frequencies for $PbMn_7O_{12}$ (sample 2) on heating at 90 kOe. The insets show enlarged fragments.

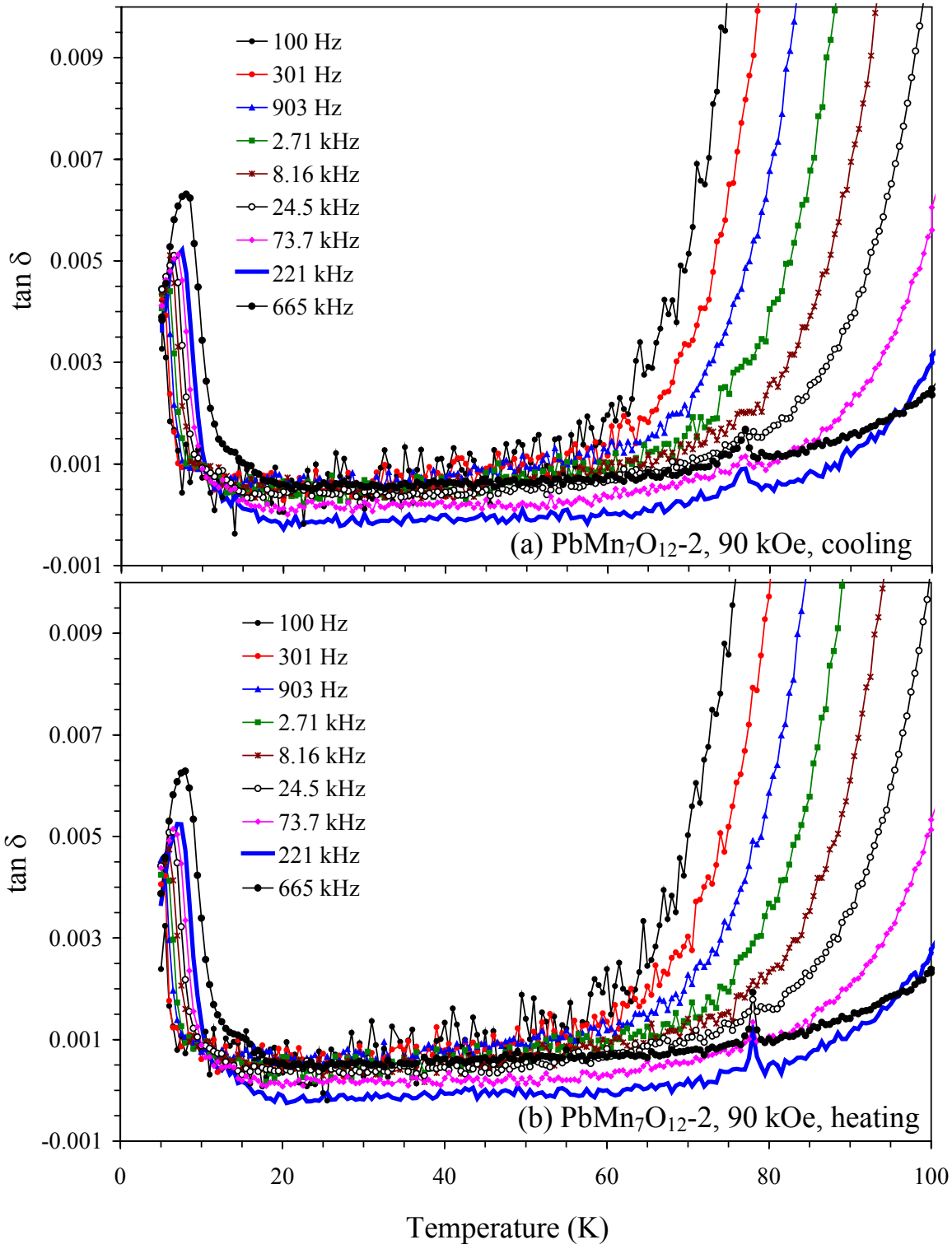

Figure S28. Dielectric Properties of $PbMn_7O_{12}$.
(Up) Dielectric loss at different frequencies for $PbMn_7O_{12}$ (sample 2) on cooling at 90 kOe. (Down) Dielectric loss at different frequencies for $PbMn_7O_{12}$ (sample 2) on heating at 90 kOe.

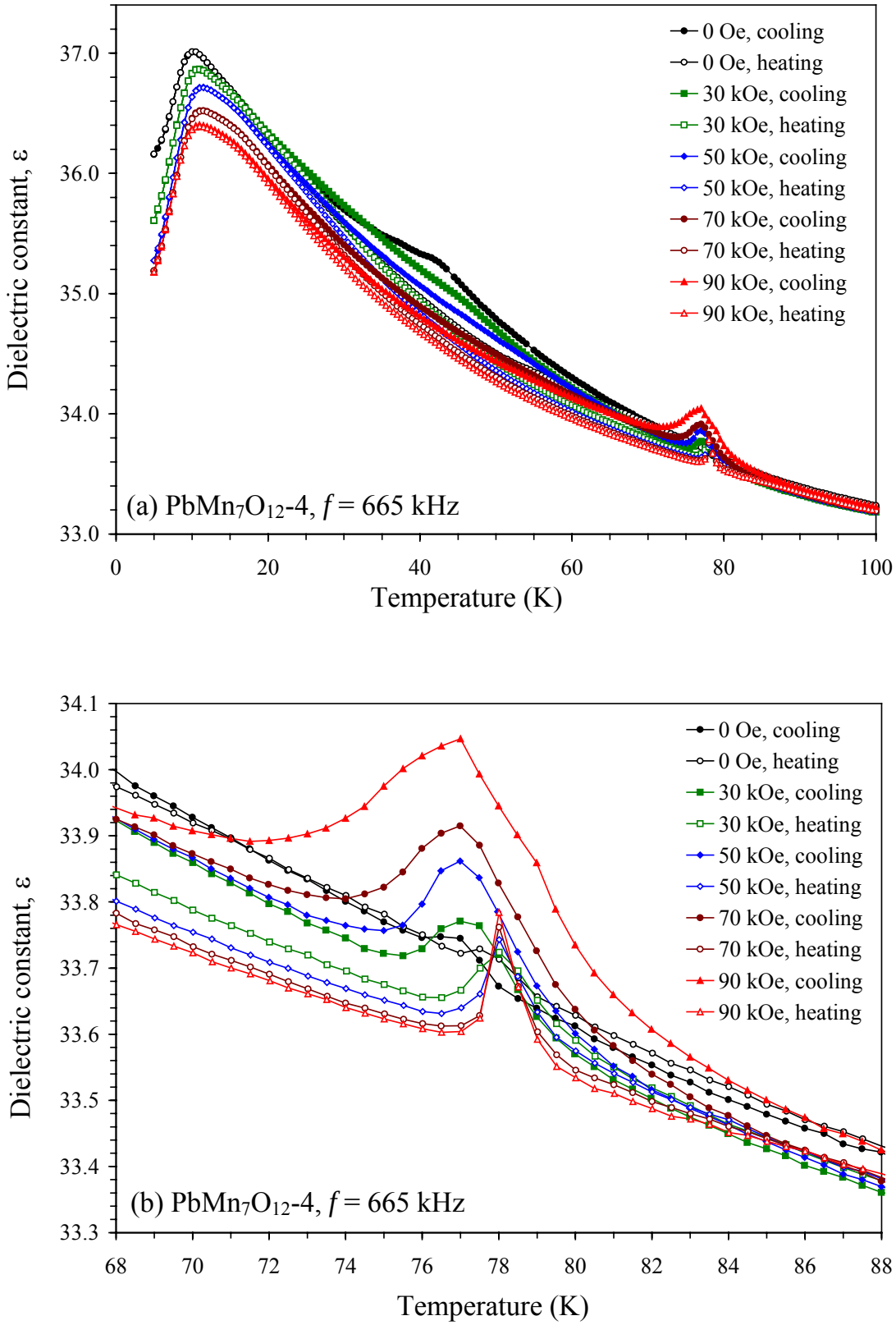

Figure S29a. Dielectric Properties of $PbMn_7O_{12}$.
(Up) Dielectric constant at frequency of 665 kHz for $PbMn_7O_{12}$ (sample 4) on heating and cooling at 0, 30, 50, 70, and 90 kOe.
(Down) Details of the same curves between 68 and 88 K.

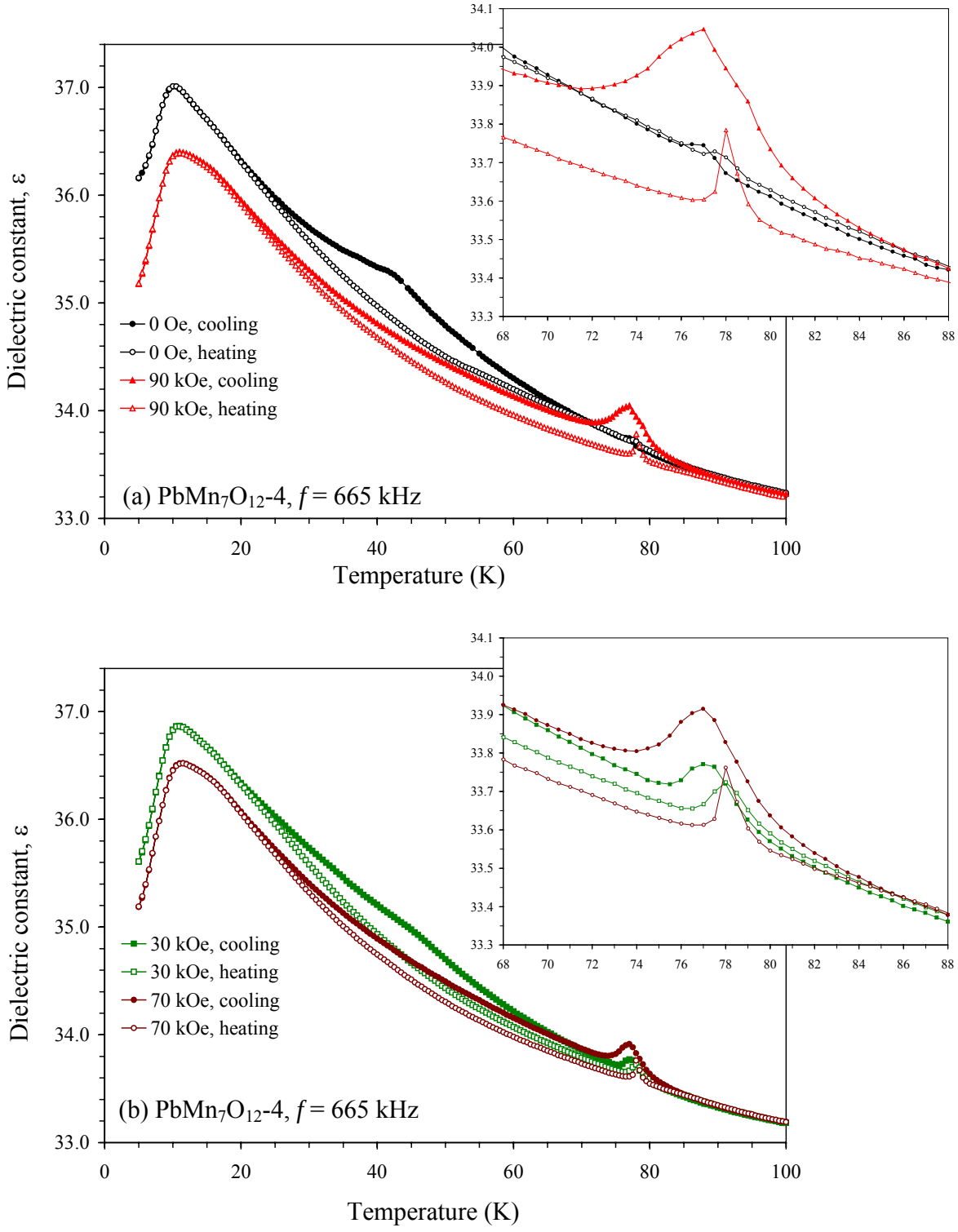

Figure S29b. Dielectric Properties of $PbMn_7O_{12}$.
(Up) Dielectric constant at frequency of 665 kHz for $PbMn_7O_{12}$ (sample 4) on heating and cooling at 0 and 90 kOe. Inset shows details of the same curves between 68 and 88 K.
(Down) Dielectric constant at frequency of 665 kHz for $PbMn_7O_{12}$ (sample 4) on heating and cooling at 30 and 70 kOe. Inset shows details of the same curves between 68 and 88 K.

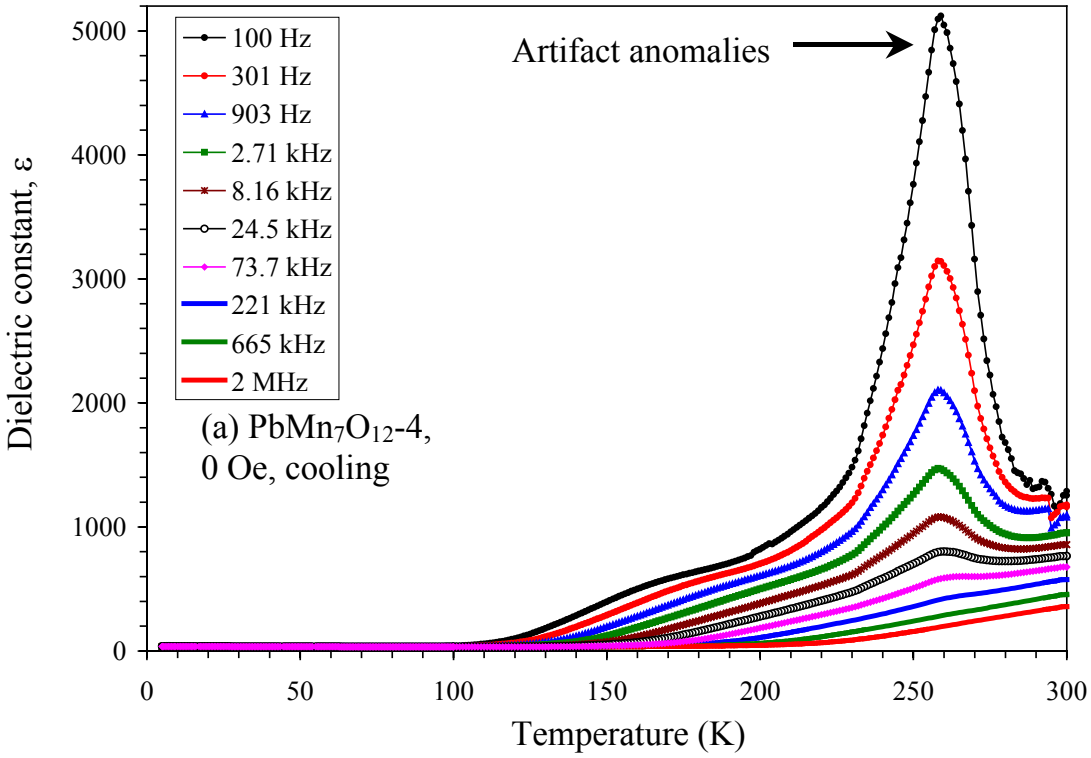

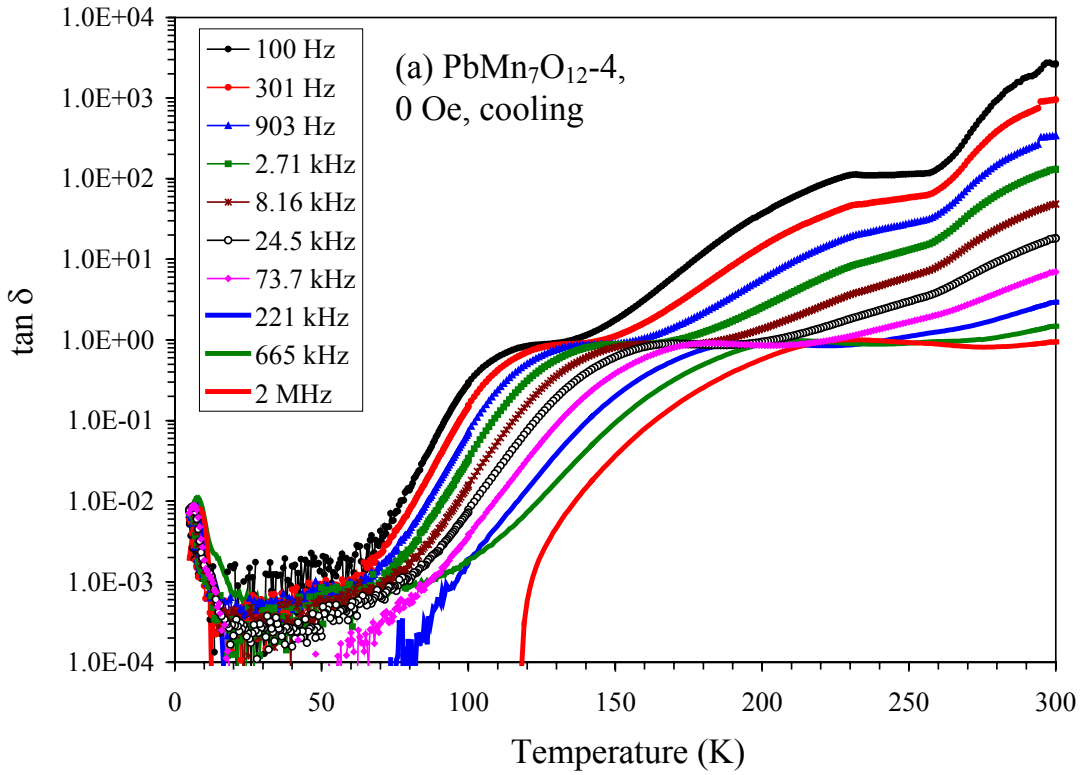

Figure S30a. Dielectric Properties of $PbMn_7O_{12}$.
(Up) Dielectric constant at different frequencies for $PbMn_7O_{12}$ (sample 4) measured at 0 Oe on cooling.
(Down) Dielectric loss (tanδ) in the logarithmic scale at different frequencies for $PbMn_7O_{12}$ (sample 4) measured at 0 Oe on cooling.

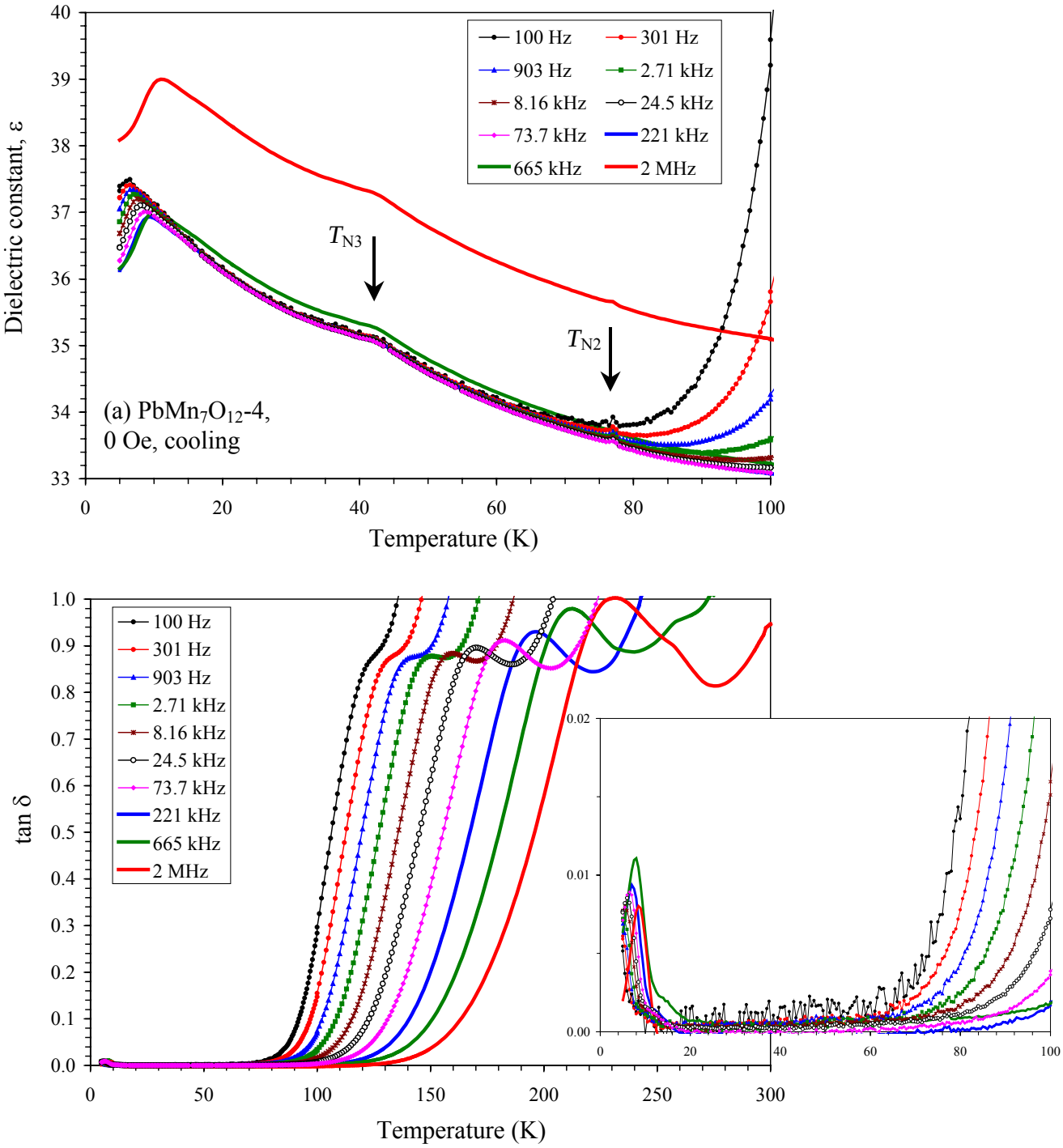

Figure S30b. Dielectric Properties of $PbMn_7O_{12}$.
(Up) Details of dielectric constant at different frequencies for $PbMn_7O_{12}$ (sample 4) measured at 0 Oe on cooling.
(Down) Details of dielectric loss (tanδ) in the linear scale at different frequencies for $PbMn_7O_{12}$ (sample 4) measured at 0 Oe on cooling.

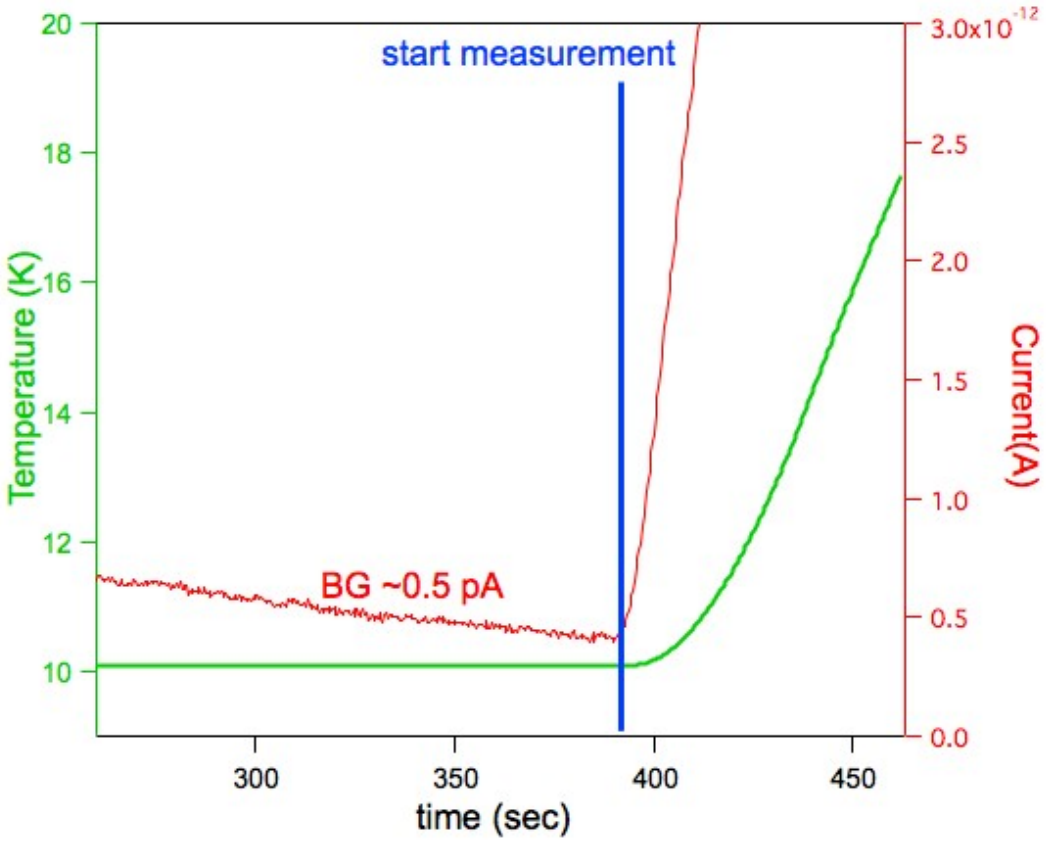

Figure S31a. Pyroelectric Measurements of $PbMn_7O_{12}$.
Time dependence of background (BG) current (after shortening electrodes) in $PbMn_7O_{12}$ (sample 2).

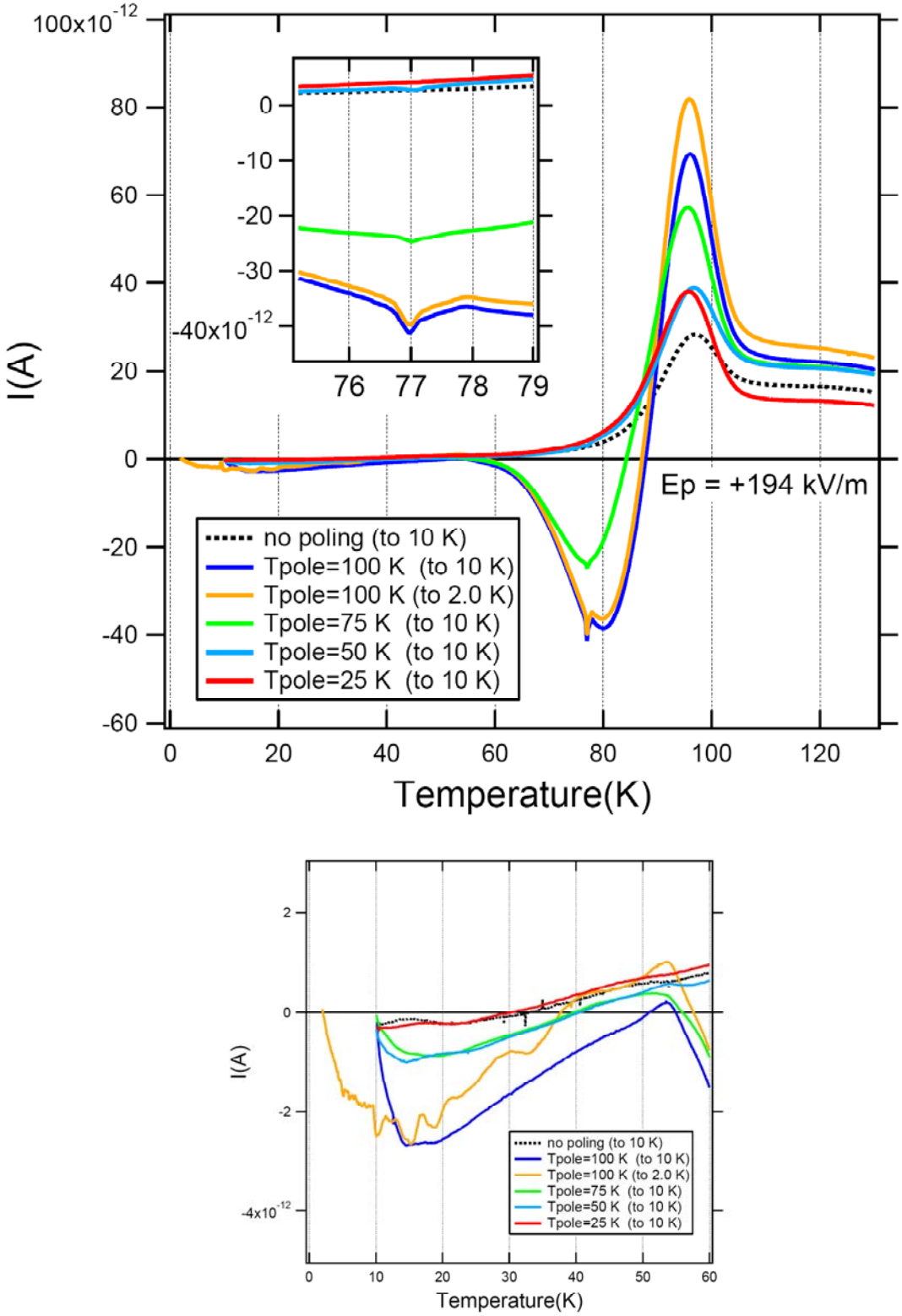

Figure S31b. Pyroelectric Measurements of $PbMn_7O_{12}$ (sample 4).
Results of pyroelectric current measurements for $PbMn_7O_{12}$ (sample 4). Poling conditions are specified on the figure. The insets show details near T_{N2} (the top inset) and between 2 and 60 K (the bottom inset). Note that a maximum of the broad peak is shifted to 80 K in comparison with 75 K in sample 2 (Figure 12 in the main text).

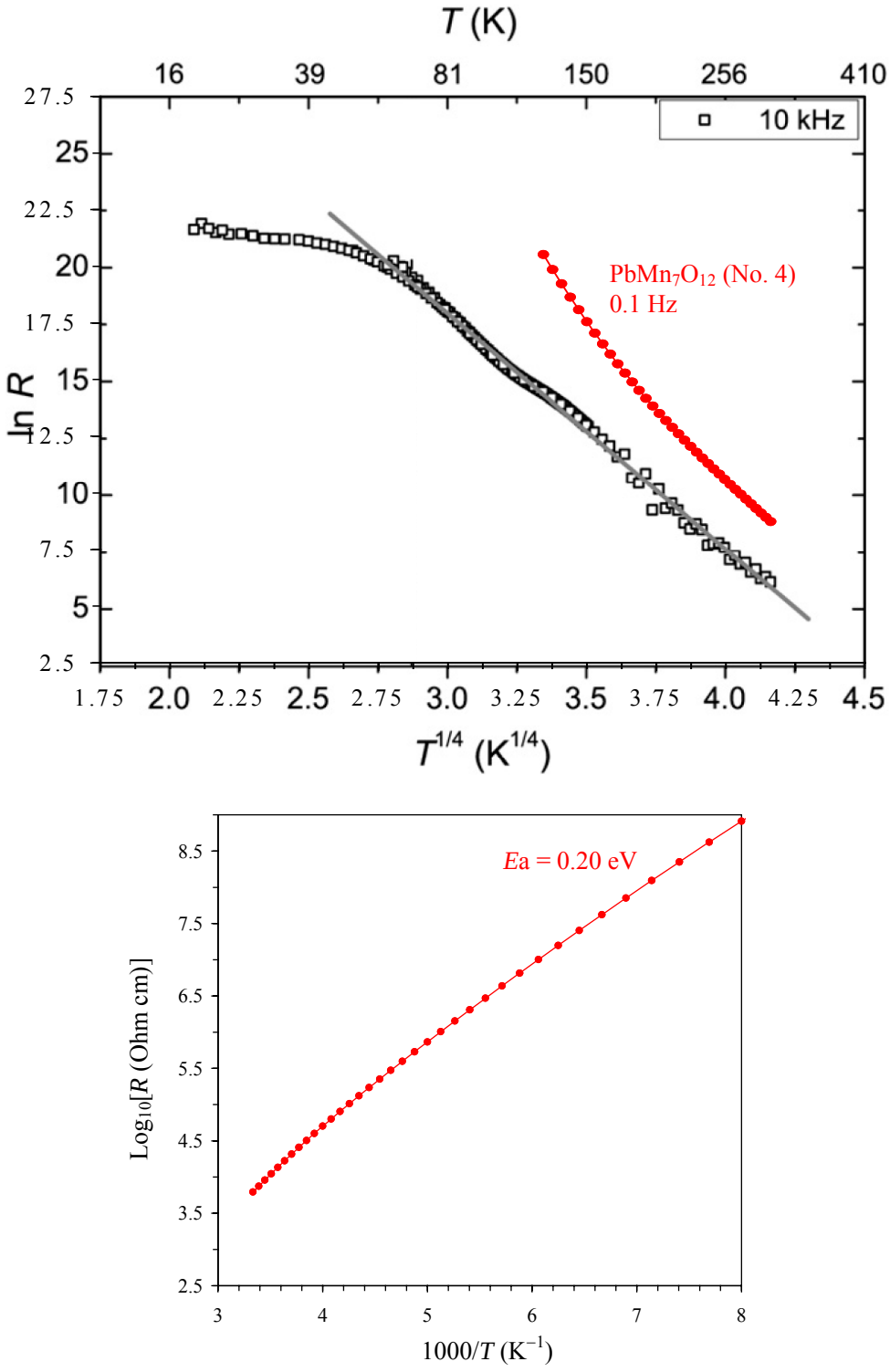

Figure S32. Resistivity of $PbMn_7O_{12}$ (Sample 4).
(Up) Total resistivity of $PbMn_7O_{12}$ at 0.1 Hz (Sample 4; red circles) in comparison with resistivity of $PbMn_7O_{12}$ from [Locherer, T.; Dinnebier, R.; Kremer, R. K.; Greenblatt, M.; Jansen, M. Synthesis and Properties of a New Quadruple Perovskite: A-Site-Ordered $PbMn_3Mn_4O_{12}$. *J. Solid State Chem.* **2012**, *190*, 277-284]. The plot is ln(R) vs $T^{1/4}$.
(Down) Total resistivity of $PbMn_7O_{12}$ (Sample 4; red circles) between 125 and 300 K plotted as log(R) vs 1000/T.

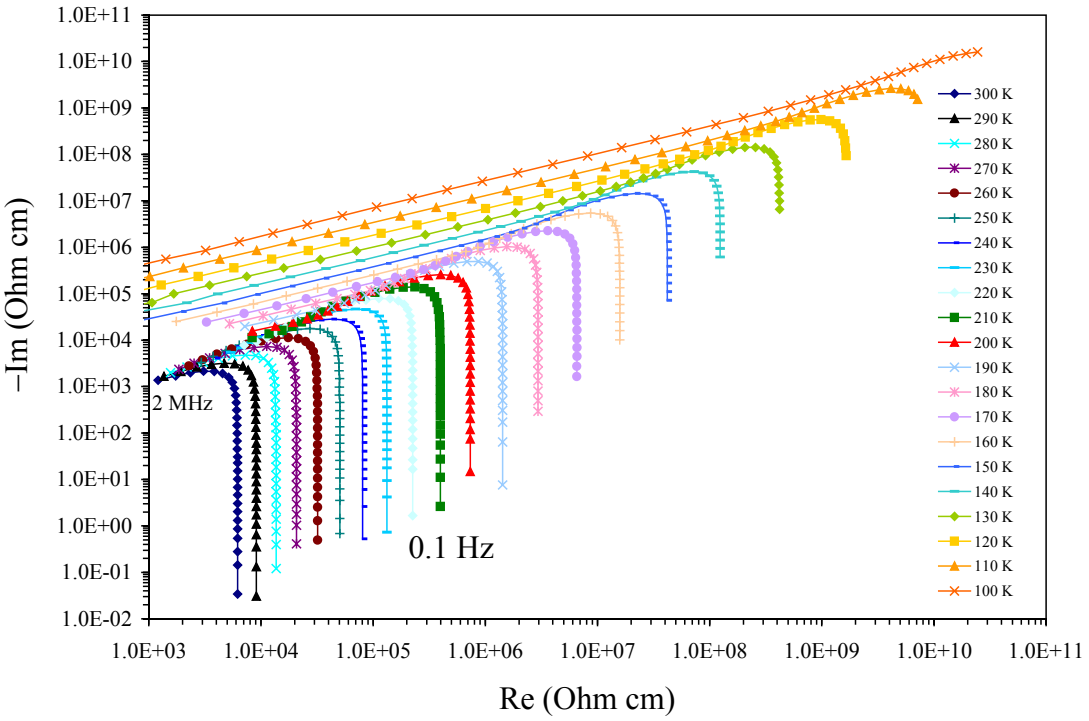

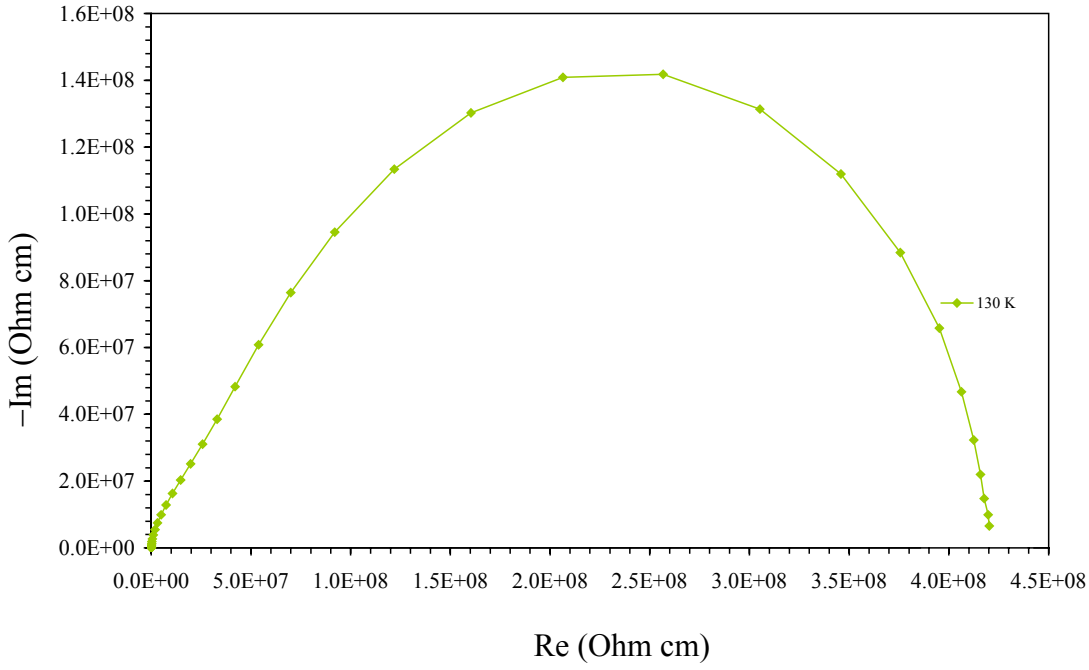

Figure S33. Complex impedance of $PbMn_7O_{12}$ (Sample 4).
(Up) Complex impedance of $PbMn_7O_{12}$ (Sample 4) at different temperatures. The data were used to extract total resistivity shown on Figure S32. (Data are shown with a step of 10 K; measurements were performed with a step of 5 K). Resistivity could be obtained between 300 and about 125 K. Below 120 K, the semi-circle was far from completion because of high resistivity.
(Down) A typical complex impedance plot at 130 K in the linear scale. A distorted (at high frequencies) semicircle is seen.

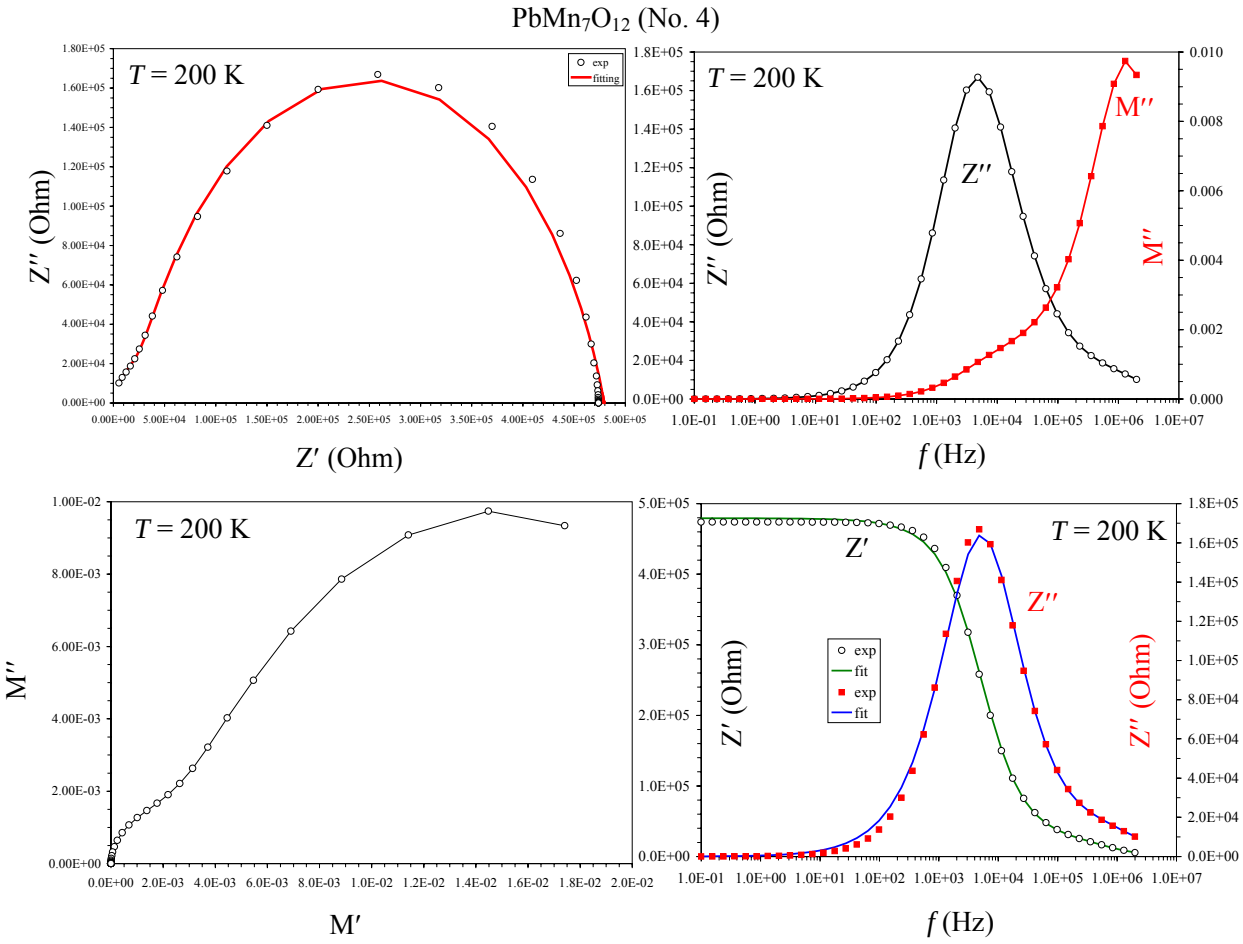

Fitting Parameters at 200 K:

Parameter	Value	Error (%)
R_1 (grain boundary), Ohm	457440	0.45
R_2 (grain), Ohm	21922	3.0
P_1	5.8808E-10	1.36
n_1	0.79084	0.13
P_2	1.3536E-10	3.6
n_2	0.8338	0.26

Equivalent electric circuit used in fitting
(CPE – a constant phase element):

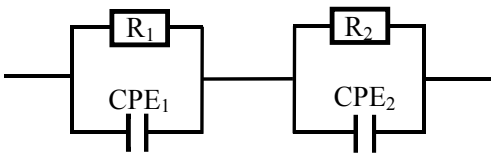

Figure S34. Complex impedance data of $PbMn_7O_{12}$ (Sample 4).
Different plots for $PbMn_7O_{12}$ (Sample 4) at 200 K. (Up, left) Experimental complex impedance (symbols) with fitting results (the red line); fitting parameters are given in the table. (Up, right) Experimental imaginary impedance Z′′ and modulus M′′ vs frequency (symbols with lines). (Down, left) Experimental complex modulus (symbols with lines). (Down, right) Frequency dependence of experimental complex impedance (symbols) with fitting results (green and blue lines).

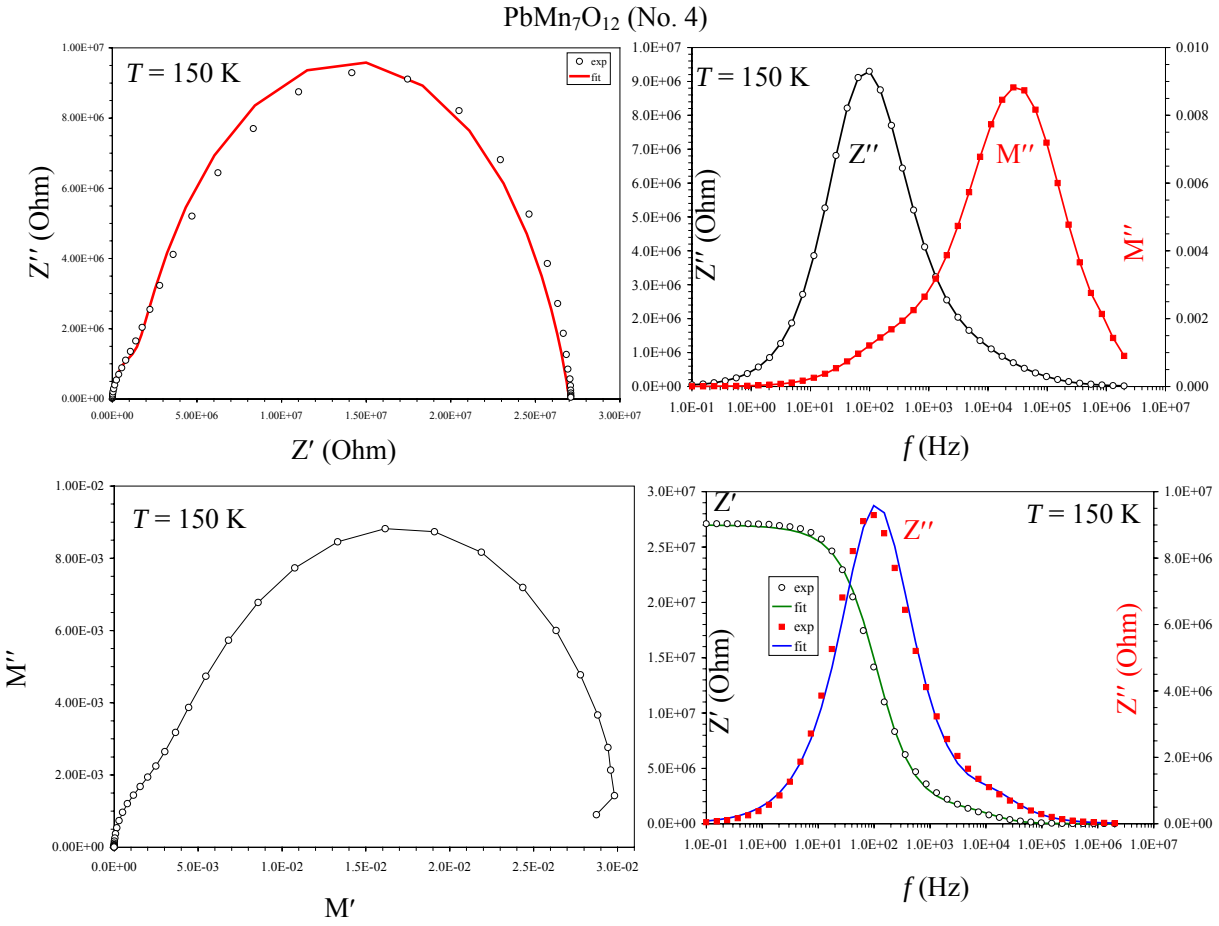

Fitting Parameters at 150 K:

Parameter	Value	Error (%)
R_1 (grain boundary), Ohm	25781000	4.8637
R_2 (grain), Ohm	1220300	15.819
P_1	1.8786E-10	6.9764
n_1	0.81489	0.80269
P_2	1.4010E-11	9.6519
n_2	0.9647	0.67924

Equivalent electric circuit used in fitting
(CPE – a constant phase element):

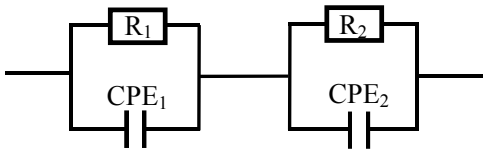

Figure S35. Complex impedance data of $PbMn_7O_{12}$ (Sample 4).
Different plots for $PbMn_7O_{12}$ (Sample 4) at 150 K. (Up, left) Experimental complex impedance (symbols) with fitting results (the red line); fitting parameters are given in the table. (Up, right) Experimental imaginary impedance Z′′ and modulus M′′ vs frequency (symbols with lines). (Down, left) Experimental complex modulus (symbols with lines). (Down, right) Frequency dependence of experimental complex impedance (symbols) with fitting results (green and blue lines).

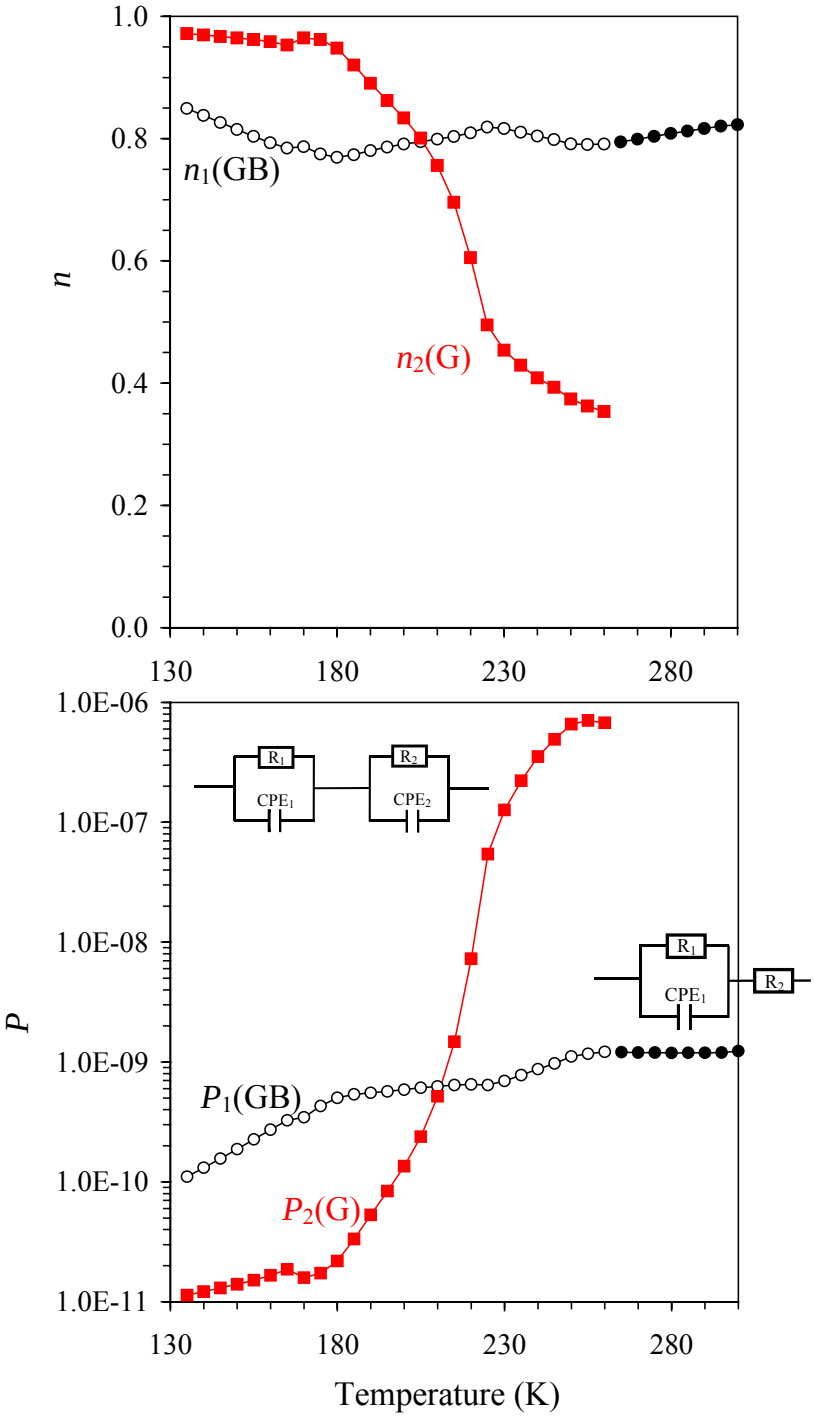

Figure S36a. Complex impedance data of $PbMn_7O_{12}$ (Sample 4).
Temperature dependence of the fitting parameters. Between 135 K and 260 K, the complex impedance was fitted using two parallel *R*-CPE elements. Between 265 K and 300 K, the complex impedance was fitted using parallel R_2 and R_1-CPE elements. CPE: a constant phase element. G: grains; GB: grain boundaries.
Below 130 K, the data could not be fitted satisfactorily with two parallel *R*-CPE elements.

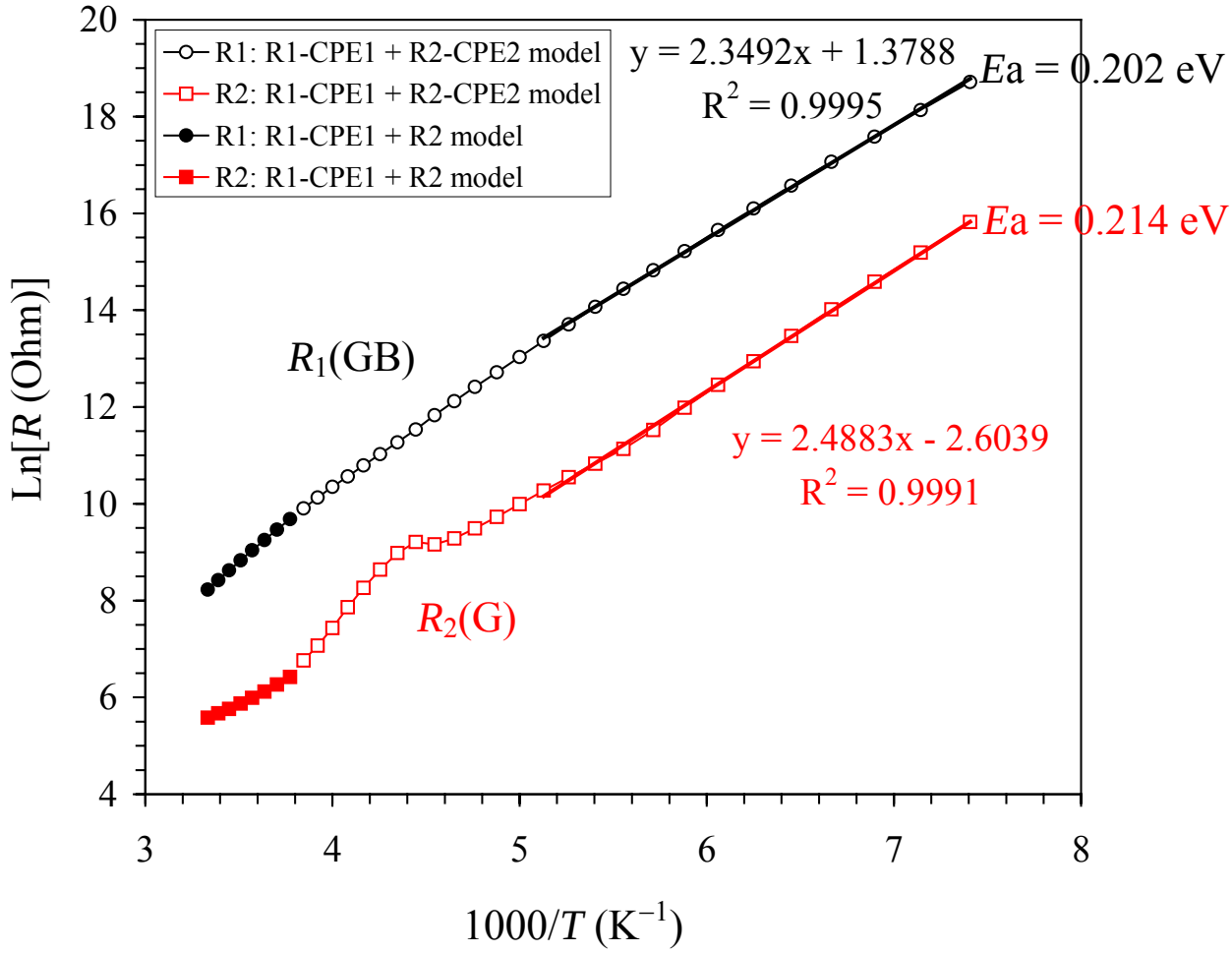

Figure S36b. Complex impedance data of $PbMn_7O_{12}$ (Sample 4).
Temperature dependence of the fitting parameters, R_1(GB) and R_2(G), plotted as ln(R) vs 1000/T. Thickness – 0.78 mm and electrode area – 12.0 mm^2 for sample 4.

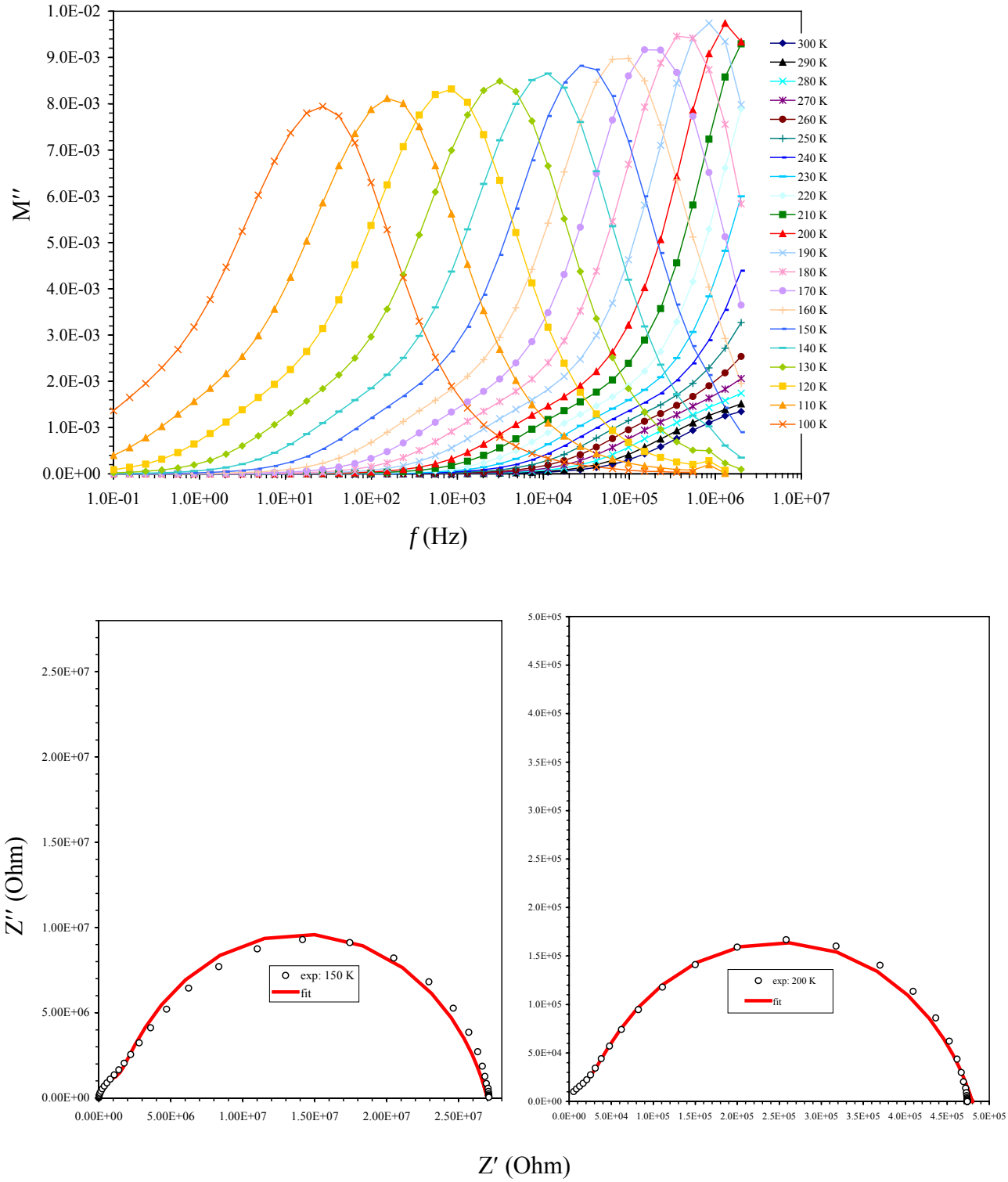

Figure S37. Complex impedance data of $PbMn_7O_{12}$ (Sample 4).
(Up) Modulus M″ spectroscopic plots as a function of temperature in $PbMn_7O_{12}$ (Sample 4). The high-frequency peak remains at about the same size at different temperatures, indicating that its capacitance value is almost constant.
(Down) Complex impedance plane plots in $PbMn_7O_{12}$ (Sample 4), when Z′ and Z″ are shown with the same scale.

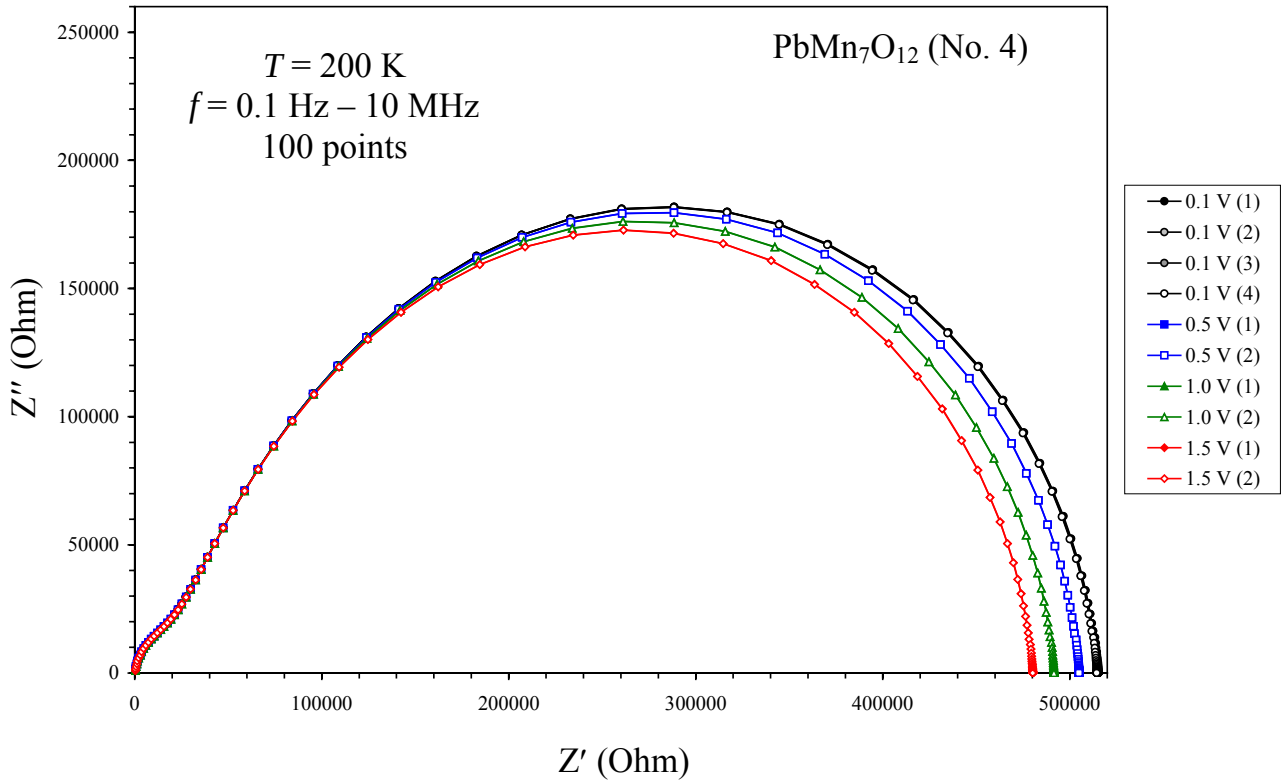

Figure S38a. Complex impedance data of $PbMn_7O_{12}$ (Sample 4).
Complex impedance plane plots in $PbMn_7O_{12}$ (Sample 4) at 200 K. Measurements were performed between 0.1 Hz and 10 MHz at 100 points on the logarithmic scale and using different ac voltage of 0.1, 0.5, 1.0, and 1.5 V. Similar voltage dependence was observed at 150 K and 300 K. The voltage dependence is usually interpreted by a noticeable contribution from sample-electrode contact impedance.

Therefore, the Z' vs Z'' data [measured between 0.1 Hz and 2 MHz at 40 points with 0.1 V (Figures S33-S37)] were also analyzed using three elements: RC1-RC2-RCPE3 (Figure S38b). With this model, the data could be fit between about 120 K and 220 K.

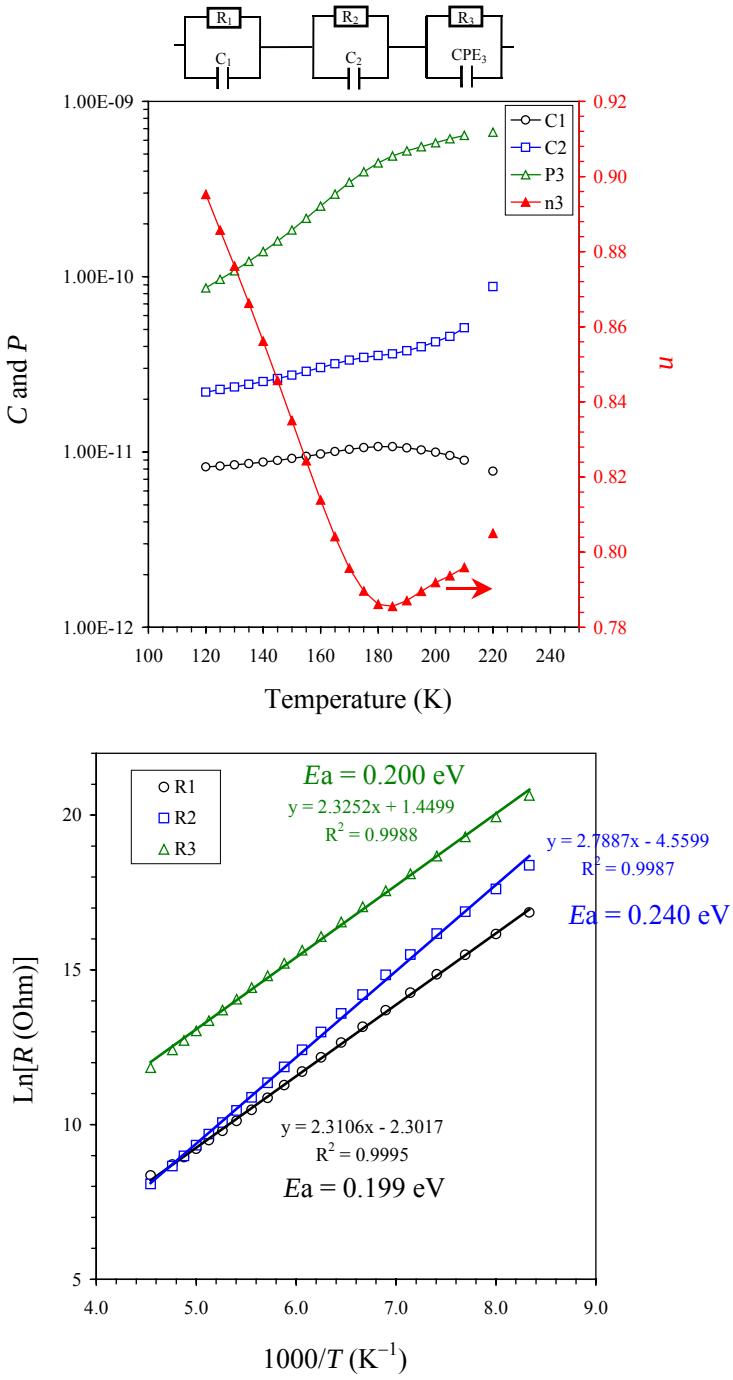

Figure S38b. Complex impedance data of $PbMn_7O_{12}$ (Sample 4).
Temperature dependence of the fitting parameters. R1 is usually interpreted as bulk, R2 – as grain boundaries, and R3 – as sample-electrode resistivity.

In all fittings (Figures S32, 36b, 38b), all activation energies are between 0.20 and 0.24 eV. These values could be either intrinsic for semiconducting $PbMn_7O_{12}$ or artifacts because the largest contribution to resistivity could dominate in fittings. It is interesting that very similar activation energy of 0.22 eV was found in $LaMn_7O_{12}$ [Prodi, A.; Gilioli, E.; Cabassi, R.; Bolzoni, F.; Licci, F.; Huang, Q.; Lynn, J. W.; Affronte, M.; Gauzzi, A.; Marezio, M. *Phys. Rev. B: Condens. Matter Mater. Phys.* **2009**, *79*, 085105]; and it was assigned to the presence of midgap defect states.